

Methanol Production from Syngas

Process modelling and design
utilising biomass gasification and
integrating hydrogen supply

Leonie E. Lücking

Technische Universiteit Delft

Methanol Production from Syngas

Process modelling and design utilising biomass
gasification and integrating hydrogen supply

by

Leonie E. Lücking

in partial fulfillment of the requirements for the degree of

Master of Science

in Sustainable Energy Technology

at the Delft University of Technology,

to be defended publicly on Tuesday December 5, 2017 at 11:30 AM.

P&E-2864

Supervisor: Prof. dr. ir. W. De Jong

Thesis committee: Prof. dr. ir. W. De Jong, TU Delft
Dr. P. V. Aravind, TU Delft
Ir. P. L. J. Swinkels, TU Delft
Ir. ing H. C. de Lathouder, Prinno bv.

An electronic version of this thesis is available at <http://repository.tudelft.nl/>.

Preface

This thesis presents the end of my master at TU Delft. I would like to thank those who helped me with my studies but also with making the last two years so enjoyable.

Firstly to my family, thank you so much for your love, your trust, your open ears and the distractions when I needed them.

For the supervision and assistance with my thesis I would like to thank Prof. Wiebren de Jong and Hans de Lathouder. Thank you to Dr. Aravind and Pieter Swinkels for reading my report and being on my committee.

Lastly, I would like to thank my friends for the lovely time in Delft. Thank you to Balaji for helping me through tough times and cheering me up. Lieke, thank you for all the coffee breaks and encouragement and being the most awesome project partner. Thank you to Abhi, for being my introduction to the crow's nest. Richard, thank you for being my study buddy and friend, and thank you to Irma, Enid, Stephanie and Camilla for making SET as enjoyable as it was.

*Leonie E. Lücking
Delft, November 2017*

Abstract

Transitioning from a heavily fuel reliant economy to a sustainable future is one of the major challenges of our time. The high energy density and good storage properties of fossil fuels have made them the most important energy source for the last centuries. Moving away from fossil fuels towards greener, biomass-based energy and energy carriers is hindered by the technological gap due to the maturity of conventional processes compared to sustainable ones. This thesis focuses on a process of converting biomass into methanol. The process is a small-scale application which is mobile so it can be moved towards the source of the biomass, with the aim to reduce transportation costs. The specific focus lies on the conversion of the gasification-derived syngas into methanol. For this an extensive literature study was conducted to find suitable technologies and process kinetics. Aspen Plus[®] with the integration of Excel was used to model the chosen technologies. The process was divided into three unit operations. The methanol reactor unit with a recycle stream, the CO₂-removal unit to prepare the gas for the reactor unit and a H₂-recycle unit to increase the utilisation of the hydrogen. Each unit operation was modelled separately to study the influence of their parameters and to determine which parameters have the largest influence. Finally, when integrating all unit operations within one model, these selected parameters were used to determine the operating conditions and process design.

The aim of the developed model was to predict and improve the process for different applications with integrated hydrogen supply from renewable sources. The disadvantage of utilising renewable energy sources for the production of hydrogen is the intermittent supply of electricity for the electrolysis of hydrogen. Therefore the process needs to be able to accommodate different levels of hydrogen production. The first case is the base case without any hydrogen input. It is given a syngas-input and the CO₂-removal unit runs at full capacity. Building upon this model, the behaviour of the system for hydrogen supply integration was modelled in the second and third case. The second case introduces additional hydrogen and therefore the CO₂-removal unit can be turned down. The third application adds CO₂, which was removed in case one, to the system and increases the hydrogen input. The study of these processes shows, that the operating pressure of the methanol reactor unit has a very large influence on the energy requirements of the process but also on the production of methanol. In respect to the power and cooling requirements of the process a low pressure is favoured but much larger quantities of methanol can be produced at higher pressures. With the chosen designs for the cases a respective methanol production of 47.6 t d⁻¹, 96.8 t d⁻¹ and 180.6 t d⁻¹ is reached. The integration of hydrogen leads to two major concerns for the process. The integration requires much larger equipment due to higher flowrates and the quality of the product decreases as a higher CO₂/CO-ratio produces more water. The thesis served its purpose by developing a model of the process which can be further used to optimise the process on a techno-economic level.

Contents

List of Figures	xi
List of Tables	xv
Abbreviations	xvii
Glossary	xix
Nomenclature	xxi
1 Introduction	1
1.1 Research Questions	4
1.2 Structure of the Thesis	4
2 Theoretical Background	5
2.1 Biomass as Energy-Feedstock for Methanol Synthesis.	5
2.1.1 Gasification	5
2.1.2 Impurities and Cleaning of Bio-Syngas	7
2.1.3 Uses of Syngas	7
2.2 Methanol Production.	8
2.2.1 Methanol Synthesis from Syngas	8
2.3 Hydrogen Production through Electrolysis.	10
3 State of the Art Methanol Reactor and Process Technology	13
3.1 Low-Pressure Methanol Synthesis Reactor.	13
3.1.1 Adiabatic Reactors	14
3.1.2 Isothermal Reactors	15
3.1.3 Other Reactor Types	15
3.1.4 Catalysts.	18
3.2 Synthesis Gas Upgrading: CO ₂ -Removal.	19
3.2.1 Absorption.	20

3.2.2	Membranes	22
3.2.3	Adsorption	22
3.2.4	Low-Temperature Distillation	24
3.3	Synthesis Gas Upgrading: Hydrogen Recycle	25
3.3.1	Adsorption	25
3.3.2	Cryogenic Distillation	25
3.3.3	Membranes	25
4	Building the Model	29
4.1	Terminology and Assumptions	30
4.2	Methanol Reactor Unit.	31
4.2.1	Modelling	31
4.2.2	Calibration and Comparison with Reactor Data.	34
4.2.3	Sensitivity Analyses	35
4.2.4	Influencing Parameters	41
4.3	CO ₂ -Removal Unit	43
4.3.1	Modelling	43
4.3.2	Validation	44
4.3.3	Sensitivity Analyses	44
4.3.4	Influencing Parameters	47
4.4	Hydrogen-Recycle	49
4.4.1	Modelling	49
4.4.2	Sensitivity Analyses	51
4.4.3	Influencing Parameters	53
4.5	Full Methanol Synthesis Unit	53
5	Evaluating the Cases	55
5.1	Case 1 - No Hydrogen Integration	56
5.1.1	Operating point	58
5.2	Case 2 - Constant Hydrogen Integration	59
5.3	Case III - Varying Hydrogen Integration	60
5.4	Comparison	61

6 Conclusion	65
6.1 Recommendations	67
Bibliography	69
A Flowsheets	i
B Flows of the cases	v

List of Figures

1.1	Global Energy Demand in quadrillion BTU, 1990-2040 (1 quadrillion BTU = 293.1 TWh) .	1
1.2	Comparing the energy resources of the planet	2
1.3	Methanol Demands and End Use.	3
1.4	Scheme of a methanol production plant. The elements of focus of this thesis are within the blue frame.	4
2.1	Effect of the reduction temperature on the product with the operating ranges for different fuels: agro fuels, refuse-derived fuels (RDF), woody biomass and coal.	7
2.2	Examples of uses of syngas and methanol and their conversion catalysts	8
2.3	Energy demand for water and steam electrolysis at 10 bar	11
3.1	Conversion profiles (solid line), equilibrium curves (dashed line) and schematics of methanol reactors	14
3.2	Conversion profile (solid line), equilibrium curve (dashed line) and schematic for an isothermal reactor with indirect cooling	15
3.3	Process technologies for CO ₂ -capture adapted from Rao and Rubin	19
3.4	Development stage of process technologies for CO ₂ -capture adapted from Figueroa <i>et al.</i>	20
3.5	Process selection chart for CO ₂ -absorption technology without H ₂ S present	21
3.6	Corrected Robeson upper-bound for H ₂ /CH ₄ polymeric membranes	27
4.1	Unit operations discussed within this thesis: H ₂ -recycle, CO ₂ -removal and methanol reactor with crude methanol separation	30
4.2	Methanol Reactor Unit for the formation of methanol from syngas and separation of crude methanol from the gas stream as modelled in Aspen Plus®	35
4.3	Concentration profile of the methanol reactor from Van den Bussche and Froment . . .	35
4.4	Concentration profile of the methanol reactor as modelled with Aspen Plus®	35
4.5	Influence of the reactor's diameter and volume on the production of methanol for a single reactor reactor	38
4.6	Influence of the reactor volume distribution on the pressure drop	38
4.7	Influence of feed pressure and temperature on the output of a single methanol reactor with the dimensions of 3.5 m length and 2 m diameter	38

4.8	Influence of the operating pressure of the MRU on the methanol output within the <i>CRU-DEMEO</i> for various pressure drops between the reactor inlet and the flash	38
4.9	Influence operating pressure of the MRU on the compressor work per lower heating value of methanol produced at various pressure drops between the reactor inlet and the flash	39
4.10	Influence operating pressure of the MRU on the compressor work per lower heating value of methanol produced at various flash temperatures	39
4.11	Influence operating pressure of the MRU on the cooling duty of the flash per lower heating value of methanol produced at various pressure drops between the reactor inlet and the flash	40
4.12	Influence operating pressure of the MRU on the cooling duty of the flash per lower heating value of methanol produced at various flash temperatures	40
4.13	Influence operating pressure of the MRU on the mass flow into the reactor due to recycle at various pressure drops between the reactor inlet and the flash	41
4.14	Influence operating pressure of the MRU on the mass flow into the reactor due to recycle at various flash temperatures	41
4.15	Influence of the flash's temperature on the composition of the <i>CRUDEMEO</i> stream at various operating pressures of the MRU	42
4.16	Influence of the flash's temperature on the composition of the <i>CRUDEMEO</i> stream at various pressure drops between the reactor inlet and the flash at the MRU's operating pressure of 60 bar	42
4.17	Value of the recycle ratio for the MRU at different percentages of purged gas	42
4.18	Influence of the recycle ratio on the methanol output of the flash	42
4.19	Influence of the recycle ratio on on the compressor work per lower heating value of methanol produced	43
4.20	Influence of the recycle ratio on on the cooling duty per lower heating value of methanol produced	43
4.21	CO_2 -removal unit (CRU) with the Selexol [®] process as the chosen technology. The split <i>Rec-Y-N</i> defines if the stream <i>F1-TOP</i> is being recycled into the distillation column or not.	44
4.22	P-xy-diagram for a binary mixture of Selexol [®] and water at 50 °C	46
4.23	P-xy-diagram for a binary mixture of Selexol [®] and CO_2 at 12 °C	46
4.24	Composition of the <i>SYN-IN</i> stream after the absorber column with the resulting stoichiometric number,SN, for different solvent flowrates	46
4.25	Energy requirement per removed CO_2 for the operation	46
4.26	Composition of the <i>SYN-IN</i> stream after the absorber column with the resulting stoichiometric number,SN, for the operation of the flash at various pressures	47
4.27	Energy requirement per removed CO_2 for the operation of the flash at various pressures	47
4.28	Composition of the <i>SYN-IN</i> stream after the absorber column with the resulting stoichiometric number,SN, for different operating pressures of the absorber	48

4.29 Energy requirement per removed CO ₂ for different operating pressures of the absorber	48
4.30 Power consumption of the CRU over the amount of removed CO ₂ for various <i>FLACHCCU</i> -pressures	48
4.31 H ₂ -recycle unit (HRU) with the membrane, modelled as a <i>USER2</i> -Module, and the feed and product streams	49
4.32 Diagram of the model by Kohl and Nielsen used in this report. The flow directions of each flow are presented.	51
4.33 Fraction of the component flow in the <i>FEED-ME</i> -stream that permeated through the membrane over the membrane size	53
4.34 Fraction of the component flow in the <i>FEED-ME</i> -stream that permeated through the membrane over the pressure of the <i>FEED-ME</i> -stream for a membrane size of 3.5 m ² . .	53
5.1 Simplified depiction of the solar irradiation during the different production periods . . .	56
5.2 CASE1: mechanical ratio (MR) (continuous line) and thermal ratio (TR) (dashed line) over the solvent flowrate for various MRU operating pressures and a recycle fraction of 0.89	57
5.3 CASE1: Stoichiometric number of the reactor feed over the solvent flowrate for various MRU operating pressures and a recycle fraction of 0.89	57
5.4 CASE1: mechanical ratio (MR) (continuous line) and thermal ratio (TR) (dashed line) over the recycle fraction for various MRU operating pressures and a solvent flowrate of 115 000 kg h ⁻¹	58
5.5 CASE1: produced methanol in the <i>CRUDEMEO</i> -stream over the recycle ratio for various MRU operating pressures and a solvent flowrate of 115 000 kg h ⁻¹	59
5.6 CASE1: volumetric flowrate of the reactor feed over the recycle ratio for various MRU operating pressures and a solvent flowrate of 115 000 kg h ⁻¹	59
5.7 CASE1: mechanical ratio (MR), thermal ratio (TR) and the fraction of hydrogen loss over the membrane area at an operating pressure of 60 bar and a solvent flowrate of 115 000 kg h ⁻¹	59
5.8 CASE1: compression work of the three pressure changers and the total flowrate of methanol in the <i>CRUDEMEO</i> -stream over the membrane at an operating pressure of 60 bar and a solvent flowrate of 115 000 kg h ⁻¹	59
5.9 CASE2: mechanical ratio and thermal ratio as well as methanol component flow in the <i>CRUDEMEO</i> -stream for various hydrogen inlet flows	60
5.10 CASE2: recycled mss flow and volumetric flow entering the reactor for various hydrogen inlet flows	60
5.11 CASE3: mechanical ratio and thermal ratio as well as methanol component flow in the <i>CRUDEMEO</i> -stream for various hydrogen inlet flows	61
5.12 CASE3: recycled mass flow and volumetric flow entering the reactor for various hydrogen inlet flows	61
A.1 Aspen Plus® Model flow-sheet for case 1: Methanol synthesis without hydrogen integration	ii

A.2 Aspen Plus® Model flow-sheet for case 2: Methanol synthesis with hydrogen integration	iii
A.3 Aspen Plus® Model flow-sheet for case 3: Methanol synthesis with hydrogen and CO ₂ integration	iv

List of Tables

2.1	Overview of energy-related biomass supply sources globally (2013)	6
2.2	Electrolysers and their characteristics	11
3.1	List of producers of low-pressure adiabatic methanol reactors and the reactors' characteristics	16
3.2	List of producers of low-pressure isothermal methanol reactors and the reactors' characteristics	17
3.3	Metal composition of catalysts provided by different manufacturers	19
3.4	Selection of CO ₂ -absorption processes and their operating conditions	22
3.5	Advantages and disadvantages of membrane separation	23
3.6	Critical point temperatures, molecular weights and molecule sizes	24
4.1	Values for the kinetic model of LHHW-type for equations 4.5 to 4.7 from Van den Bussche and Froment	32
4.2	Adjusted values for the Aspen Plus®-model of the reactor kinetics for equations 4.5 and 4.6 in the form of equation 4.10 and 4.11 respectively	33
4.3	Catalyst specifications from Chen <i>at al.</i>	34
4.4	Comparison of the product stream and the cooling water (CW) of the simulation (SIM) with the industrial data from Chen <i>at al.</i>	36
4.5	Estimated feed compositions and properties from de Lanthouder. The composition and flowrate are used for the first optimisation of the reactor and reactor unit	37
4.6	Conditions and sizes used for the optimisation of the MRU	37
4.7	Estimated feed compositions and properties from de Lanthouder as well as estimated compositions within the Solvent loop. The composition and flowrate are used for the first optimisation of CO ₂ -removal unit (CRU)	45
4.8	Base conditions and sizes used for the optimisation of the CRU for case 1 and case 2 respectively	45
4.9	Permeation rates for each component	52
4.10	Estimated feed compositions and properties from de Lanthouder. The composition and flowrate are used for the first optimisation of the membrane	52
5.1	Case overview	56

5.2	Operating variables for the operation similar to the first estimate by Lathouder	57
5.3	Characteristics of the processes from case 1 to 3	62
B.1	Stream summary for case 1: Methanol synthesis without hydrogen integration (part1) .	vi
B.2	Stream summary for case 1: Methanol synthesis without hydrogen integration (part2) .	vii
B.3	Stream summary for case 1: Methanol synthesis without hydrogen integration (part3) .	viii
B.4	Stream summary for case 2: Methanol synthesis with hydrogen integration (part1) . .	ix
B.5	Stream summary for case 2: Methanol synthesis with hydrogen integration (part2) . .	x
B.6	Stream summary for case 2: Methanol synthesis with hydrogen integration (part3) . .	xi
B.7	Stream summary for case 2: Methanol synthesis with hydrogen integration (part4) . .	xii
B.8	Stream summary for case 3: Methanol synthesis with hydrogen and CO ₂ integration (part1)	xiii
B.9	Stream summary for case 3: Methanol synthesis with hydrogen and CO ₂ integration (part2)	xiv
B.10	Stream summary for case 3: Methanol synthesis with hydrogen and CO ₂ integration (part3)	xv
B.11	Stream summary for case 3: Methanol synthesis with hydrogen and CO ₂ integration (part4)	xvi

Abbreviations

ARC	Advanced Reactor Concept	MDEA	methyldiethanolamine
BWR	boiling water reactor	MEA	monoethanolamine
CAPEX	capital expenditure	MeOH	methanol
CCS	carbon capture and storage	MOF	Metal-Organic Frameworks
CHP	combined heat and power	MR	mechanical ratio
CRU	CO ₂ -removal unit	MRU	methanol reactor unit
DEA	di-ethanol amine	MSU	methanol synthesis unit
DME	dimethyl ether	MTBE	methyl tert-butyl ether
DMT	dimethyl terephthalate	MTO	methanol-to-olefins
EIA	U.S. Energy Information Agency	MTP	methanol-to-propylene
GCR	gas-cooled reactor	MUG	make-up gas
HRU	H ₂ -recycle unit	PEG DME	Polyethylene Glycol Dimethyl Ether
HVO	hydro-treated vegetable oil	PSA	pressure swing adsorption
ICI	Imperial Chemical Industries	RWGS	reverse water-gas shift
IFP	Institut Français du Pétrole	SN	stoichiometric number
IGCC	integrated gasification combine cycle	TAME	tert-amyl methyl ether
LHHW	Langmuir-Hinshelwood-Hougen-Watson	TR	thermal ratio
LHV	lower heating value	TSA	temperature swing adsorption
LPM	low-pressure methanol	VSA	vacuum swing adsorption
		WGS	water-gas shift

Glossary

Aspen Plus®

Chemical process simulator and optimiser by AspenTechnology

Le Chatelier's Principle

If a dynamic equilibrium is disturbed by changing the conditions, the position of equilibrium moves to counteract the change

LPMEOH™

Liquid-phase technology for the production of methanol in a slurry reactor; Developed by Air Products

Rectisol®

Physical absorption process using chilled methanol

Selexol®

Physical absorption process using Polyethylene Glycol Dimethyl Ether

syngas

Syngas is a fuel gas mixture consisting primarily of hydrogen, carbon monoxide, and very often some carbon dioxide

Nomenclature

Sign	Name	Unit
<i>A</i>	area	m ²
<i>a</i>	dimensionless constant	-
<i>b</i>	dimensionless constant	-
<i>c</i>	molar concentration	kmol m ⁻³
<i>D</i>	diffusivity	m ² s ⁻¹
<i>d</i>	molecular diameter	m
<i>D_p</i>	particle diameter	m
<i>f^o</i>	adsorbed phase fugacity for pure component	Pa
<i>f</i>	constant depending on polymer	J mol ⁻¹
<i>f^A</i>	adsorbed phase fugacity	Pa
<i>f^G</i>	gas phase fugacity	Pa
<i>J</i>	molar flux	kmol s ⁻¹ m ⁻²
<i>K_{a/b/c}</i>	adsorption constant	- or Pa ⁿ
<i>k</i>	kinetic pre-factor for reaction rate	kmol kg ⁻¹ s ⁻¹ driving force ⁻¹
<i>k</i>	scaling factor	Pa
<i>k</i>	solubility coefficient	kmol m ⁻³ Pa ⁻¹
<i>K_p</i>	equilibrium constant for partial pressure	Pa or Pa ²
<i>LHV</i>	lower heating value	MJ kg ⁻¹
<i>M</i>	molar flow through membrane	kmol s ⁻¹
<i>ṁ</i>	mass flow	kg h ⁻¹
<i>MR</i>	mechanical ratio	kW _P kW _{ch} ⁻¹
<i>N</i>	molar flow on feed/retentate side	kmol s ⁻¹
<i>ṅ</i>	molar flowrate	kmol h ⁻¹
<i>n</i>	slope	-
<i>O</i>	molar flow on permeate side	kmol s ⁻¹
<i>P</i>	permeability	mol m ⁻¹ s ⁻¹ Pa ⁻¹
<i>P</i>	power	kW
<i>P</i>	pressure	Pa
<i>p</i>	partial pressure	Pa
<i>Q</i>	cooling duty	kW
<i>R</i>	permeation rate	kmol m ⁻² s ⁻¹ Pa ⁻¹
<i>r</i>	reaction rate	mol kg ⁻¹ s ⁻¹
<i>RR</i>	recycle ratio	-
<i>S</i>	solubility	mol m ³ Pa ⁻¹
<i>SN</i>	stoichiometric number	-
<i>T</i>	temperature	°C
<i>TR</i>	thermal ratio	kW _Q kW _{ch} ⁻¹
<i>U</i>	superficial velocity	m s ⁻¹
<i>m</i>	distance through membrane	m
<i>x</i>	mole fraction in adsorbed phase	-
<i>y</i>	mole fraction in vapour phase	-
<i>z</i>	reactor length	m
<i>α</i>	selectivity	-
<i>ε</i>	void fraction	-
<i>η</i>	system efficiency	-
<i>η_{CO2}</i>	CO ₂ removal efficiency	kJ mol ⁻¹
<i>γ</i>	adsorbed phase activity coefficient	-

Sign	Name	Unit
μ	fluid viscosity	Pa s
ϕ_i^G	fugacity coefficient of component i in the vapour phase	-
ϕ_s	particle shape factor	-
Π	pressure of adsorbed solution	N m^{-1}
π	pressure of system	Pa
ρ	density	kg m^{-3}

Index	Name
H ₂ prod	produced hydrogen
i	component i
i	more permeable gas
j	less permeable gas
MeOH	methanol
P	power
Q	cooling
RWGS	reverse water-gas shift

1

Introduction

In the face of global warming associated climate change the biggest challenge is to continue being able to cover the global energy need while simultaneously reducing the emission of greenhouse gases and reducing the dependency on fossil fuels as decided upon in the Paris Agreement [1]. This problem is exacerbated by the predicted¹ increase of the global energy demand (figure 1.1). To accomplish the goals set by the Paris Agreement, a move towards renewable energy sources needs to happen. Renewable energy sources are defined through their ability to naturally replenish within the human timeframe and their carbon neutral transformation into useable energy. These energy sources include solar, wind, hydropower, biomass and geothermal energy. They can be used to provide different forms of energy for the end-user: electricity, heat and fuels.

Of these energy sources hydro, wind and solar energy have the highest installed capacity for power

¹The U.S. Energy Information Agency (EIA) uses their *IEO2016 Reference case* to project the energy demand, sources and emissions for up to 2040. The reference case "assumes known technologies and technological and demographic trends, generally reflects the effects of current policies, and does not anticipate new policies that have not been announced" [2].

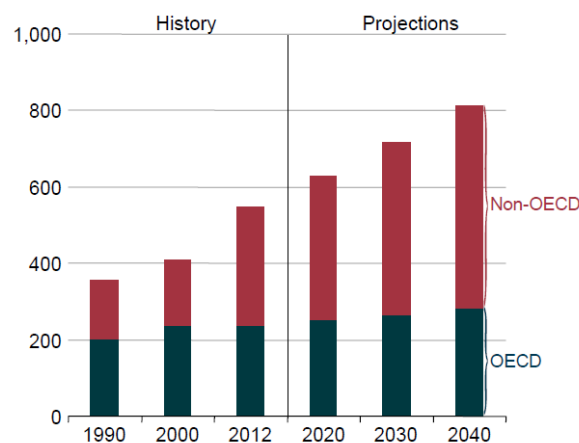


Figure 1.1: Global Energy Demand in quadrillion BTU, 1990-2040 (1 quadrillion BTU = 293.1 TWh) [2]

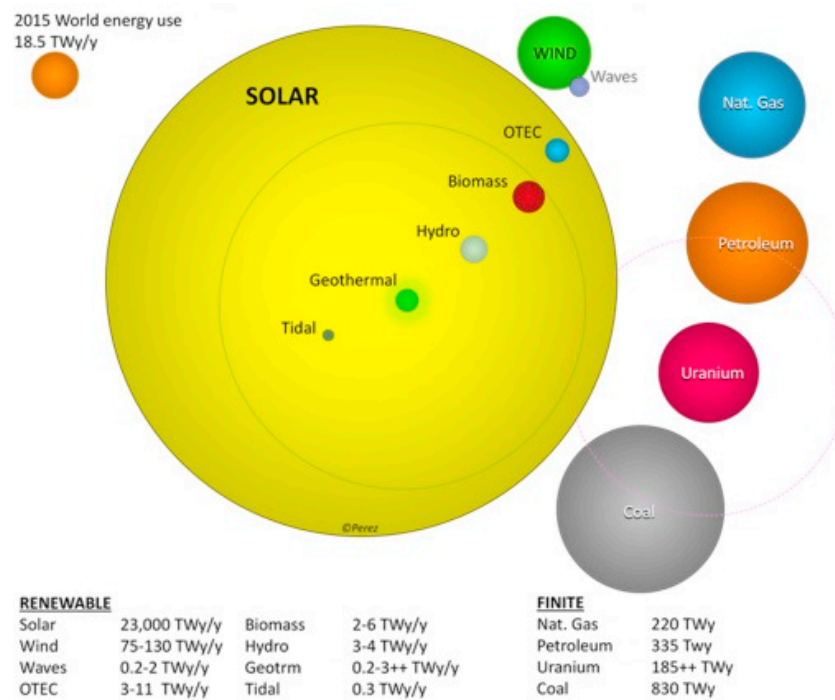


Figure 1.2: Comparing the energy resources of the planet: renewable resources are shown with their yearly value, finite resource with their total value (adapted from Perez and Perez [4]).

generation [3]. Figure 1.2 illustrates the energy resources available for each primary energy source. The renewable sources are presented with their yearly quantity while the finite resources are shown with their total quantity. It shows that for the renewable resources solar has by far the largest supply quantity and both solar and wind energy could cover the world's total energy demand by themselves. However, both wind and solar energy are highly variable and depend on the season, the time of the day and the weather. This non-controllable variance in the available energy can be combated on two fronts. On one side, storage technologies can work as a bridge to overlap the production and demand curve. On the other side, other energy resources, which are more constant and dispatchable, can be added to the energy mix to cover the gap between production and demand.

One possible energy source is biomass. It is available nearly everywhere and can be stored and used when necessary. However, one of the bigger challenges of biomass is the low energy density and the decentralised production. Due to these two factors supply of biomass is relatively inefficient and often over long distances [5, 6]. The energy stored in biomass can be directly transformed into heat or it can be processed first to create more energy dense products like liquid fuels.

One such liquid fuel is methanol. Methanol is a simple alcohol with the formula CH_3OH . It has many uses, such as fuel for combustion to generate heat and/or electrical energy, fuel for vehicles and as solvent and feedstock for the generation of other chemicals. In 2015 the total demand of methanol was 70 Mt [7]. The different areas of demand are shown in figure 1.3. Of these, methanol-to-olefins (MTO) and formaldehyde are the most common products.

The production of methanol is well established. It became more prominent in the 1960s when Imperial Chemical Industries (ICI) developed a low-pressure methanol (LPM) process that allowed for mild reaction conditions [9]. For this process the feed for the reactor is syngas, a gas consisting of carbon

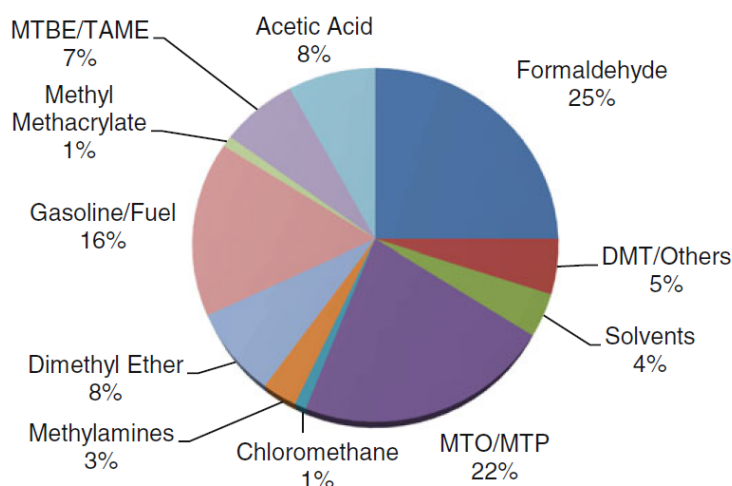


Figure 1.3: Methanol Demands and End Use. DMT: dimethyl terephthalate, MTBE/TAME: methyl tert-butyl ether/tert-amyl methyl ether, MTO: methanol-to-olefins, MTP: methanol-to-propylene [8]

dioxide (CO_2), carbon monoxide (CO) and hydrogen (H_2). Syngas can be produced from different feedstocks. The main feedstock is natural gas. Natural gas can be converted to become syngas through steam reforming and/or autothermal reforming and through partial oxidation. However other sources such as coal, higher hydrocarbons and biomass can be used as well [9].

Using biomass as the feedstock for syngas has various advantages. The main advantage is the potentially carbon-neutral product, as the carbon stored in biomass has been captured from the air. Some main disadvantages are in the many cleaning steps that are required to avoid poisoning of the catalysts, the storage of the biomass before processing and the transport of the biomass to the production plants. The disadvantage of transportation comes from the biomass' low energy density and long transport paths before it arrives at the production plant. One solution is a pre-treatment closer to the area where the biomass is sourced. This pre-treatment increases the energy density and thus reduces the amount of fuel needed for transportation.

This thesis explores a small production plant developed by de Lathouder [10]. The plant is transportable and allows for an installation in a factory hall and a quick set up at the production site. This targets the transportation problem as it moves the plant to the source of the biomass. It is envisioned to produce $50 \text{ t}_{\text{MeOH}} \text{ d}^{-1}$ from an input of 5 t d^{-1} of dry biomass. The source for the biomass in this study is lignocellulosic biomass such as woody waste from agriculture and forestry with the overall formula $\text{CH}_{1.17}\text{O}_{0.7}$ and a lower heating value (LHV) of 18.0 MJ kg^{-1} .

The plant consists of a fluidised bed gasification, gas cleaning, hydrogen recycle, CO_2 -removal, methanol conversion and distillation of the product (see figure 1.4). To build such a small plant a review and analysis of the technologies used needs to be conducted. This thesis focuses on the downstream production of methanol starting after the cleaning of the syngas and ending before the distillation.

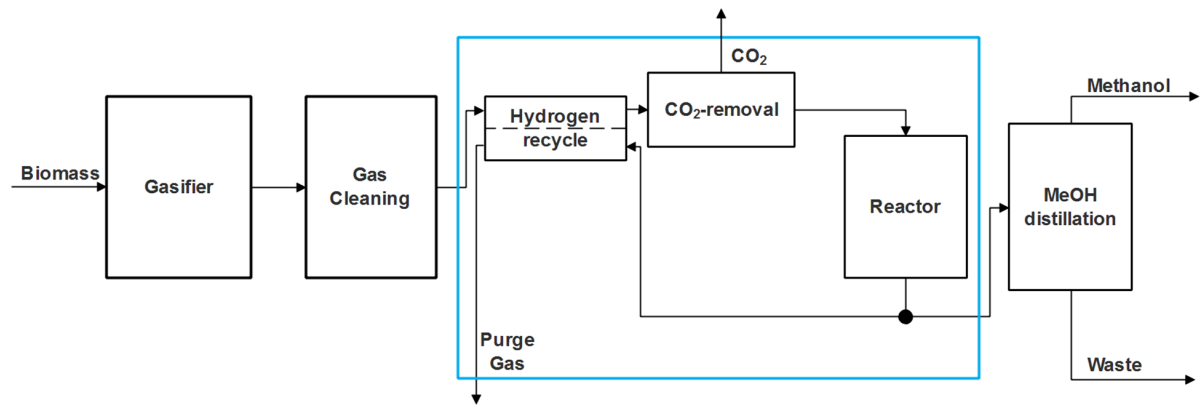


Figure 1.4: Scheme of a methanol production plant. The elements of focus of this thesis are within the blue frame.

1.1. Research Questions

The aim of this thesis is to answer two questions and their subquestions about the process:

1. What are the best reactor and separation technologies and optimal operation conditions for the production of methanol in a small-scale transportable process plant with an estimated daily production of $50 \text{ t}_{\text{MeOH}} \text{ d}^{-1}$?
 - (a) Is the obtainable production volume within the desired range?
 - (b) Given that the raw product stream still has to be distilled, how do the operation conditions of the process influence the quality of the product?
2. How can the integration of hydrogen supply improve the process yield and how does it influence the design of the process?

1.2. Structure of the Thesis

To answer the research questions this thesis will first give background information on the synthesis of methanol from syngas, biomass as a feedstock for methanol synthesis and hydrogen production in fuelcells in chapter 2. This theoretical background is followed in chapter 3 by a literature review of the current state of the art technologies available for each unit of the process. Subsequently, in chapter 4, the process units are modelled in Aspen Plus[®] and analysed for their behaviours at different conditions.

After generating a model for the process, it will be evaluated in chapter 5 for the questions posed by this thesis. For this, three different cases are assessed to find feasible operation conditions and equipment sizes.

Finally, the thesis will conclude in chapter 6 by answering the research question and giving recommendations for future research.

2

Theoretical Background

This chapter will give the background information necessary for the building of the model and understanding of the individual process units' working principles. First, biomass as a feedstock for the synthesis of methanol is introduced with all the significant steps for the production of syngas. Following the production of syngas, the actual kinetics of the formation of methanol are explained. Finally, the production of hydrogen by means of water electrolysis for the additional integration into the process is detailed.

2.1. Biomass as Energy-Feedstock for Methanol Synthesis

The biomass used for gasification is usually dry and solid. This biomass could also be used for direct combustion with steam generation which can be integrated in a combined heat and power (CHP) plant. The sources of the globally produced biomass are presented in table 2.1. In 2013, a total of 57.7 EJ of biomass was supplied as primary energy, of this 82 % was delivered as final energy. Most biomass energy is consumed in the residential sector (74 %) followed by the industries (17 %) and the transport sector (5.7 %) [11].

2.1.1. Gasification

Gasification is the process of converting a liquid or solid feed into a gas or vapour phase and a solid phase. In the following, an overview of the process will be given, for more detailed information see Basu *et al.* [12]. The process of biomass gasification consists of four main steps. These steps are:

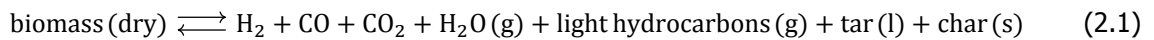
1. Drying
2. Pyrolysis
3. Oxidation
4. Reduction

Table 2.1: Overview of energy-related biomass supply sources globally (2013) [11]

Sector	Fuel	Share	
Forestry	Fuelwood	68 %	88 %
	Pellets	0.8 %	
	Charcoal	10 %	
	Forest residues	1.8 %	
	Black liquor	6.8 %	
	Wood industry residues	0.8 %	
Agriculture	Bioethanol from crops	4.0 %	9 %
	Biodiesel from crops	2.1 %	
	Hydro-treated vegetable oil (HVO)	0.3 %	
	Biogas from crops/animal	2.6 %	
Waste	Municipal waste	2.6 %	3 %

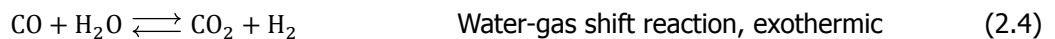
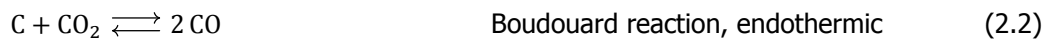
Drying: In the drying process the water in the moist fuel is evaporated to produce dry fuel. The higher the moisture content the higher the heat requirement of the gasification process.

Pyrolysis: This step is the thermochemical decomposition of the dry fuel at temperatures between 250 °C and 700 °C. During this decomposition the biomass is converted into gases, liquids and solids as presented in equation 2.1.



Oxidation: This step is exothermic and provides the heat for the other steps which are all endothermic. The fuel for the oxidation can come from the gasification itself by providing char or hydrogen from the converted biomass. The products of this stage are mainly CO₂, CO and water. If air is used for the oxidation, then nitrogen will be present in the product gas.

Reduction: The solid and gaseous products from the oxidation and pyrolysis are mixed and react together to form more syngas. The most common reactions are listed in equations 2.2 to 2.5.



These reactions result in a globally endothermic process step. In addition, the temperature of the process determines the composition of the product. A higher temperature increases the conversion of char and reduces the formation of tars, a lower temperature increases the energy content of the syngas and lowers the risk of ash sintering in the process. Figure 2.1 depicts the effect of temperature on the product. The current processes for gasification are designed for temperatures between 800 °C and 1100 °C, however temperatures between 500 °C and 1600 °C are possible if oxygen instead of air is used for the oxidation step [13].

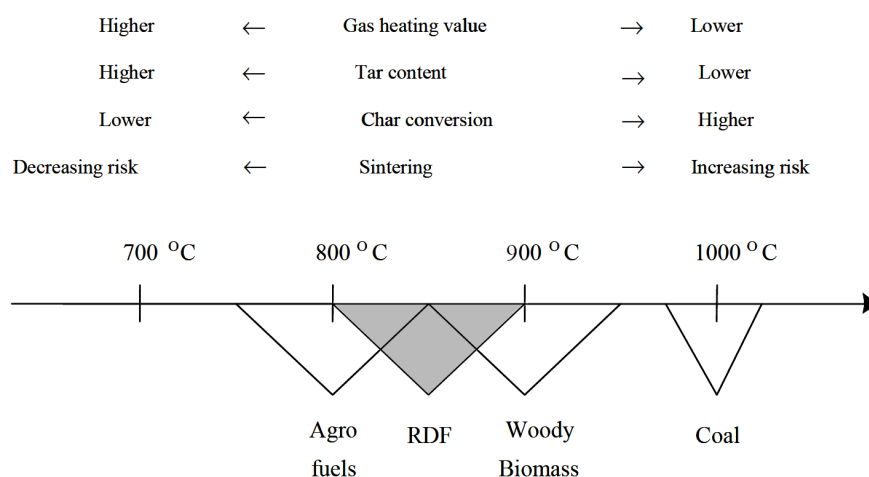


Figure 2.1: Effect of the reduction temperature on the product with the operating ranges for different fuels: agro fuels, refuse-derived fuels (RDF), woody biomass and coal. [14]

2.1.2. Impurities and Cleaning of Bio-Syngas

Additionally to the tars and nitrogen species mentioned in the previous section, other impurities are present in the output gas from the gasifier. These include ash, particles from un-reduced char as well as inert materials from the fuel, and unwanted gaseous byproducts from the reaction. These byproducts can be NH_3 and inorganic acid gases, like H_2S and HCl . As these impurities can affect the downstream processes they are usually removed. There are different technologies for the cleaning of syngas. At hot temperatures 'dry' processes are used as opposed to 'wet' processes at lower temperatures.

The removal of particulates is performed through various techniques based on inertial separation, barrier filtration and/or electrostatic interaction for hot gas temperatures and wet-scrubbing for lower temperatures. The removal of tars is usually combined with the particulate removal at low temperatures due to their condensation. High temperatures not only allow for physical removal, but also thermal or catalytic cracking of the tars. The other compounds can be removed through absorption or adsorption [15]. These principles are discussed in more detail in section 3.2.

2.1.3. Uses of Syngas

There is a wide variety of uses for syngas and syngas derived products. Next to the combustion to generate heat and electricity in a CHP plant, syngas can be converted into other chemicals. Figure 2.2 depicts a selection of chemicals derived from syngas and their conversion paths and catalysts.

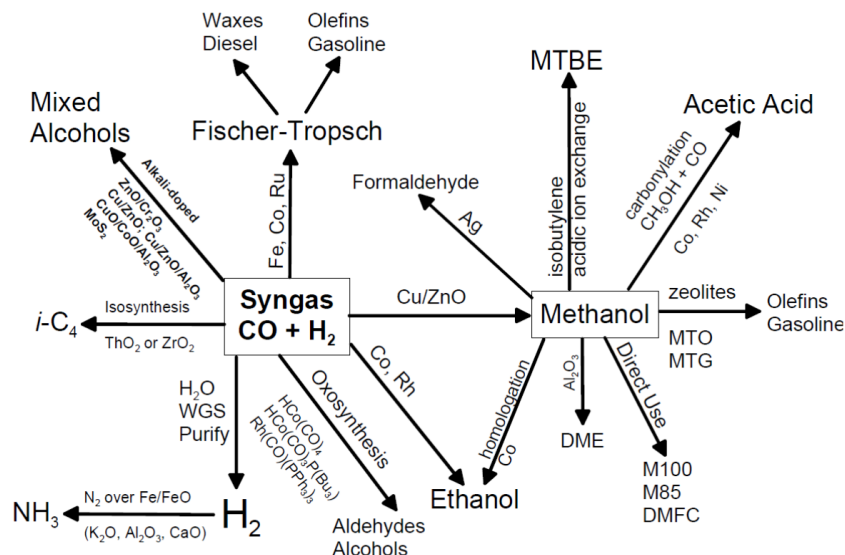


Figure 2.2: Examples of uses of syngas and methanol and their conversion catalysts [16]

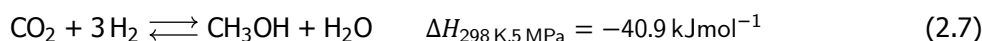
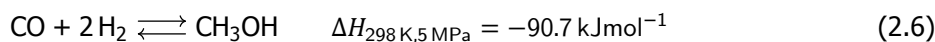
2.2. Methanol Production

Methanol is an important feedstock for the chemical industry as well as the future energy and fuel industry. The current globally installed production capacity of methanol is around 110 billion metric tonnes per year [7] to meet the demand of 70 billion metric tonnes. At the moment nearly all methanol is produced from natural gas through reforming and catalytic conversion. However, the use of biomass and other feedstock for syngas generation is being researched and implemented. The change of feedstock is supported by the similarity of syngas produced from natural gas and from other feedstock.

2.2.1. Methanol Synthesis from Syngas

The prevailing technology for producing methanol is the low-pressure catalytic reaction of syngas. The low pressure allows for operating conditions which favour the conversion of methanol and nearly completely inhibit the production of by-products. This leads to a high selectivity of > 99 % [16]. The most common catalyst used in low-pressure methanol production is a Copper-Zinc Oxide catalyst with Aluminium Oxide or Chromium(III) Oxide (Cu–ZnO–Al₂O₃/Cu–ZnO–Cr₂O₃).

The reactions relevant for the production of methanol have been known for long. Carbon dioxide and carbon monoxide can react with hydrogen to form methanol with water as a side-product. Equations 2.6 and 2.7 show the stoichiometry of these reactions and their reaction enthalpy [17].



As these reactions are exothermic and lead to a decrease of the amount of molecules present, the productivity can be increased by increasing pressure and reducing temperature, according to Le Chatelier's Principle. Resulting from the reactions' stoichiometries, the stoichiometric number (SN) for the compos-

ition of the feed is derived (see eq. 2.8). For the synthesis of methanol the ideal value of SN is slightly above two, indicating an excess of hydrogen [9].

$$SN = \frac{[H_2] - [CO_2]}{[CO] + [CO_2]} \quad (2.8)$$

Next to the two methanol producing reactions, the water-gas shift (WGS) reaction takes place.



As the WGS reaction connects equation 2.6 and 2.7, only two of these three reactions are stoichiometrically independent and need to be considered for the overall reaction. In literature the opinions whether the methanol is formed due to CO-hydrogenation or CO₂-hydrogenation differ and so do the calculations for the reaction rates.

There are a lot of studies focused on determining the kinetics of the formation of methanol from syngas. Graaf *et al.* [18] studied the chemical equilibrium for the process and determined that the behaviour of the non-ideal gas mixture is best predicted by the Soave-Redlich-Kwong equation of state. Additionally, the equilibrium constants based on partial pressures were calculated for the hydrogenation of CO and for the reverse water-gas shift (RWGS) reaction. The values are as follows:

$$\log_{10} K_{pCO} = \frac{5139}{T} - 12.621 \quad (2.10)$$

$$\log_{10} K_{pRWGS} = \frac{-2073}{T} + 2.029 \quad (2.11)$$

where K_{pCO} = equilibrium constant for the hydrogenation of CO [bar⁻²]

K_{pRWGS} = equilibrium constant for the RWGS reaction [-]

In a later study Graaf *et al.* [19] developed a kinetic model and compared it to models from literature. Similar to previous studies their model is based on the dual-site Langmuir-Hinshelwood mechanism: CO and CO₂ are absorbed on one site while H₂ and H₂O are absorbed on the other site.

Skrzypek *et al.* [20, 21] published kinetics and thermodynamics of LPM synthesis on a CuO/ZnO/Al₂O₃-catalyst based on the hydrogenation of CO₂. In their experiments they determined that syngas consisting only of CO and H₂ without any CO₂ or H₂O does not produce methanol. This indicates that methanol is formed from CO after WGS reaction and subsequent hydrogenation of CO₂.

Van den Bussche and Froment [22] determined the values for their steady-state kinetic model based on the same dual-site approach as Graaf *et al.* [18, 19]. In their model, methanol is formed through hydrogenation of CO₂ and the RWGS reaction on a Cu/ZnO/Al₂O₃-catalyst. This model was derived from literature and experimental work. In their approach they use the equilibrium constants from Graaf *et al.* [18] and conducted experiments to determine the remaining parameters for the kinetics.

The experimental data was gathered at feed temperatures between 180 °C and 280 °C, pressures of 15 bar to 51 bar, and a feed ratio of p_{CO}/p_{CO_2} from 0 to 4.1.

Several studies based their reactor calculations on the model of Van den Bussche and Froment [22] and received comparable results to industrial processes [23, 24]. While Van den Bussche and Froment

[22] validated their values for an adiabatic reactor, Chen *et al.* [23] used the model for an isothermal reactor and Luyben [24] used a reactor with cooling.

Mignard and Pritchard [25] adjusted the activation energy of reaction 2.7 and 2.9 from Van den Bussche and Froment [22] to match the results at lower temperatures from Klier *et al.* [26] and reactions at pressures up to 71 bar. The adjustments are kept within the confidence interval set by Van den Bussche and Froment [22]. This change does not change the composition of the equilibrium but it does alter the rate of the reactions as well as the composition of the gas inside the reactor until it reaches the equilibrium. Due to a shortage of literature based on Mignard and Pritchard [25]’s kinetics, the more established kinetics by Van den Bussche and Froment [22] will be used within this thesis.

Reactor types which are used to produce methanol are listed in chapter 3.1.

2.3. Hydrogen Production through Electrolysis

The integration of hydrogen supply into the proposed process is possible through various technologies. The most reasonable path for the utilisation of electricity is electrolysis. Other sources for hydrogen are fossil fuel processing or biological hydrogen from algae, fermentation and other biological processes [27]. However, electrolysis is the only process where electricity is transformed into hydrogen with only clean water as the feed. The basic reaction behind electrolysis is presented in equation 2.12. The minimum energy required changes depending on the temperature of the process. Figure 2.3 shows the change in minimum required energy for temperatures from 0 °C to 1200 °C. As the temperature rises, less electrical energy is required and more thermal energy is needed.



Electrolysis works on the principle of an electric DC current passing through two electrodes and splitting water into hydrogen and oxygen. The two electrodes are separated by a membrane which only allows one kind of ion to pass. Which ion travels through the diaphragm depends on the technology used. Table 2.2 gives an overview of the three most common hydrogen electrolysis technologies. For the combination of renewable energies with hydrogen production, the proton exchange membrane electrolyser is the best option. It reacts quickly and fluctuations effect the electrolyte very little [29]. However, it has a high investment cost compared to alkaline electrolysers and are still in the development phase [27].

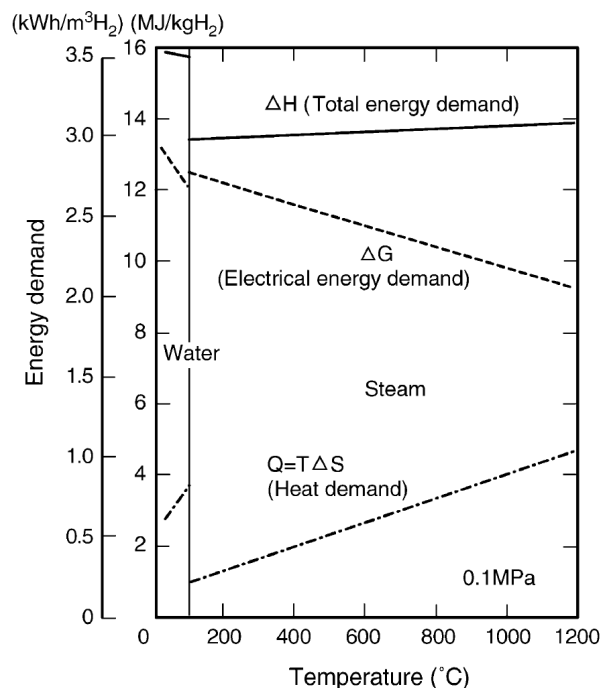


Figure 2.3: Energy demand for water and steam electrolysis at 10 bar [28]

Table 2.2: Electrolysers and their characteristics

	AE	PEM	SOEC
Full name	alkaline electrolyser	proton exchange membrane electrolyser	solid oxide electrolysis cells
Electrolyte	aqueous alkaline electrolyte ≈ 30 wt% KOH or NaOH	solid polymeric membrane	solid ceramic membrane (yttria-stabilized zirconia (YSZ))
Electrode material	nickel with coating	noble metals	cathode: cermet of YSZ and nickel anode: composite of perovskites and YSZ
Anode reaction	$4\text{OH}^- \longrightarrow \text{O}_2 + 2\text{H}_2\text{O} + 4\text{e}^-$	$2\text{H}_2\text{O} \longrightarrow \text{O}_2 + 4\text{H}^+ + 4\text{e}^-$	$\text{O}^{2-} \longrightarrow \frac{1}{2}\text{O}_2 + 2\text{e}^-$
Cathode reaction	$2\text{H}_2\text{O} + 2\text{e}^- \longrightarrow \text{H}_2 + 2\text{OH}^-$	$4\text{H}^+ + 4\text{e}^- \longrightarrow 2\text{H}_2$	$\text{H}_2\text{O} + 2\text{e}^- \longrightarrow \text{H}_2 + \text{O}^{2-}$
Charge carrier	OH^-	H^+	O^{2-}
Temperature	$< 100^\circ\text{C}$	$< 80^\circ\text{C}$	600 to 900°C
Pressure	ambient	up to 85 bar	-
Efficiency	50 to 60 %	55 to 70 %	between 40 and 60 %
Max. purity	99.9 %	99.999 %	n/a
Response time	slow	fast	slow (heat up)
Implementation stage	commercial	demonstration	R&D
Source	[27, 29]	[27, 30, 31]	[27, 30, 32]

3

State of the Art Methanol Reactor and Process Technology

The investigated unit operations in this report can be implemented with different technologies and set-ups. Within this chapter the most common and established technologies for these unit operations are discussed. More experimental technologies that are only in the research and development phase are mentioned but not considered for the final process definition.

3.1. Low-Pressure Methanol Synthesis Reactor

For the methanol synthesis two main reactor types are being used: adiabatic reactors or cooled reactors. They differ in how they control the developed heat [33, 34]. The temperature within the reactor influences the conversion (rate) profile, the production of unwanted byproducts and the recycle rate. A recycle of the non-reacted gas is necessary as the equilibrium conversion of the reaction is very low. In commercial plants, the per-pass conversion of methanol is limited to 25 %. However, a conversion of up to 80 % can be achieved with ideal compositions and processes [9, 35].

There are three parameters that describe the reactor's performance (eq. 3.1 to 3.3) [36]. Assuming that the CO_2 is the main source of carbon in the conversion to methanol, the stoichiometric factor of hydrogen is taken as 3 from equation 2.7. The base of the parameters is hydrogen, as it is the limiting component of the process.

$$\text{Conversion} = \frac{\dot{n}_{\text{H}_2, \text{in}} - \dot{n}_{\text{H}_2, \text{out}}}{\dot{n}_{\text{H}_2, \text{in}}} \quad (3.1)$$

$$\text{Selectivity} = \frac{\dot{n}_{\text{MeOH}, \text{out}} - \dot{n}_{\text{MeOH}, \text{in}}}{(\dot{n}_{\text{H}_2, \text{in}} - \dot{n}_{\text{H}_2, \text{out}})} \times 3 \quad (3.2)$$

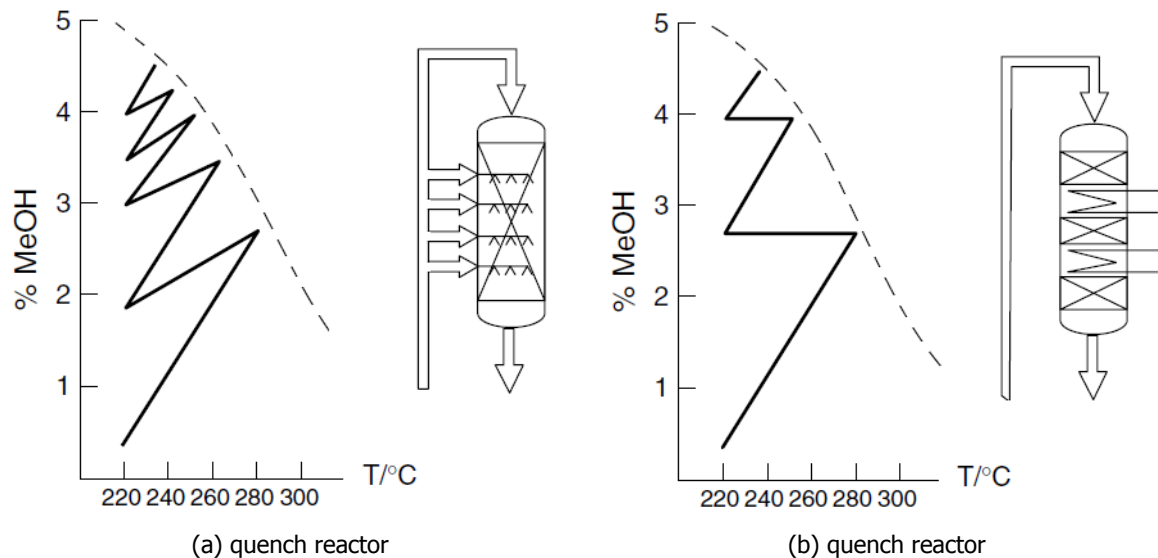


Figure 3.1: Conversion profiles (solid line), equilibrium curves (dashed line) and schematics of methanol reactors [17]. In the quench reactor cold feed is introduced into the reactor reducing the temperature but also the methanol fraction. In the adiabatic reactor the feed is cooled so the temperature is reduced but the fraction remains constant in the cooler

$$\text{Reactor yield} = \frac{\dot{n}_{\text{MeOH},\text{out}} - \dot{n}_{\text{MeOH},\text{in}}}{(\dot{n}_{\text{H}_2,\text{in}})} \times 3 \quad (3.3)$$

As the WGS reaction and the methanol reaction are exothermic, a high reactor temperature leads to a lower methanol fraction in the chemical equilibrium. This in turn means that the gas has to be recycled more often than for lower reactor temperatures, increasing the recycling ratio. The advantages of the low-pressure methanol technology, besides the lower energy requirements for the compressors and equipment, is the high selectivity of methanol. It is produced with a selectivity of above 99 % with very few by-products [16]. These by-products include formaldehyde, formic acid, ethers (such as dimethyl ether (DME)), ketones and others due to CO-hydrogenation [37, 38].

3.1.1. Adiabatic Reactors

Adiabatic reactors are characterised by not having an external cooling system within their reaction zone. There are different types of adiabatic reactors. Quench reactors cool the reaction gas by adding cold reaction gas throughout the reactor. Other reactors are a series of smaller catalyst beds with intermediate cooling. The general design of a quench reactor is shown in figure 3.1a. The conversion profile shows the injection points of the quench gas at which the temperature of the gas decreases but also the methanol fraction. In comparison, the reactor with intermediate cooling only reduces the temperature while keeping the methanol fraction constant, figure 3.1b.

The problem of adiabatic reactors is the temperature levels within the reactors. High temperatures can develop, which leads to a reduction in production and shortening of the catalyst's lifetime due to sintering (see section 3.1.4). The traditional flow direction of these reactors is axial, which leads to a very simple design but results in relatively large pressure drops or large vessel diameters, as small diameters cause high gas velocities. Larger diameters result in high material costs so different companies have developed radial flow reactors which exhibit low pressure drops, can easily be scaled

but require more complicated designs and are thus more expensive.

This more complicated design stands in contrast to the advantages of adiabatic reactors of having an easy design, easy operation and low cost. Adiabatic reactors are mostly applied for smaller scales, e.g. the adiabatic reactor by Johnson Matthews produces up to 3000 t d^{-1} [33, 34]. Table 3.1 gives an overview of the most commonly used methanol reactors and their producers.

3.1.2. Isothermal Reactors

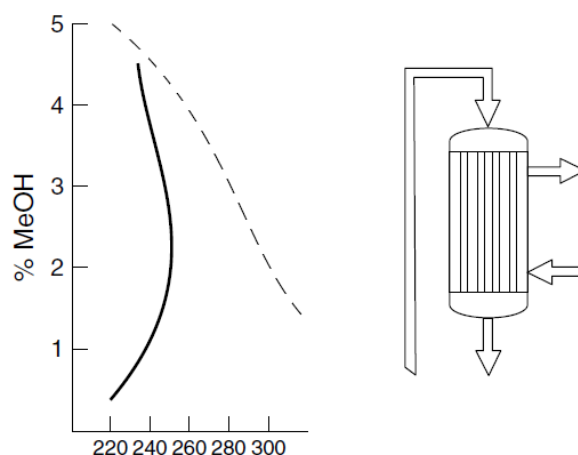


Figure 3.2: Conversion profile (solid line), equilibrium curve (dashed line) and schematic for an isothermal reactor with indirect cooling [17]

The aim of isothermal reactors is to keep the temperature constant at a low level through cooling, realising a quasi-isothermal process. In contrast to the adiabatic reactors, isothermal reactors do this by cooling the reactor, catalyst and reaction gas. The cooling is done indirectly to not dilute the reaction gas. The two most common cooling technologies are gas-cooling (gas-cooled reactor (GCR)) and cooling through steam generation (boiling water reactor (BWR)). The advantages of these technologies are the longer lifetime of the catalyst, the higher yield due to the methanol-favouring equilibrium, and the energy recovery in the coolant. Figure 3.2 shows an example of the methanol production within an isothermal reactor. In comparison to the other two reactors shown in figure 3.1, the gas within the isothermal reactor never reaches high temperatures.

The main technologies used in plants are licensed by Lurgi (27%), Johnson Matthew/Davy (25%) and Haldor Topsøe (16%) [33]

3.1.3. Other Reactor Types

Next to the adiabatic and isothermal reactors, research is being conducted into other new technologies. Of these, the two most promising are the liquid-phase reactors and membrane reactors.

The LPMEOH™, a slurry reactor developed by Air Products, is a good example of liquid-phase reactors. The reactor has catalyst particles suspended in inert mineral oil. The feed gas is bubbled through the oil where it reacts on the catalyst surface. The advantage of the reactor is the high tolerance for

Table 3.1: List of producers of low-pressure adiabatic methanol reactors and the reactors' characteristics

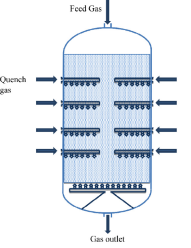
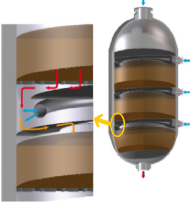

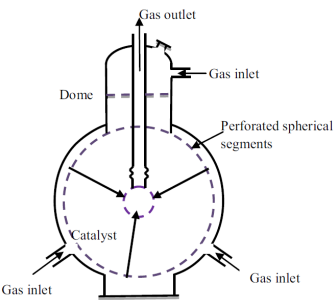
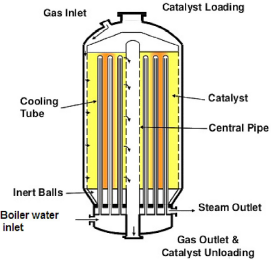
Company	Specifics	Source
Johnson Matthey/ Process Davy Technology	<ul style="list-style-type: none"> • 50 to 100 bar • 270 °C • quench reactor • flow in axial or radial direction • axial direction: simple but large • radial direction: complicated internal design but compact • for small scale applications 	[33, 34]
		
Casale and ICI	<ul style="list-style-type: none"> • similar to Johnson Matthey/ Davy Process Technology reactor • improved quench gas redistribution • separated catalyst beds • methanol production capacity increased by 20 % 	[34]
		
Haldor Topsøe	<ul style="list-style-type: none"> • Collect-Mix-Distribute reactor • quench reactor • radial flow through catalyst bed, axial flow to quench • catalyst beds arranged plates and separated by vertical support beams • increased conversion and better temperature control 	[33, 34, 39]
		
Kellogg, Brown and Root	<ul style="list-style-type: none"> • series of adiabatic reactors with intermediate cooling • spherical shape • gas enters from outside towards inner shell • catalyst loaded around inner shell • thin external walls possible → low cost of transport and manufacture 	[34]
		
Toyo Engineering Company	<ul style="list-style-type: none"> • radial flow with concentric catalyst beds • intermediate cooling • boiling water cooling • good temperature control • catalyst bed 30 % smaller than conventional quench reactors • good heat recovery • low pressured drop independent of reactor height • easy scale-up by increasing reactor height 	[34, 40, 41]
		

Table 3.2: List of producers of low-pressure isothermal methanol reactors and the reactors' characteristics

Company	Specifics	Sources
Linde	<ul style="list-style-type: none"> axial flow of gas indirect cooling helical cooling tubes inside catalyst bed no axial temperature variations → avoids stresses 	[34, 42]
Lurgi	single-stage: <ul style="list-style-type: none"> single indirectly cooled reactor boiling water reactor (BWR) shell and tube with catalyst on the tube side methanol yield: $1.8 \text{ kg}_{\text{MeOH}} \text{ l}_{\text{catalyst}}^{-1}$ 	[34, 43]
	MegaMethanol: <ul style="list-style-type: none"> two reactors: the simple BWR and a gas-cooled reactor (GCR) cooling gas of the GCR is the unreacted syngas → only a small preheater required GCR is a shell and tube with catalyst on shell side due to the second reactor the BWR can be smaller high conversion efficiency → half the recycle ratio as single stage BWR lower investment costs through smaller BWR, discarded large pre-heater and generally smaller equipment due to lower recycle ratio designed for large-scale processes 	[34, 43, 44]
Mitsubishi Heavy Industries	<ul style="list-style-type: none"> double-walled tube and shell reactor combined GCR and BWR feed-gas as coolant in the inner tube boiling water as coolant on the shellside reaction between inner and outer tube 	[33, 34]

CO and low H₂/CO ratios, making it a good choice for coal derived-syngas which is high in CO [45]. The reactor is still at the laboratory stage of development due to modelling and scaling-up issues. It, therefore requires more studying [34].

Membrane reactors are being investigated as a possibility to increase the methanol yield by removing the product (MeOH and H₂O) from the reacting gas. The possibility to remove water from the reaction by using a silica/alumina composite membrane reactor has been investigated by Sea and Lee [46]. They showed that using a membrane reactor can improve the methanol yield by up to 1.5 times compared to a traditional reactor. Similarly, Gallucci *et al.* [47] showed the influence of temperature on the production rate of a zeolite membrane reactor which utilises a sorption-enhanced equilibrium to improve the yield. Compared with the operation of a traditional reactor at the same conditions, an increase in methanol-selectivity as well as CO₂-conversion was observed for all temperatures. However, this research found no industrial scale implementation or experience.

3.1.4. Catalysts

Through the development of a copper-zinc catalyst, that is made thermally stable due to the support structure of alumina, ICI was able to produce methanol at pressures around 5 MPa. This catalyst has now been adapted by a lot of companies with different atomic ratios of the metal components (see table 3.3).

The catalysts have a strong vulnerability towards poisoning due to the susceptibility of copper. They are especially susceptible to sulphur and chlorine compounds. While the addition of ZnO reduces the sensitivity of the catalyst towards sulphur, the amount of sulphur species in the gas is limited to 0.5 ppmv. A concentration of above 0.8 wt% of sulphur on the catalyst deactivates it completely [16, 37]. This limit excludes COS which does not poison the catalyst for concentration of 0.6-9 ppm in its gas state. The catalysts show no COS adsorption or dissociation at operation conditions for methanol formation [16]. The limit of chlorine species content, in any form, is of the order of magnitude of 1 ppb, as it deactivates the catalyst by strongly reacting with copper and additionally increasing the sulphur poisoning [48].

Next to sulphur and chlorine compounds, liquid water can lead to premature deactivation of the catalyst as it quickens the growth of copper crystals and destroys the catalyst's matrix. This water can come from high CO₂ content in the feed gas and the resulting RWGS reaction [37].

Next to the poisoning of the catalyst, sintering of the copper, which leads to the formation of copper crystals, can lead to deactivation. A maximum operating temperature of 300 °C is considered to be acceptable [16].

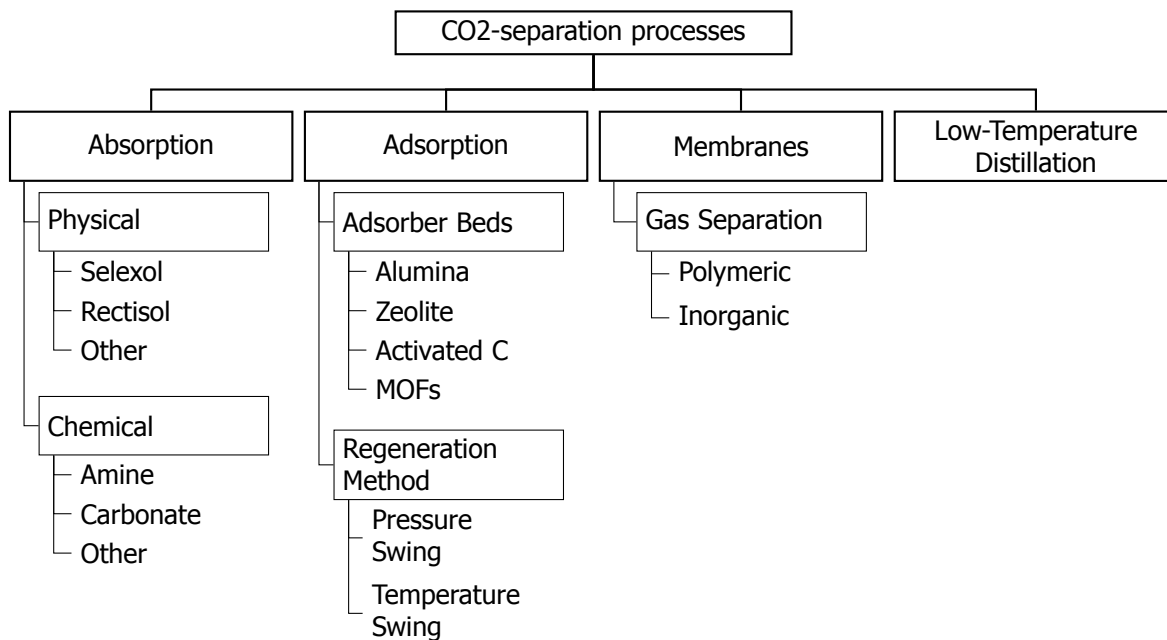
All these factors together contribute to the catalysts' average industrial lifetime of 2-5 years [37].

Table 3.3: Metal composition of catalysts provided by different manufacturers [16]

Manufacturer	Cu at%	Zn at%	Al at%	Other (at%)
IFP	45-70	15-35	4-20	Zr (2-18)
ICI	20-35	15-50	4-20	Mg
BASF	38.5	48.8	12.9	
Shell	71	24		Rare Earth oxide (5)
Sud Chemie	65	22	12	
Dupont	50	19	31	
United Catalysts	62	21	17	
Haldor Topsoe MK-121	>55	21-25	8-10	

3.2. Synthesis Gas Upgrading: CO₂-Removal

The CO₂-removal to achieve a stoichiometric number (SN) of above two in the reactor feed can be implemented through different separation technologies. These technologies include chemical and physical absorption, membranes, adsorption, and cryogenic distillation. Figure 3.3 gives an overview of the technologies used for CO₂-separation. One largely researched area of CO₂-separation is carbon capture and storage (CCS). For this application the required purity of the separated CO₂ is very high to allow for high pressure storage additionally a high degree of separation is desired. Leung *et al.* [49] give an overview of the mature and novel technologies employed for CCS.

Figure 3.3: Process technologies for CO₂-capture adapted from Rao and Rubin [50]

CCS can be used in three fuel combustion configurations: post-, pre- and oxy-combustion. In post-combustion CCS the CO₂ is separated from the flue gas. The main characteristics of this separation is the low partial pressure of CO₂ and the presence of high amounts of oxygen and nitrogen from air. In pre-combustion the fuel is transformed into syngas at high pressures. The separation happens before the combustion and therefore at high pressures and without air present in the stream. The last configuration separates oxygen from air and uses it to combust the fuel. This way the flue gas can be up to 95 % CO₂ which can be purified even more through condensation or other methods [51].

The maturity of the different technologies for post-, pre- and oxy-combustion are visualised by Figueroa *et al.* [52] in figure 3.4 with their possible cost reduction benefit for an installed CCS process. The technologies applicable for the correction of the CO₂ content in the process studied in this thesis are similar to the technologies applied in the pre-combustion carbon dioxide capture as these are also based on syngas with high concentrations of CO₂ at high partial pressure [53].

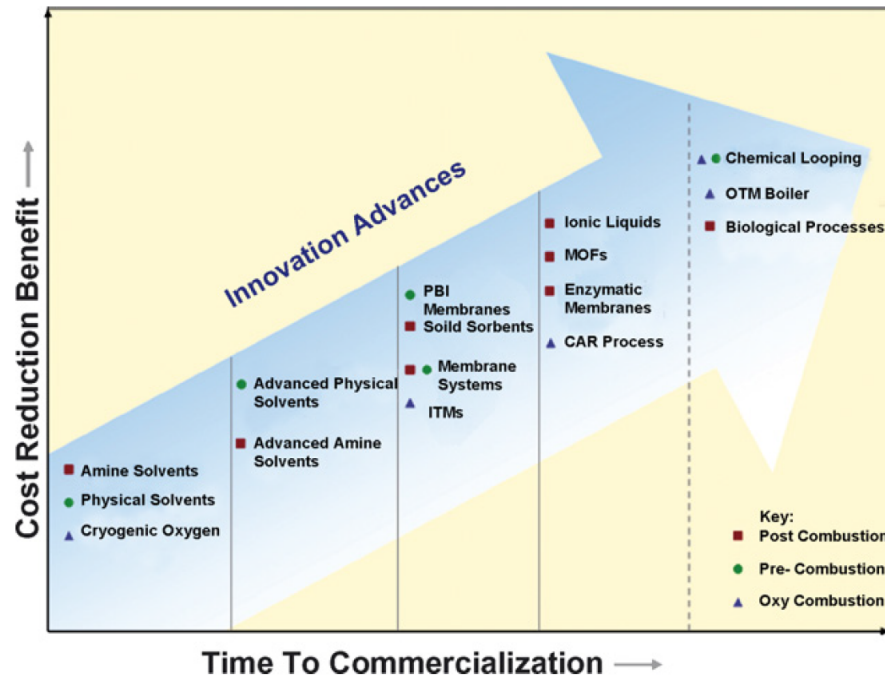


Figure 3.4: Development stage of process technologies for CO₂-capture adapted from Figueroa *et al.* [52]

3.2.1. Absorption

Absorption is the process of dissolution of molecules from a fluid into a solvent. The absorbed compounds are stored within the volume of the solvent. The separation through absorption can be performed with a chemical or physical solvent. The processes differ in temperature and pressure of the absorption and desorption column. This form of CO₂-separation is currently the most mature technology [49].

The applications for the absorption processes are within the areas of pre- and post-combustion. Chemical absorption is more suitable to post-combustion processes, due to the low pressure (normally atmospheric pressure) and low CO₂ partial pressure. Physical absorption becomes relevant for pre-combustion as it requires higher pressure and higher partial pressure of CO₂ [52, 54, 55]. The selection of a suitable process is displayed in figure 3.5 for the given partial pressure in the feed and the required partial pressure of CO₂ in the removed gas. The "hybrid" within the diagram is a hybrid between absorption and membranes which works well for large partial pressure differences between feed and product.

Chemical absorption processes generally require heat to regenerate the solvent while the solvent for physical absorption is regenerated using different pressures. Due to chemical reactions chemical solvents have lower flow rates for the same absorption rate which results in lower power consumption

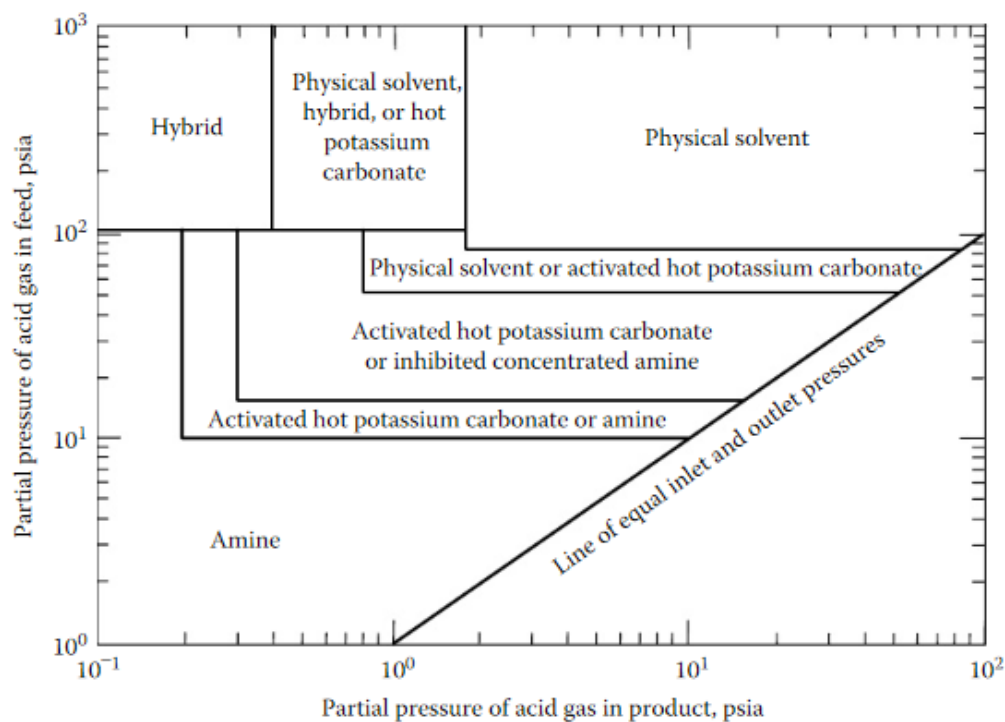


Figure 3.5: Process selection chart for CO₂-absorption technology without H₂S present [56] (adapted from Tennyson and Schaaf [57])

for the pumps [58] but higher heat requirements due to the regeneration.

The most common technologies for physical solvents are Selexol[®] and Rectisol[®]. Selexol[®] is a process licensed by UOP LLC [59] and uses as a solvent a mixture of Polyethylene Glycol Dimethyl Ether (PEG DME) with the formula $\text{CH}_3\text{O}(\text{C}_2\text{H}_4\text{O})_n\text{CH}_3$ where n ranges from 2 to 9 [60]. The Rectisol[®] process, licensed by Linde and Lurgi, uses chilled methanol as the solvent [61].

For chemical absorption there are several different solvents available. The most common ones are monoethanolamine (MEA), di-ethanol amine (DEA), methyldiethanolamine (MDEA) and mixed amines (Sulfinol[™], Amisol[™]) [55]. These solvents work by providing the alkalinity necessary to absorb the CO₂.

Koytsoumpa *et al.* [55] compared different acid gas removal technologies based on a desired 97% removal of CO₂. For this, they simulated two physical absorption solvents (Selexol[®] and Rectisol[®]) and two chemical absorption solvents (K₂CO₃ and MDEA) within Aspen Plus[®]. The results of the simulations show that the absorption processes with these solvents differ in power and heat requirement as well as amount of solvent needed. The authors do not decide on specific technologies as this is determined by the requirements and conditions of the complete process. The physical absorption processes are favoured for higher concentrations of CO₂ and lower temperatures compared to the chemical absorption.

A process system comparison in Aspen Plus[®] by Padurean *et al.* [58] of different gas-liquid absorption technologies for a pre-combustion coal-biomass syngas shows Selexol[®] and Rectisol[®] to be the best options for physical absorption with Selexol[®] using marginally less power, cooling and heating per kilogram of captured CO₂ than the other solvents. Padurean *et al.* [58] recommends Selexol[®] due to

its higher capture rate. Additionally, the authors give a list of the operation conditions for Rectisol[®], Selexol[®] and MDEA given in table 3.4.

Table 3.4: Selection of CO₂-absorption processes and their operating conditions [55]

Process	Rectisol	Selexol	MDEA
Solvent	Chilled methanol	PEG DME	methyldiethanolamine
Operating P_{opt}	~20 bar	~20 bar	~20 bar
Operating T_{opt}	-75 to -30 °C	0 to 25 °C	30 to 50 °C
Minimum CO ₂ in treated gas (ppmv)	10 to 100 CO ₂	300 CO ₂	Bulk gas CO ₂

3.2.2. Membranes

A compact option for the separation of gases are membranes. Membranes are selective barriers of which the driving forces of gas separation are concentration gradients of the components. Separation is achieved due to differences in the permeation and selectivity [62]. This leads to a not entirely selective separation of components, as all components can permeate through the membrane and the concentration gradient makes it impossible to achieve complete extraction. It is possible to gain high purities through multi-stage operation with recycle streams [62–64]. There are different kinds of membranes. They can be categorised as dense and porous and as polymeric and inorganic. Additionally the membranes can be used in different operations, these are gas separation, where both sides of the membrane are gaseous, and gas absorption, where the extracted compounds are absorbed by a solvent.

Many studies on the separation of CO₂ from syngas have been focused on high pressure and high temperatures. The pre-combustion gas separation within an integrated gasification combine cycle (IGCC) is one possible application of the membranes. Ramasubramanian *et al.* [53] reviewed the prospects of using membranes for CO₂-capture to obtain lower cost of electricity compared to established absorption processes like Selexol[®]. They conclude that while membranes can offer a good alternative to the current state of the art separation processes polymeric membranes need to be improved in terms of selectivity and inorganic membranes need to be more easily scale-able to actually be competitive. Scholes *et al.* [65] examined the use of CO₂-selective membranes, especially rubbery polymeric membranes and facilitated transport membranes. They emphasised that in order to achieve adequate CO₂-separation, membranes, which have a high solubility selectivity and low diffusivity selectivity, are needed, as H₂ is a very small molecule and diffuses more easily than CO₂.

The advantages and disadvantages of using membranes to separate CO₂ from the syngas are listed in table 3.5.

3.2.3. Adsorption

Solid adsorbents used to remove CO₂ from flue gas by adsorption form a new and promising class of technology [66]. Adsorption works similar to absorption with the distinction, that the adsorbed compounds are bound to the surface and not to the volume. Solid sorbents are used in a temperature

Table 3.5: Advantages and disadvantages of membrane separation [53, 62, 65]

Advantage	Disadvantage
Ease of installation	No ideal material
Easy scale-up	Problems with durability
Low operating costs	Contamination
No moving parts	Fouling
No auxiliary equipment needed	Small economy of scale

swing adsorption (TSA) or pressure swing adsorption (PSA) process. The CO₂ in the acid gas is adsorbed by a solid sorbent. This sorbent then needs to be regenerated. This can either be done by increasing the temperature or by lowering the pressure.

Berger and Bhowan [67] have developed a model and screening methodology to analyse the energy penalty of post-combustion CCS. They applied this model to a database containing over 4 million possible sorbents and have found that solid sorbents can have up to 30% lower energy requirement than the more established absorption with monoethanolamine (MEA). The main advantage to chemical absorption in aqueous solvents is the lower heat requirement due to not having to provide the heat of vapourisation in the desorption column.

In a review by Samanta *et al.* [68] different sorbents for post-combustion adsorption are discussed and analysed. The main categories of sorbents are similar to absorption processes as they are physical sorbents and chemisorbents. Among the physical sorbents activated-carbon-based solid sorbents have very low cost and are widely applied, zeolite sorbents have shown great potential for the separation of CO₂ and Metal-Organic Frameworks (MOF) are a novel class of solid sorbents whose crystalline structure is controllable (pore size, pore shape, etc). The chemisorbents have the advantage over the physical sorbents at low CO₂ partial pressures due to higher selectivity and capacities. Similar to the liquid-based absorption the most common chemisorbents are from the carbonate-group or the amine-group.

To regenerate the sorbents two major processes can be used: PSA and TSA. Both processes operate by changing the thermodynamic parameters of the system. The phase equilibrium between the adsorbed and the gas phase is defined by the gas phase fugacity, f_i^G , and adsorbed phase fugacity, f_i^A , of each element as described by equation 3.4 [69]:

$$f_i^G = f_i^A \quad (3.4)$$

with

$$f_i^G = y_i \phi_i^G \{T, P, y\} P \quad (3.5)$$

and

$$f_i^A = x_i f_i^{\circ} \{T, \Pi\} \gamma_i \{T, \Pi, x\} \quad (3.6)$$

where y_i = mole fraction of component i in the vapour phase

ϕ_i^G = fugacity coefficient of component i in the vapour phase, value dependent on T, P, y

T = System temperature

P = system pressure

y = composition of the gas phase

x_i = mole fraction of component i in the adsorbed phase

f_i° = fugacity coefficient of pure i in the adsorbed phase, value dependent on T, Π

γ_i = activity coefficient of i in the adsorbed phase, value dependent on T, Π, x

Π = pressure of adsorbed solution, similar to surface tension

x = composition of the adsorbed phase

The driving force of the PSA is the pressure ratio between absorption and desorption. These pressures can range from high-pressure adsorption to vacuum regeneration [70, 71]. The effects of the process parameters on the post-combustion PSA with 13X zeolite have been investigated by Ho *et al.* [70] and Zhang *et al.* [71] with the former comparing a regeneration at atmospheric pressure to one at vacuum. They conclude that vacuum swing adsorption (VSA) is the more feasible option.

For the operation of a TSA process the driving force is the temperature difference between absorption and desorption. The sorbents regenerated by an increase in temperature have to have good thermal stability at the operating conditions [72]. Sjostrom and Krutka [73] evaluated different sorbents for their regeneration energy and selected an amine sorbent to be tested in a pilot plant [74]. They conclude that there are still issues with the regeneration as this specific sorbent does not regenerate in a pure CO₂ environment, making a pure product impossible. However, other sorbents might not have that problem.

Overall, there is still a lot of research necessary to implement solid sorbents on an industrial scale [66–68, 75]. This research includes a deeper understanding of the materials' characteristics and their manufacture [67], data on sorbent performance and process integration [68], the reactor sizing and economic evaluation [66], and the regeneration technology [75].

3.2.4. Low-Temperature Distillation

Low-temperature, or cryogenic, distillation is the distillation of gases at very low temperatures. Table 3.6 lists the critical temperatures of the components of the plant discussed in this report. As can be seen, there is a gap between the gases needed for methanol production (CO and H₂) and CO₂. This means it is possible to use cryogenic distillation for the separation of CO₂.

Table 3.6: Critical point temperatures, molecular weights and molecule sizes [76, 77]

Component	T_c °C	MW g mol ⁻¹	Kinetic Diameter pm
H ₂	-240.21	2.016	289
CO	-140.29	28.010	376
CH ₄	-82.59	16.043	380
CO ₂	30.98	44.010	330
CH ₃ OH	239.16	32.042	400
H ₂ O	373.95	18.015	265

Berstad *et al.* [78] analyse the application of low-temperature distillation on pre-combustion syngas from coal gasification. The advantage of this technology is the CO₂ is separated in a state at which

it does not need further cooling or compression for storage. This also means that the remaining syngas exits the unit at lower temperatures. In a following study Berstad *et al.* [79] compared the low-temperature CO₂ capture with Selexol® capture and concluded that low-temperature capture units have a higher electrical efficiency despite the high compression energy need. However, the assumption of this comparison was the absence of water in the gas stream which requires thorough drying units before the unit operation as it can lead to process blockage [78, 80].

3.3. Synthesis Gas Upgrading: Hydrogen Recycle

Most hydrogen separation technologies applied today have the aim to separate hydrogen with very high purity. For the proposed process scheme of this project, this is not necessary. The aim is to recycle as much hydrogen as possible while also having a vent. Thus the technologies need to be examined for the application in recycle rather than purification. Especially the selectivity of H₂ to CH₄ and H₂ to N₂ is important as the other compounds of the gas can be recycled into the process.

Similar to the CO₂-removal unit the hydrogen recycle is a gas separation unit and can be achieved through various technologies. The three commercial and most prominent ones are PSA with sorbents such as zeolite, cryogenic distillation and membranes [81].

3.3.1. Adsorption

In PSA the hydrogen permeates through the sorbent while the impurities get adsorbed. This can give a hydrogen purity of 99-99.999 % with a series of adsorbers using zeolite [81]. The technology has been described in detail in section 3.2.3.

3.3.2. Cryogenic Distillation

To separate the hydrogen from the gas mixture the temperature needs to be reduced to condense the other gases. As this process would be performed at temperatures just above hydrogen condensation it is called cryogenic distillation instead of low-temperature distillation for CO₂ separation. However, the general process is similar and requires a large compression and cooling duty.

3.3.3. Membranes

The use of membranes for the separation of hydrogen can be categorised into polymeric, inorganic, facilitated transport and hybrid, dense and porous membranes. The small kinetic diameter of hydrogen compared to the other components (see table 3.6) means that separation is predominately diffusion based [53, 82]. Adhikari and Fernando [83] reviewed membrane separation techniques for hydrogen. They list membranes as advantageous compared to other techniques due to their lower energy consumption, ease of operation and cost effectiveness.

The most commonly used membrane material are polymeric, microporous inorganic or metallic membranes. Polymer membranes are used to separate hydrogen from gas mixtures with hydrocarbons,

nitrogen and carbon monoxide. However, there is a trade-off between selectivity of hydrogen to other components (α) and the H_2 permeability (P). Figure 3.6 shows the current upper bound of this trade-off for H_2/CH_4 separation. The x-axis is the permeability of hydrogen in barrers¹. This is plotted against the selectivity, α , of hydrogen to CH_4 for current existing membranes on the y-axis. An optimal membrane would be located at the top right corner, due to the trade-off this can not be reached with current materials and technologies. The trade-off results in an upper bound which can be described by equations 3.7 to 3.9.

$$P_i = k\alpha_{ij}^n = k\left(\frac{P_i}{P_j}\right)^n \quad (3.7)$$

$$-\frac{1}{n} = \left[\frac{d_j + d_i}{d_i^2}\right](d_j - d_i) \approx \Delta d_{ji} \quad (3.8)$$

$$k^{-1/n} = \frac{S_i}{S_j} S_i^{-1/n} \exp\left\{\frac{1}{n}\left[b - f\left(\frac{1-a}{RT}\right)\right]\right\} \quad (3.9)$$

where P_i = permeability of the more permeable gas [$\text{mol m}^{-1} \text{s}^{-1} \text{Pa}^{-1}$]

i = more permeable gas

j = less permeable gas

α = selectivity of the membrane [-]

k = scaling factor

n = slope of log-log limit in figure 3.6 [-]

d = molecular diameter [m]

S = solubility of the gas in the membrane [$\text{mol m}^{-3} \text{Pa}^{-1}$]

a, b = dimensionless constants depending on membrane properties

f = constant depending on chosen polymer [J mol^{-1}]

The values for this bound are predicted by Robeson [84] and Freeman [85]. With the inverse of the slope approximately equal to the molecular diameter of the two gases, as proven with empirical data, the upper bounds for various gas pairs can be calculated if the permeabilities and solubilities are known. The difference between the 'prior upper bound' and the 'present upper bound' in figure 3.6 results from optimisations of the polymers to improve their solution/diffusion transport. The trade-off between permeability and selectivity leads to high investment costs when a very pure product is required. To achieve high purities large membrane areas are needed to compensate for the low permeability.

Dense metallic membranes such as Palladium or Palladium-alloys can produce nearly pure hydrogen (99.99% [83]). The obstacles concerning the use of this type of membrane is the cost of the metal, the membrane lifetime and the poisoning by other gases such as CO [65].

¹1 barrer = $10^{-10} \text{ cm}_{\text{STP}}^3 \text{ cm}_{\text{th}} \text{ cm}_{\text{A}}^{-2} \text{ s}^{-1} \text{ cmHg}^{-1}$ with cm_{STP}^3 as the amount of molecule in a cubic centimetre at standard conditions, cm_{th} the thickness of the membrane, cm_{A}^2 the area of the membrane and cmHg the pressure drop over the membrane.

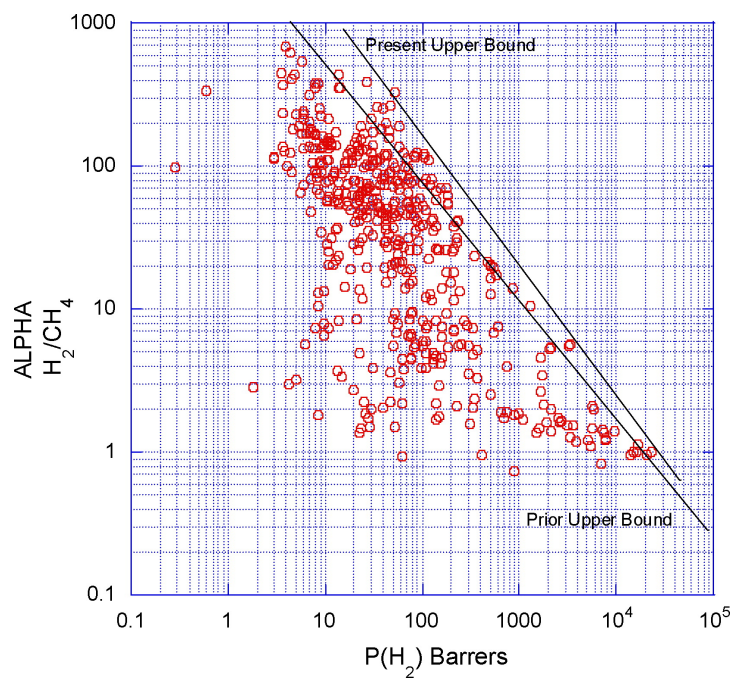


Figure 3.6: Corrected Robeson upper-bound for H_2/CH_4 polymeric membranes [84]

4

Building the Model

The process described in basics in figure 1.4 and more detailed in figure 4.1 shows the different unit operations that are analysed for this thesis. These unit operations include the methanol reactor unit (MRU) with the heat-exchangers and compressors, the CO₂-removal unit (CRU) and the H₂-recycle unit (HRU). The models of these units are analysed separately based on estimates of the streams, before they are being combined into one model and optimised with hydrogen supply integration. The assumptions made for the models are listed and discussed, followed by the descriptions of the models and sensitivity analyses to identify the most influential variables. For the analyses of the units, a first estimate of the streams provided by de Lathouder [10] is used for the input streams.

For the synthesis of methanol from clean syngas the following unit operations were chosen:

1. The adiabatic reactor was chosen due to its simple design and the process' small scale (desired production volume of 50 t d⁻¹)
2. The Selexol[®]-process was selected for the removal of CO₂ from the syngas. This process was chosen as it is one of the most mature technologies and the partial pressure of CO₂ is within the working range of absorption, specifically physical absorption (see figure 3.5). Additionally, physical absorption has a lower heat requirement than chemical absorption (see chapter 3.2) making it easier to integrate into the process.
3. For the recycle of hydrogen from the purge stream a polymeric membrane was chosen, as it has very low operational costs and little required equipment. Also, there is no need for a strict separation of the components except for the non-reacting CH₄ and N₂

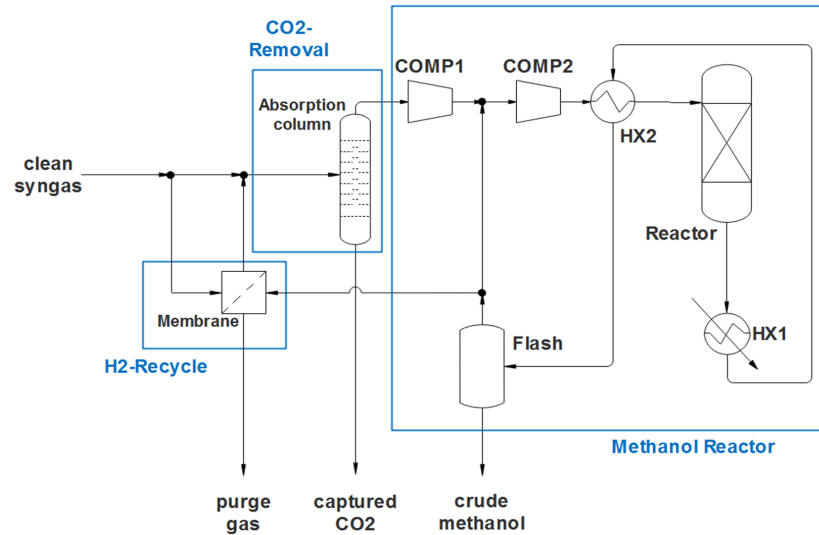


Figure 4.1: Unit operations discussed within this thesis: H₂-recycle, CO₂-removal and methanol reactor with crude methanol separation

4.1. Terminology and Assumptions

The process model within this chapter is based on a section of the process designed by de Lathouder [10]. The full process from biomass to methanol includes a fluidised bed gasifier followed by a gas cleaning unit. The crude methanol produced within the here modelled methanol synthesis unit (MSU) is purified in a distillation column. The purged gas stream could be used to produce steam for the compression turbines through combustion or it could be sold.

The ratio of work put into the system to the lower heating value (LHV) of the produced methanol in the *CRUDEMEO*-stream (eq. 4.1) will be referred to as the mechanical ratio (MR). Similarly, the ratio of the thermal energy put into the system to the LHV of produced methanol in the *CRUDEMEO*-stream (eq. 4.2) will be called thermal ratio (TR).

$$MR = \frac{\sum P_i}{LHV_{MeOH} * \dot{m}_{MeOH, CRUDEMEO}} \quad (4.1)$$

$$TR = \frac{\sum Q_i}{LHV_{MeOH} * \dot{m}_{MeOH, CRUDEMEO}} \quad (4.2)$$

where MR = mechanical ratio [$kW_p kW_{ch}^{-1}$]

TR = thermal ratio [$kW_Q kW_{ch}^{-1}$]

P_i = power input [kW]

Q_i = cooling input [kW]

LHV_{MeOH} = lower heating value of methanol [$MJ kg^{-1}$]

$\dot{m}_{MeOH, CRUDEMEO}$ = methanol in the *CRUDEMEO*-stream [$kg h^{-1}$]

The equipment that is grouped together within the blue frames in figure 4.1 will be called *unit*. The

three units are: H₂-recycle unit (HRU), CO₂-removal unit (CRU) and methanol reactor unit (MRU). The whole process depicted in figure 4.1 is called the methanol synthesis unit (MSU).

Basic assumptions:

- The only components considered within this process: H₂, CO, CO₂, N₂, CH₄, H₂O, MeOH, Selexol
- Perfectly clean syngas at the entry of the process section. No H₂S or other impurities
- MRU:
 - No by-products formed in the reactor
 - No limitations due to mass or heat transfer
- CRU:
 - The storage or disposal of the extracted CO₂-rich gas is ignored
- HRU:
 - behaviour follows simple solution-diffusion mechanism
 - permeation rate independent of pressure, temperature and composition

4.2. Methanol Reactor Unit

An adiabatic reactor was chosen due to the high CO₂ content in the feed. The conversion of CO₂ and H₂ to methanol is less exothermic than for CO and thus does not generate as much heat [86]. A cooling system is not necessary as the deactivation temperature of the catalyst is not reached.

4.2.1. Modelling

To model this unit operation a functioning reactor model is needed before the reactor can be integrated into the methanol reactor unit (MRU). In the following analysis, limitations due to diffusion or other wise were neglected. Lee [87] analysed the influence of pore-diffusion for the production of methanol under low-pressure conditions. He concluded that for commercially applied conditions limitations are present, however, there is no criterion to accurately determine the influence. It should be determined through experiments. Smaller catalyst particle sizes reduce the influence and can turn the process into a kinetic driven one [88].

Methanol Reactor

For the modelling of the reactor the plugflow-module of Aspen Plus[®] with the Langmuir-Hinshelwood-Hougen-Watson (LHHW) kinetic model is used. Two reactions are modelled: the formation of methanol from CO₂ (eq. 4.3) and the RWGS-reaction (eq. 4.4):



The kinetic model used is the previously discussed model by Van den Bussche and Froment [22] with the reaction rates for methanol formation (eq. 4.5) and for RWGS-reaction (eq. 4.6). The validated area for this kinetic model is 15 to 51 bar, 180 to 280 °C and a ratio of CO/CO₂ of 0 to 4.1. The reaction

rate is calculated from three components:

1. the kinetic factor, k , which incorporates the activation energy
2. the driving force, the numerator of the equation, as a difference between partial pressures of the forward and backward reaction with the equilibrium constant
3. the adsorption term, the denominator of the equation, which describes the behaviour of adsorption on the catalyst

$$r_{\text{MeOH}} = k_{\text{MeOH}} \frac{(p_{\text{CO}_2} p_{\text{H}_2}) - (1/K_{p\text{MeOH}}) (p_{\text{CH}_3\text{OH}} p_{\text{H}_2\text{O}} / p_{\text{H}_2^2})}{(1 + K_a (p_{\text{H}_2\text{O}} / p_{\text{H}_2}) + K_b \sqrt{p_{\text{H}_2}} + K_c p_{\text{H}_2\text{O}})^3} \quad (4.5)$$

$$r_{\text{RWGS}} = k_{\text{RWGS}} \frac{p_{\text{CO}_2} - (1/K_{p\text{RWGS}}) (p_{\text{CO}} p_{\text{H}_2\text{O}} / p_{\text{H}_2})}{(1 + K_a (p_{\text{H}_2\text{O}} / p_{\text{H}_2}) + K_b \sqrt{p_{\text{H}_2}} + K_c p_{\text{H}_2\text{O}})} \quad (4.6)$$

where r_i = reaction rate [$\text{mol kg}_{\text{cat}}^{-1} \text{s}^{-1}$]

k_i = kinetic factor [$\text{kmol kg}_{\text{cat}}^{-1} \text{s}^{-1} \text{bar}^{-1}$] or [$\text{kmol kg}_{\text{cat}}^{-1} \text{s}^{-1} \text{bar}^{-2}$]

p_i = partial pressure [bar]

K_{p_i} = equilibrium constant [-] or [bar^{-2}]

$K_{a/b/c}$ = adsorption constants [bar^n]

The values for the reactions rate are given in table 4.1 where the values are given in the form of equation 4.7.

$$k_i \quad \text{or} \quad K_i = A_i^* \exp\left(\frac{B_i^*}{RT}\right) \quad (4.7)$$

Table 4.1: Values for the kinetic model of LHHW-type for equations 4.5 to 4.7 from Van den Bussche and Froment [22]

Variable	Unit	A_i^*	B_i^*
k_{MeOH}	$\text{mol kg}_{\text{cat}}^{-1} \text{s}^{-1} \text{bar}^{-2}$	1.07	36 696
k_{RWGS}	$\text{mol kg}_{\text{cat}}^{-1} \text{s}^{-1} \text{bar}^{-1}$	1.22×10^{10}	-94 765
K_a	-	3453.38	-
K_b	$\text{bar}^{-0.5}$	0.499	17 197
K_c	bar^{-1}	6.62×10^{-11}	124 119

Additionally the equilibrium constants based on partial pressure, K_{p_i} , are taken from Graaf *et al.* [18] where the units need to be changed for partial pressures in Pa which results in the two equations 4.8 and 4.9.

$$\ln K_{p\text{MeOH}} = \frac{7059.73}{T} - 47.415 \quad (4.8)$$

$$\ln K_{p\text{RWGS}} = \frac{-4773.26}{T} + 4.672 \quad (4.9)$$

The kinetic model described above needs to be adjusted to be integrated into the Aspen Plus® model. First, the units of pressure need to be changed into Pascal and the kinetic expression needs to be changed to kmol. Additionally the kinetic pre-factor needs to be presented in the form of equation 4.10 and the other terms need to be adapted into the form of equation 4.11. The final values entered into the Aspen Plus® model are in table 4.2.

Table 4.2: Adjusted values for the Aspen Plus®-model of the the reactor kinetics for equations 4.5 and 4.6 in the form of equation 4.10 and 4.11 respectively

Variable	$k_{i,0}$	E_i
k_{MeOH}	1.07×10^{-13} kmol kg _{cat} ⁻¹ s ⁻¹ Pa ⁻²	-36 696 kJ kmol ⁻¹
k_{RWGS}	1.22×10^2 kmol kg _{cat} ⁻¹ s ⁻¹ Pa ⁻¹	94 765 kJ kmol ⁻¹

Variable	A_i	B_i
$\ln \frac{1}{K_{p\text{MeOH}}}$	47.415	-7059.73
$\ln \frac{1}{K_{p\text{RWGS}}}$	-4.672	4773.26
$\ln K_a$	8.1471	-
$\ln K_b$	-6.4522	2068.44
$\ln K_c$	-34.9526	14 928.92

$$k_i = k_{i,0} \exp\left(-\frac{E_i}{RT}\right) \quad (4.10)$$

$$\ln K_i = A_i + \frac{B_i}{T} \quad (4.11)$$

The pressure drop within the reactor is modelled with the Ergun equation as suggested by Towler and Sinnott [89]. Within Aspen Plus® the Ergun equation has the following form:

$$-\frac{dP}{dz} = 150 \frac{(1-\varepsilon)^2}{\varepsilon^3} \frac{\mu U}{\phi_s^2 D_p^2} + 1.75 \frac{1-\varepsilon}{\varepsilon^3} \frac{\rho U^2}{\phi_s D_p} \quad (4.12)$$

where $\frac{dP}{dz}$ = change of pressure over the length dz [Pa m⁻¹]

ε = void fraction [-]

μ = fluid viscosity [Pa s]

U = superficial velocity [m s⁻¹]

ϕ_s = particle shape factor [-]

D_p = particle diameter [m]

ρ = fluid density [kg m⁻³]

Aspen Plus® needs the diameter, shape factor and void fraction of the catalyst and catalyst bed to

calculate the pressure drop. The other values are determined through the simulation. In this model, the catalyst data from Chen *et al.* [23] was used (see table 4.3).

Table 4.3: Catalyst specifications from Chen *et al.* [23]

Shape	cylindrical
Diameter [mm]	5.4
Height [mm]	5.2
Density [kg m^{-3}]	1190
Void fraction of bed [$\text{m}^3 \text{m}^{-3}$]	0.285

Methanol Reactor Unit

The full unit consists of two compressors (*COMP1* and *COMP2*), two heat exchangers (*HX1* and *HX2*), the reactor (*REACTOR*), a flash (*FLASH*) and the splitter (*SPLITREA*). The two compressors are needed to first compress the feed and after mixing it with the recycle stream recompress the mixed stream to the required feed conditions of the reactor. The heat developed in the reactor is used to evaporate a water stream in *HX1* and to heat up the feed gas of the reactor to feed conditions. The produced methanol needs to be separated from the product stream to recycle the non-reacted gas. This can be done within a flash as the boiling point of MeOH is much higher than of H_2 , CO and CO_2 (see table 3.6). Finally, a part of the recycle stream needs to be purged in *SPLITREA* to prevent the inert gases (N_2 , CH_4) from accumulating.

The final design of the reactor within Aspen Plus[®] can be seen in figure 4.2. This flowsheet-section includes a heater between the heat exchanger (*HX1*) and the reactor to ensure that the simulation converges. If the model runs properly, the heater's duty is 0. However, if there is an issue during the convergence and in one loop the temperature of the reactor input is below 200 °C, then the reaction within the reactor becomes endothermic. This leads to a cold reactor output which cannot warm up the reactor input. To avoid this error in the convergence of the simulation the heater is placed before the reactor to ensure that the inlet temperature is always high enough. A cooler (*COOLER*) is placed after the first compressor. In case of high compression, the output from *COMP1* becomes very hot which increases the compression duty of *COMP2*. To avoid this a cooler is used when the temperature of the mixed gas entering *COMP2* exceeds 60 °C.

4.2.2. Calibration and Comparison with Reactor Data

The main component of this unit, that needs to be checked, is the reactor with its kinetics. This is done by using the same input streams as used by Van den Bussche and Froment [22] and Chen *et al.* [23] and observing the operation conditions and output of the system.

Figure 4.3 shows the concentration profile of the reactor from Van den Bussche and Froment while figure 4.4 shows the equivalent profile for the reactor modelled in this report. As can be seen the profiles are very similar. The comparison of the graphs shows that the speed as well as the reached equilibrium are comparable. Thus, the kinetics have been correctly converted for use in the Aspen Plus[®] model.

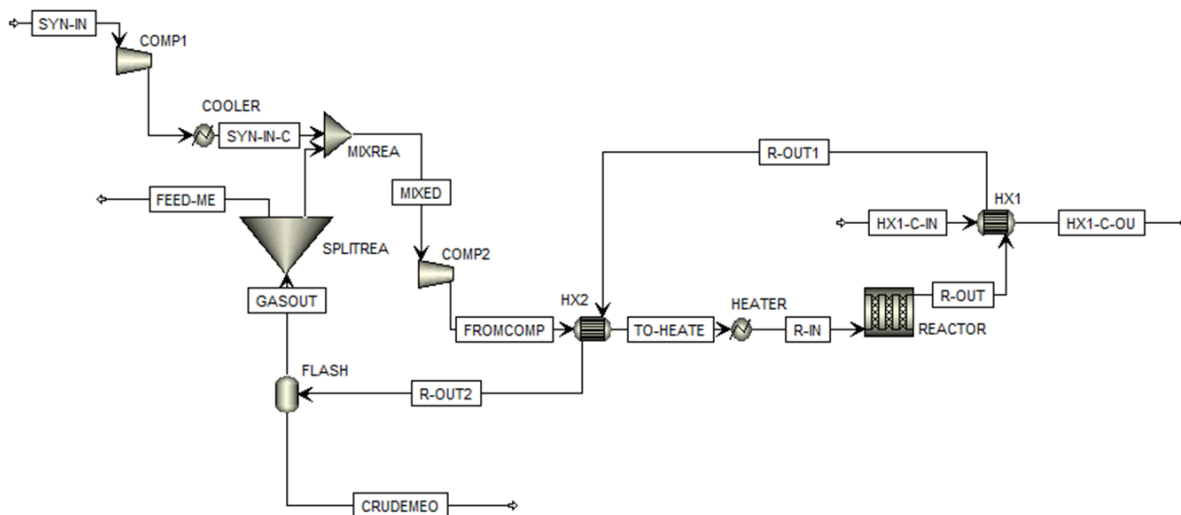


Figure 4.2: Methanol Reactor Unit for the formation of methanol from syngas and separation of crude methanol from the gas stream as modelled in Aspen Plus®

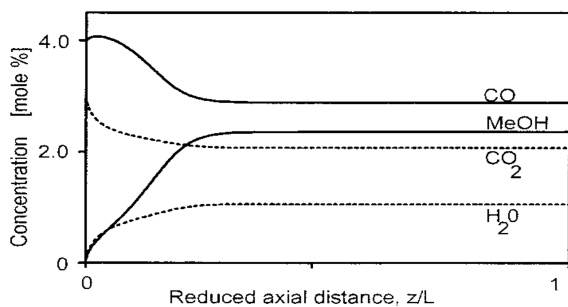


Figure 4.3: Concentration profile of the methanol reactor from Van den Bussche and Froment [22]

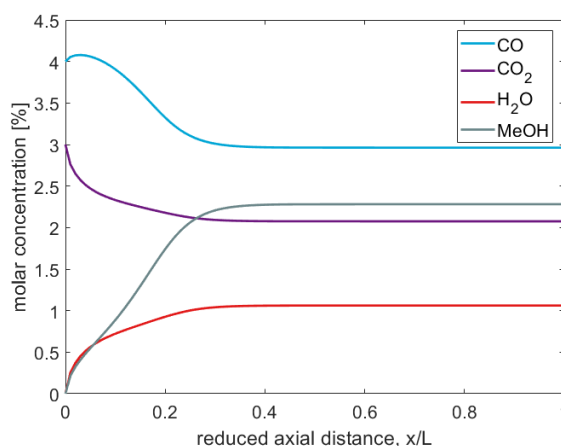


Figure 4.4: Concentration profile of the methanol reactor as modelled with Aspen Plus®

To further validate the model, it is compared to the Lurgi reactor from Chen *et al.*'s paper [23]. The Lurgi reactor is operated with an isothermal cooling stream. The in- and output streams of the industrial methanol synthesis reactor and the here presented model are listed in table 4.4. It can be seen that there is a good comparison between the model and the practical case. The difference is in large part due to the side reactions generating ethanol, propanol and methyl formate which are assumed negligible in this model.

A validation of the whole unit is done by mass and energy balances within Aspen Plus®. The differences between in and output lie within the range of 1×10^{-6} and are therefore considered to be acceptable.

4.2.3. Sensitivity Analyses

There are many variables that can influence the performance of the model. The ones with the largest influence are assumed to be:

Table 4.4: Comparison of the product stream and the cooling water (CW) of the simulation (SIM) with the industrial data from Chen *et al.* [23]

		INPUT		OUTPUT			
		FEED	CW	PRODUCT		CW	
				Chen	SIM	Chen	SIM
Temperature	°C	225	220	255	256	231.2	230.8
Pressure	bar	69.7	29	66.7	66.69	29	29
Vapor Frac	-	1	0	1	1	0.805	0.805
Mole Flow	kmol hr ⁻¹	6264.8	766	5592	5607.1	766.0	766.0
Mass Flow	kg hr ⁻¹	57 282.8	13 800	57 282.8	57 282.8	13 800	13 800
Component Flow	kg hr ⁻¹						
H2		9586.5		8013.7	8015.7		
CO		10 727.9		4921	4919.9		
CO2		23 684.2		18 316.4	18 336.7		
N2		8072		8071.9	8072		
CH4		4333.1		4333.1	4333.1		
WATER		108.8	13 800	2309.3	2297.8	13 800	13 800
METHANOL		756.7		11 283.1	11 294.0		
ETHANOL		0.6		8.7	0.6		
PROPANOL		-		0.1	-		
METHYL-FORMATE		13		25.6	13.0		

- Length and width of the reactor
- Feed temperature of the reactor
- Feed pressure of the reactor
- Feed composition
- Flash operation conditions
- Purge fraction and recycle ratio

For the analysis of this unit the feed composition and total flow is considered fixed. However, they are subject to change in the full model in chapter 5. The following sensitivity analyses shall show a trend of operation lines.

The feed flow and composition is specified in table 4.5 with the stream names in reference to figure 4.2. If not otherwise defined in the study, the operation conditions and sizing in table 4.6 apply.

Length and Width

The length and width of the single tube reactor defines the reaction volume as well as the pressure drop within the reactor. The larger the volume, the longer the residence time, eventually leading to the reacting gas reaching chemical equilibrium. To find the ideal reactor size, economics have to be considered. A smaller reactor leads to less conversion which in turn means a smaller methanol yield, but it also means the investment costs for the reactor will be less.

Figure 4.5 shows the production for different diameters and volumes. A clear drop in production can be observed for similar volumes with smaller diameters. This drop can be explained with the pressure drop within the reactor. This pressure drop increases for reactors with same volume but smaller diameters as shown in figure 4.6. At a lower pressure, the equilibrium of the reaction moves towards the left side

Table 4.5: Estimated feed compositions and properties from de Lathouder [10]. The composition and flowrate are used for the first optimisation of the reactor and reactor unit

		Reactor Input	MRU Input
Stream Name		R-IN	SYN-IN
Temperature	°C	206.28	31.96
Pressure	bar	87.8	31.9
Mass Flow	kg hr ⁻¹	33 172.7	6943.41
Component Flow	kg hr ⁻¹		
H ₂		2445.7	654.74
CO		2520.7	692.91
CO ₂		15 460.4	4233.76
N ₂		1078.9	119.19
CH ₄		11 105.8	1227.99
WATER		88.4	14.82
METHANOL		472.9	-

Table 4.6: Conditions and sizes used for the optimisation of the MRU

Length <i>REACTOR</i>	m	3.5
Diameter <i>REACTOR</i>	m	2.5
Output Pressure <i>COMP1</i>	bar	48
Output Pressure <i>COMP2</i>	bar	50
Pressure Difference <i>REACTOR</i> and <i>FLASH</i>	bar	2
Temperature <i>FLASH</i>	°C	50
Purge fraction	%	11
Temperature of <i>R-OUT1</i> at output of <i>HX1</i>	°C	220
Temperature of <i>R-IN</i> at output of <i>HX2</i>	°C	210

of equations 2.6 and 2.7 as explained in chapter 2.2.1. This leads to a lower methanol output.

Equation 4.12 reveals how a smaller diameter leads to a higher pressure drop. While most variables do not change with the diameter, the velocity of the gas changes with the decrease of the cross-sectional area. As the velocity and the pressure drop are proportional to one another the pressure drop per length increases with decreasing diameter.

The final geometry of the reactor is determined by the required conversion. Towler and Sinnott [89] recommend a reactor where the gas flows down through the catalyst bed preventing fluidisation. That way, there are no velocity restrictions in respect to fluidisation. Furthermore, they propose a ratio of height to diameter of 1:1 to 4:1 for the reactor vessel. Additional height to accommodate inert ceramic balls at the top and bottom of the catalyst beds is recommended. These ceramic balls allow for a more efficient use of the catalyst as they distribute the gas before it reaches the catalyst and they help to hold back the catalyst.

Temperature and Pressure at Reactor Inlet

Another factor influencing the yield and conversion of the reactor are the state of the inflow. By varying the pressure and temperature of the reactor's inlet stream and comparing it to the production of the reactor an operating temperature between 200 °C and 210 °C is determined depending on the operating pressure (see figure 4.7). Higher temperatures produce less methanol while lower temperatures

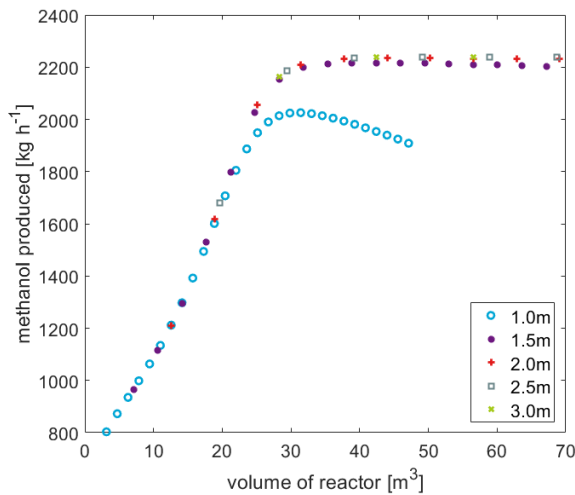


Figure 4.5: Influence of the reactor's diameter and volume on the production of methanol for a single reactor reactor

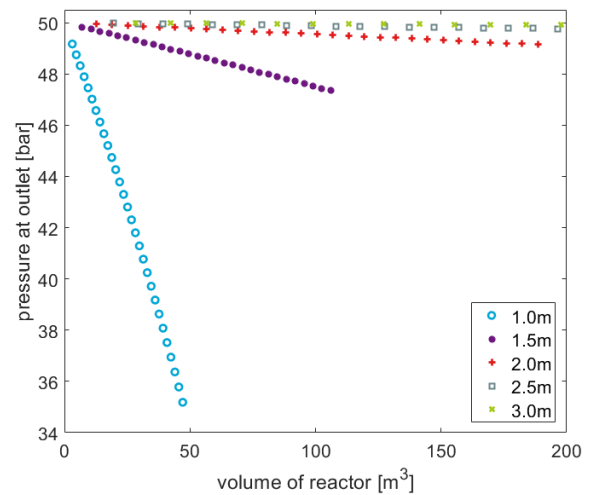


Figure 4.6: Influence of the reactor volume distribution on the pressure drop

produce considerably less methanol for higher pressures. The behaviour in this figure is given for the reactor size from table 4.6. The reason for the drop in production for lower temperatures lies in the size of the reactor. Due to the lower temperature, the reaction does not happen as fast and the equilibrium is not reached. Thus the feed stream can be at lower temperatures when using a larger reactor.

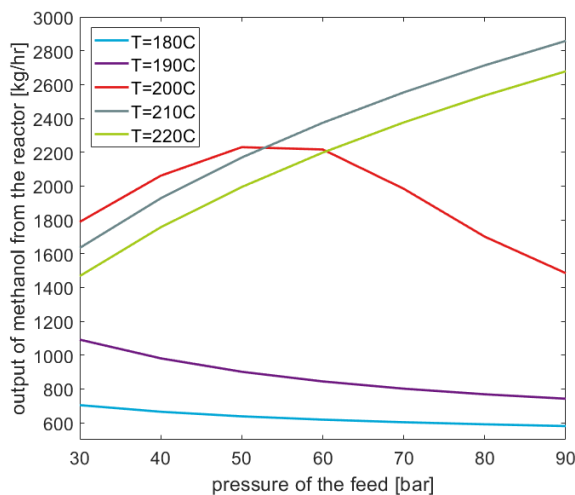


Figure 4.7: Influence of feed pressure and temperature on the output of a single methanol reactor with the dimensions of 3.5 m length and 2 m diameter

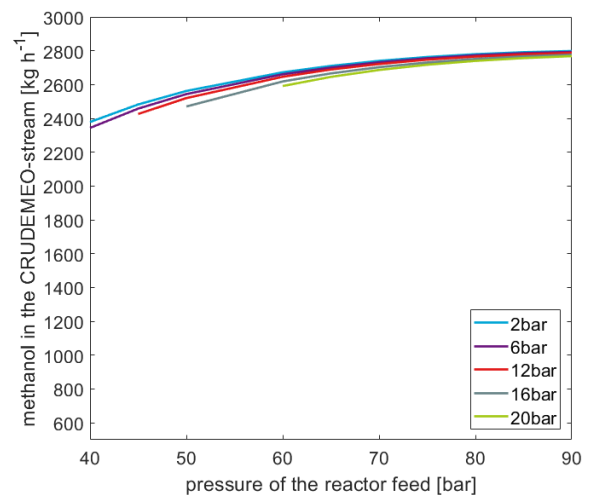


Figure 4.8: Influence of the operating pressure of the MRU on the methanol output within the *CRUDEMEO* for various pressure drops between the reactor inlet and the flash

Pressure of the Unit

The pressure of the reactor's feed stream, the operating pressure of the MRU, does not only influence the chemical equilibrium within the reactor but also the energy demand of the whole unit. The production of methanol within the MRU (see figure 4.8) follows a similar trend to the operation of the single reactor (figure 4.7). However, due to the recycling of the unreacted gas, the feed composition is different from this reactor. Thus the pressure of the unit has a lower influence on the output of methanol than for a single reactor, as long as the other equipment changes their capacity to accommodate the increase in recycled gas.

With a higher operating pressure the compressors require more energy. At a lower pressure the reactor produces less methanol. With a lower heating value (LHV) of methanol of $20.096 \text{ MJ kg}^{-1}$ [90], figure 4.9 and 4.10 show the energy demand of the compressors per LHV of methanol produced. Looking at the graph for a pressure drop of 2 bar and a flash temperature of 50°C as specified in table 4.6 the compressor work per LHV of produced methanol increases with increasing pressure. This is due to the increase in work being larger than the increase in methanol production.

Figure 4.11 and 4.12 show a the ratio of the cooling duty of the flash per LHV of produced methanol. For a small pressure drop and a higher *FLASH* temperature, the cooling demand is the lowest. However, with increasing operating pressure, the cooling duty increases. This is due to the heat developed during the compression of the gas. The higher the pressure ratio of *COMP1*, the higher the output temperature. This means, that the gas feeding the reactor has a lower heat requirement to reach the necessary feed temperature, thus increasing the duty of the flash. A cooler *FLASH* temperature ultimately increases the cooling requirement of the system.

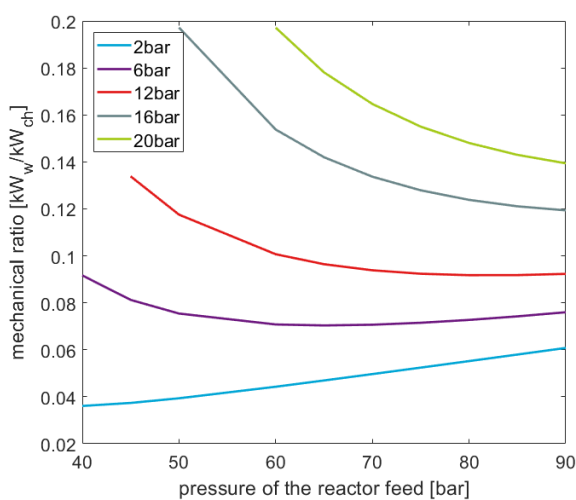


Figure 4.9: Influence operating pressure of the MRU on the compressor work per lower heating value of methanol produced at various pressure drops between the reactor inlet and the flash

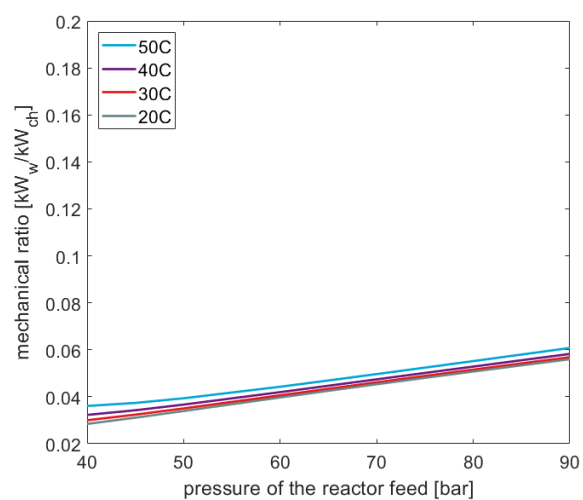


Figure 4.10: Influence operating pressure of the MRU on the compressor work per lower heating value of methanol produced at various flash temperatures

Flash Operation Conditions

The pressure and temperature of the flash influence the separation of the non-converted gas and the methanol. A good separation of the methanol from the recycle stream needs to be achieved. If possible the water content should be low, however, this is secondary, as the methanol is distilled in a downstream unit operation. Temperature and pressure of the flash influence the compressor duty and the cooling duty of the unit, the amount of gas recycled and the composition and quantity of the *CRUDEMEO* stream.

First the change in compressor work is analysed. Figure 4.9 and 4.10 show the influence of the flash's pressure and temperature on the mechanical ratio (MR) for different operating pressures of the methanol reactor unit. The two figures show that the pressure drop between the reactor inlet stream and the flash has a larger influence on the MR than the temperature to which the stream is cooled within the flash. The great increase in MR for increasing pressure drops results from the re-pressurising

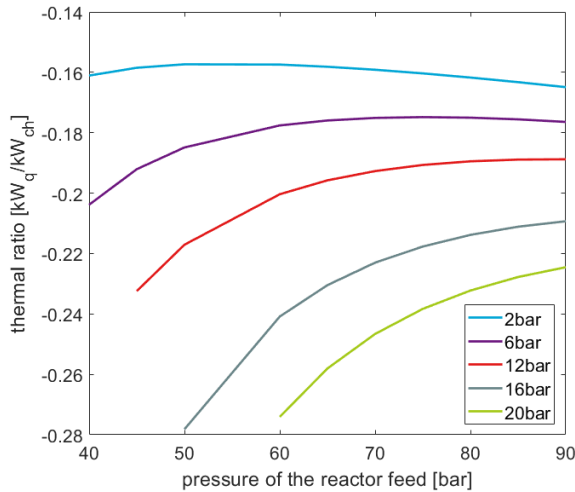


Figure 4.11: Influence operating pressure of the MRU on the cooling duty of the flash per lower heating value of methanol produced at various pressure drops between the reactor inlet and the flash

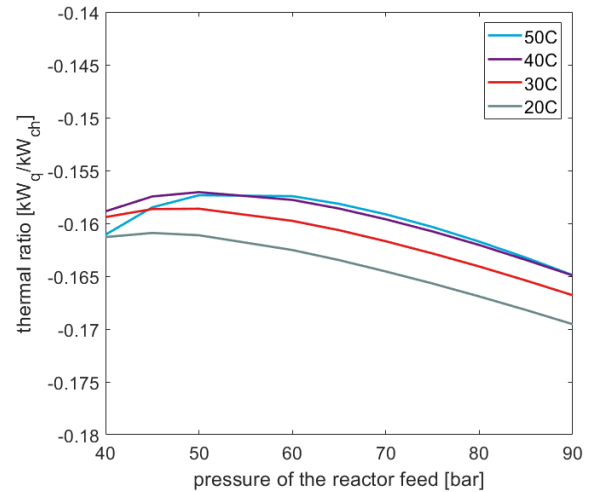


Figure 4.12: Influence operating pressure of the MRU on the cooling duty of the flash per lower heating value of methanol produced at various flash temperatures

of the stream. The decrease of the MR for lower temperatures results from the compression work in *COMP2*. A lower feed temperature lowers the compression duty.

Secondly, the cooling duty is evaluated. Here, a similar behaviour can be observed in figures 4.11 and 4.12 compared to the compressor work. The pressure drop has a much larger influence than the flash's temperature.

These trends, as well as the trends within each figure can be explained by figures 4.13 and 4.14. For fixed operating conditions (temperature and pressure drop) of the *FLASH*, the massflow into the reactor decreases for higher operating pressures. At a higher operating pressure more methanol and water is formed within the reactor. These two components are largely condensed and separated within the flash, reducing the amount of gas recycled back to the reactor. For an increase in the pressure drop from reactor inlet to flash, less methanol and water is condensed and separated, which increases the mass flow and reduces the production of methanol. The higher the operating pressure is, the more similar the compression ratio of *COMP2* becomes and the MRs for different pressure drops become closer in value leading to the trend shown in figure 4.9. With more massflow also comes an increase in the cooling duty, but the dramatic increase in cooling duty in figure 4.11 also results from the re-compression. The more the gas has to be re-compressed, the hotter it is at the output of *COMP2*. A hotter gas needs less heating by the reacted gas thus increasing the temperature of stream *R-OUT2*. This increase in temperature reveals itself in the increase of cooling needed.

Recycle Ratio

The recycle ratio of the unit has a large influence on the size of the equipment as well as the production rate. The ratio is a result of the loss of mass due to the separation in the flash and the purge. Equation 4.13 shows how the ratio is obtained while figure 4.17 demonstrates the relation with the percentage of purge gas at the conditions stated in table 4.6.

$$RR = \frac{\dot{m}_{RECYCLE}}{\dot{m}_{SYN-IN}} = \frac{\dot{m}_{R-IN} - (\dot{m}_{CRUDEMEIO} + \dot{m}_{FEED-ME})}{\dot{m}_{SYN-IN}} \quad (4.13)$$

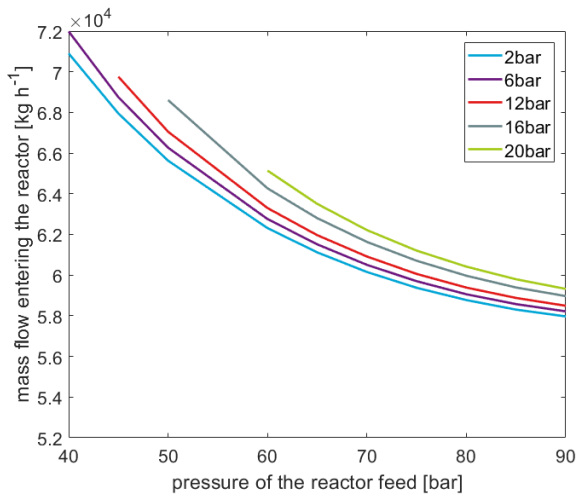


Figure 4.13: Influence operating pressure of the MRU on the mass flow into the reactor due to recycle at various pressure drops between the reactor inlet and the flash

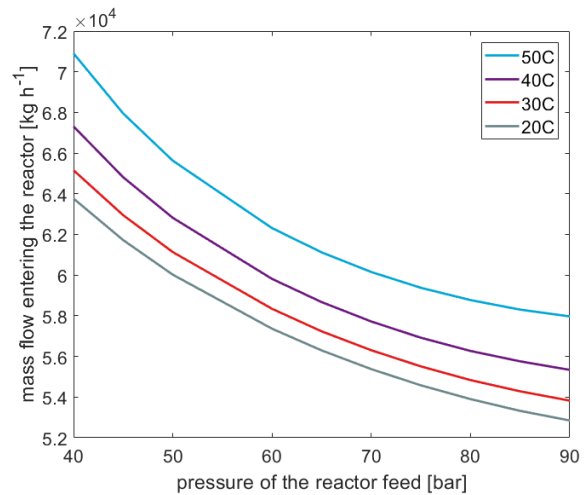


Figure 4.14: Influence operating pressure of the MRU on the mass flow into the reactor due to recycle at various flash temperatures

where $RR = \text{Recycle Ratio [-]}$

$\dot{m}_{RECYCLE} = \text{mass flow of the RECYCLE stream [kg h}^{-1}\text{]}$

$\dot{m}_{SYN-IN} = \text{mass flow of the SYN-IN stream [kg h}^{-1}\text{]}$

$\dot{m}_{CRUDEMEEO} = \text{mass flow of the CRUDEMEEO stream [kg h}^{-1}\text{]}$

$\dot{m}_{FEED-ME} = \text{mass flow of the FEED-ME stream [kg h}^{-1}\text{]}$

With a lower purge fraction comes a higher recycle ratio. A higher recycle ratio also leads to a higher methanol production as can be seen in figure 4.18

While a higher recycle ratio yields more methanol, it also requires more compressor work and more cooling. Figures 4.19 and 4.20 show the trade-off between gaining more methanol and requiring more energy. Both figures show an optimum for the given process conditions. Besides the energy requirements, the recycle ratio largely influences the size of the unit. For a recycle ratio of 3 a massflow of 20.77 t h^{-1} is recycled back into the reactor. This increases up to a massflow of 65.61 t h^{-1} for a recycle ratio of 9.4. Tripling the massflow not only increases the volume of the unit but also the investment costs. This has to be taken into consideration for the final optimisation.

4.2.4. Influencing Parameters

From the sensitivity analyses conducted in section 4.2.3 the major influencing parameters for the operation of the MRU can be identified. These parameters are the pressure of the reactor feed and the recycle ratio. Both have a large influence on flow rate, energy consumption and methanol production.

The other parameters are considered small influences. In none of the scenarios is a large pressure drop between the reactor and the flash favourable. Thus, the smallest pressure drop is chosen. Additionally, the temperature of the flash is preferred to be low as it reduces the flow rate that is being recycled. The limit on the temperature is given by the cooling system used for condensing the crudemethanol. The size of the reactor is influenced by the maximum velocity through the catalyst and the required

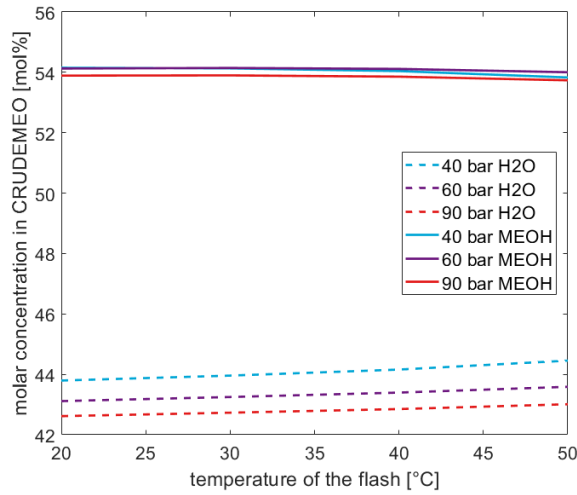


Figure 4.15: Influence of the flash's temperature on the composition of the CRUDEMEEO stream at various operating pressures of the MRU

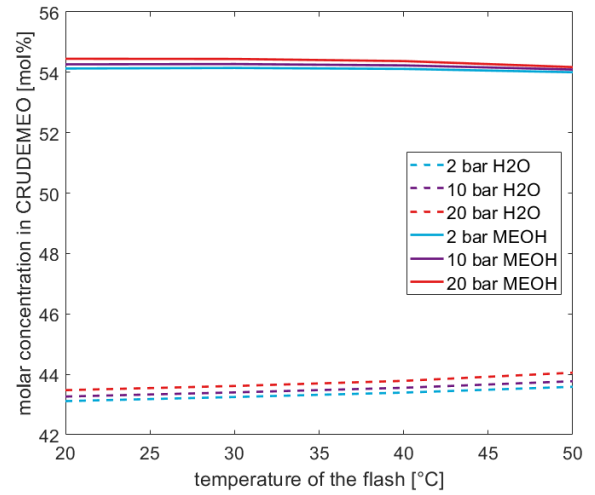


Figure 4.16: Influence of the flash's temperature on the composition of the CRUDEMEEO stream at various pressure drops between the reactor inlet and the flash at the MRU's operating pressure of 60 bar

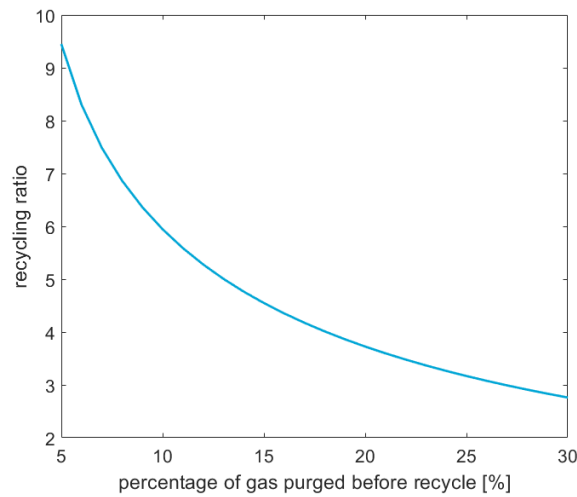


Figure 4.17: Value of the recycle ratio for the MRU at different percentages of purged gas

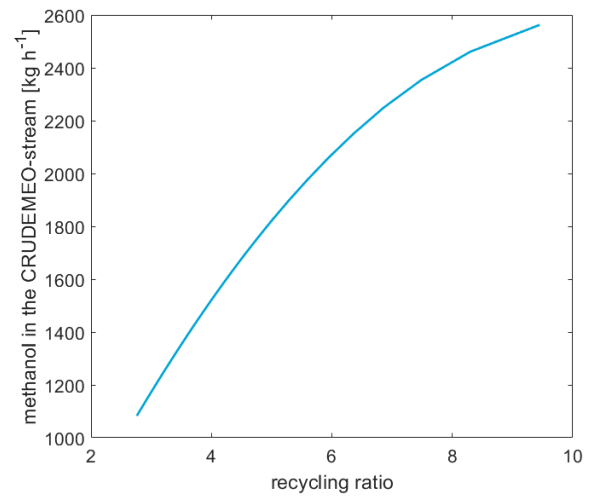


Figure 4.18: Influence of the recycle ratio on the methanol output of the flash

capacity and will be adjusted in the end.

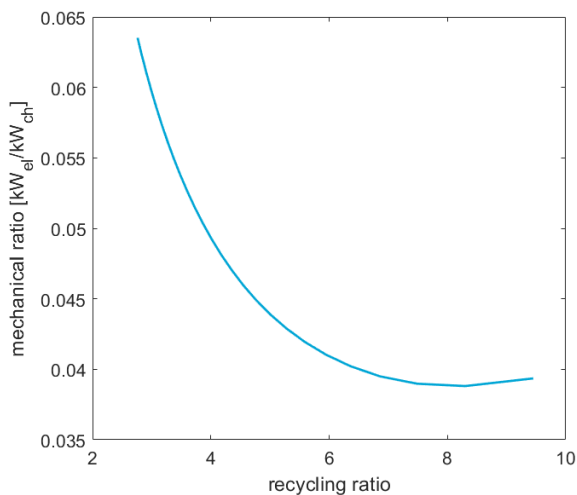


Figure 4.19: Influence of the recycle ratio on on the compressor work per lower heating value of methanol produced

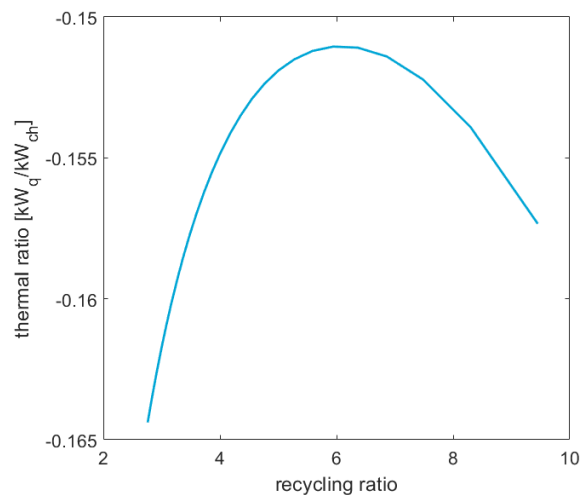


Figure 4.20: Influence of the recycle ratio on on the cooling duty per lower heating value of methanol produced

4.3. CO₂-Removal Unit

As method for the CO₂-removal the Selexol[®] process is chosen. It is one of the most mature technologies and its requirements of high partial pressure are fulfilled. This makes it more favourable than chemical absorption and other kinds of separation. In comparison with most applications of this process, the CO₂ does not need to be removed to very low fractions nor does it have to be entirely pure at the end of the process. This simplifies the process as the Selexol[®] can be regenerated in flashes rather than a distillation column.

4.3.1. Modelling

The process for the separation of CO₂ from the syngas stream operates with a closed loop for the solvent with flashes for the solvent regeneration. The syngas enters the absorption column at the bottom and exits it at the top. The absorption is done at high pressures while the liquid is relaxed during regeneration to release the absorbed gas. Figure 4.21 shows the process as simulated within Aspen Plus[®].

The lean solvent enters the absorber (*ABSORBER*) at the top and exits at the bottom enriched with CO₂ and other components of the gas. In the flash (*FLASHCCU*) the solvent is regenerated before a fraction of the regenerated solvent is purged in the splitter (*SPLITCCU*) to avoid a build-up of impurities. The remaining solvent is refilled with pure solvent to replace the purged amount and then pressurised in the pump (*PUMP*). Finally the solvent-stream is cooled in a chiller (*COOL-REC*) to have the right conditions for re-entry of the absorption column.

The compound Selexol[®] is modelled with the Aspen Plus[®] model for a CO₂ capture process. Using the *PC-SAFT* property method [91] and the experimental data from Polyethylene Glycol Dimethyl Ether (PEG DME) Aspen Technology developed a model to simulate the behaviour of Selexol[®] [92].

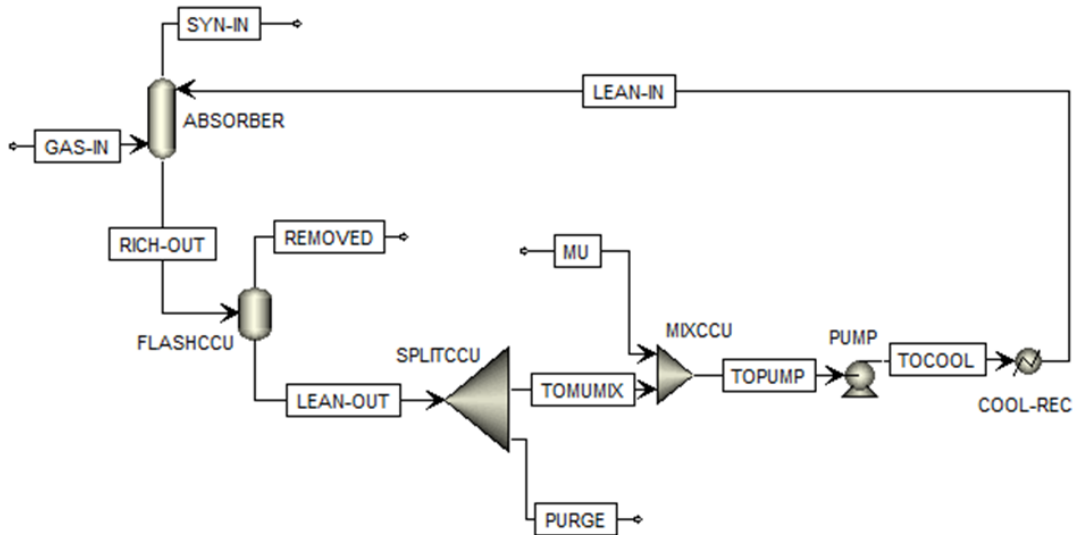


Figure 4.21: CO₂-removal unit (CRU) with the Selexol[®] process as the chosen technology. The split *Rec-Y-N* defines if the stream *F1-TOP* is being recycled into the distillation column or not.

4.3.2. Validation

A validation of the process is difficult, as the application is uncommon. No comparable data for a similar gas mixture and removal fraction could be found. The data for the solubility and properties of Selexol[®] have been compared to experimental data by Aspen Technology [92].

4.3.3. Sensitivity Analyses

The process as described in section 4.3 can be optimised by adjusting process conditions and operations. The following variables are determined to have the largest influence on the optimisation.

- Flowrate and composition solvent (*LEAN-IN*)
- Flowrate purge (*PURGE*) and make-up (*MU*)
- Operating pressure and cooling duties of the flashes (*FLASH1*) and (*FLASH2*)
- Pressure and temperature of the solvent stream (*LEAN-IN*) and absorption column (*ABSORBER*)

To get an idea of their influence on the performance of the process, a sensitivity analysis is performed. The comparison of the energetic efficiency is based on the power and thermal removal efficiencies of the process (η_{W,CO_2} and η_{Q,CO_2}) as described in equations 4.14 and 4.15:

$$\eta_{CO_2,P} = \frac{\sum P_i}{\dot{n}_{CO_2}} \quad (4.14)$$

$$\eta_{CO_2,Q} = \frac{\sum Q_i}{\dot{n}_{CO_2}} \quad (4.15)$$

where η_{CO_2} = CO₂ removal efficiency [kJ mol⁻¹]

P_i = power input [kW]

$$Q_i = \text{cooling input [kW]}$$

$$\dot{n}_{\text{CO}_2} = \text{removed CO}_2 \text{ [kmol h}^{-1}\text{]}$$

The starting values for this study are given in table 4.7. If not otherwise defined, the operation conditions and sizes listed in table 4.8 apply.

Table 4.7: Estimated feed compositions and properties from de Lathouder [10] as well as estimated compositions within the Solvent loop. The composition and flowrate are used for the first optimisation of CO₂-removal unit (CRU)

		CRU Input	Solvent Input	Solvent Mock-Up
Stream Name		<i>GAS-IN</i>	<i>LEAN-IN</i>	<i>MU</i>
Temperature	°C	33.69	10.00	25.00
Pressure	bar	31.95	30.00	3.50
Mass Flow	kg hr ⁻¹	11 914.0	190 800.0	18.6
Component Flow	kg hr ⁻¹			
H ₂		654.7	trace	-
CO		692.9	0.3	-
CO ₂		9204.3	3850.0	-
N ₂		119.2	trace	-
CH ₄		1228.0	3.1	-
WATER		14.8	6535.3	0.8
METHANOL		-	-	-
SELEXOL		-	636.2	17.8

Table 4.8: Base conditions and sizes used for the optimisation of the CRU for case 1 and case 2 respectively

Solvent stream	kg h ⁻¹	120 000
Pressure top stage <i>ABSORBER</i>	bar	31
Pressure <i>FLASHCCU</i>	bar	1
Pressure <i>PUMP</i>	bar	30
Temperature at <i>COOL-REC</i> output	°C	10
no compression of <i>GAS-IN</i> before column		

Solvent's Flowrate and Composition

The best case for this process would be a very pure solvent at a low flowrate. The first would improve the separation and absorption while the second would lead to a reduction of equipment size. To achieve a pure solvent, a good separation between the absorbed compounds and the solvent is necessary. Figure 4.22 and figure 4.23 show the p-xy-diagram for a binary mixture of Selexol[®] and water at 50 °C and the p-xy-diagram for a binary mixture of Selexol[®] and CO₂ at 12 °C respectively. The graphs show that a separation of Selexol[®] and CO₂ is possible at reasonable pressures and temperatures while it will require more extreme conditions (high temperatures and/or vacuum pressures) to separate the water from the Selexol[®].

The composition of the solvent is dependent on the purge rate and the regeneration of the solvent. After a thorough regeneration the solvent will be pure while it will still contain absorbed compounds if not regenerated completely. A complete regeneration would require a distillation column and possibly a drying unit. To keep the setup simple, only a flash is used. This results in a large amount of water staying absorbed within the solvent.

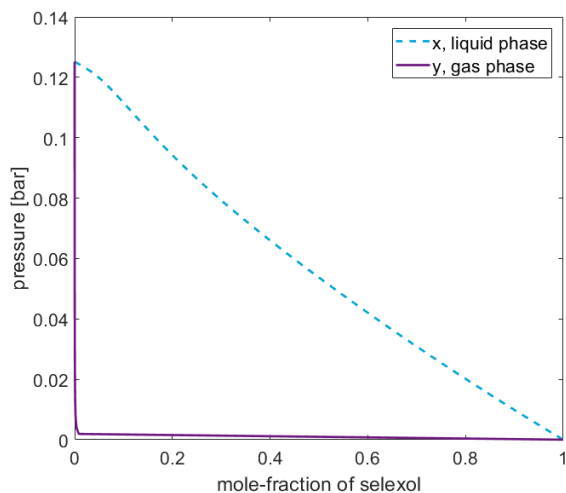


Figure 4.22: P-xy-diagram for a binary mixture of Selexol® and water at 50 °C

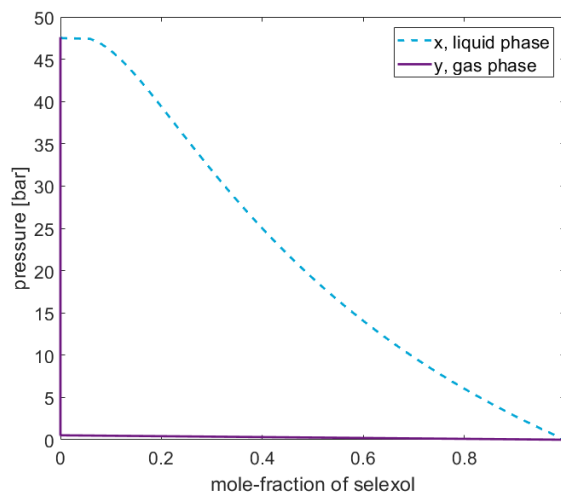


Figure 4.23: P-xy-diagram for a binary mixture of Selexol® and CO₂ at 12 °C

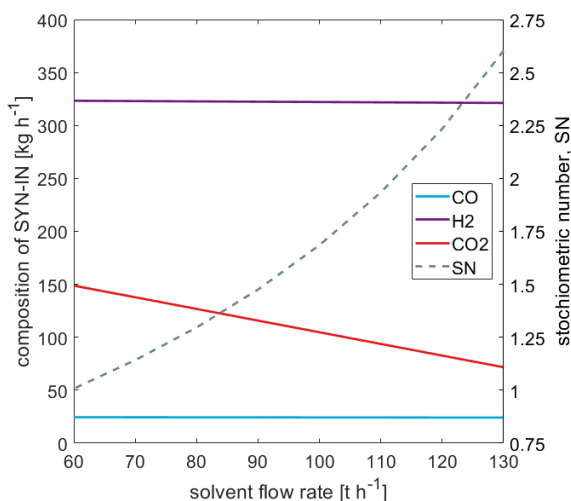


Figure 4.24: Composition of the SYN-IN stream after the absorber column with the resulting stoichiometric number, SN, for different solvent flowrates

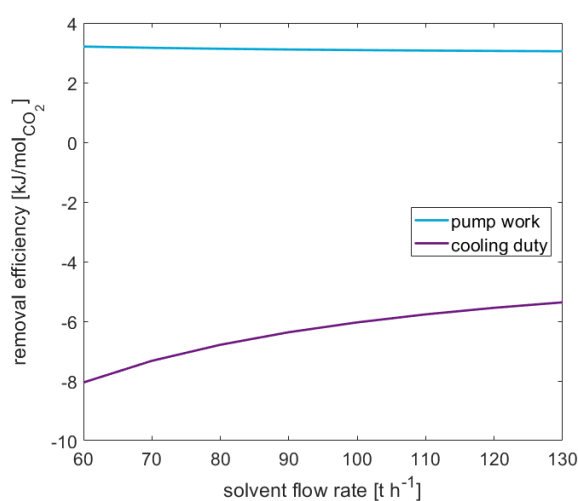


Figure 4.25: Energy requirement per removed CO₂ for the operation

The flowrate influences the amount of removed CO₂ as shown in figure 4.24 for an absorption pressure of 30 bar. More solvent leads to a higher removal of CO₂. Figure 4.25 shows the change in removal efficiency for the absorption process for different solvent flowrates in relation to the removed CO₂. The trend for power consumption and cooling duty both prefer a higher flowrate. Both observations together show, that a higher removal of CO₂ has a higher removal efficiency.

Flash operation

The FLASHCCU can be operated at different pressures and temperatures. As shown in figure 4.23 a pressure between 1 bar and 5 bar should lead to a high regeneration of the solvent. Figures 4.26 and 4.27 show the operation at different pressures. The main change that can be observed is the increase of CO₂ in the SYN-IN-stream as well as the decrease in removal efficiency for higher pressures within the FLASHCCU.

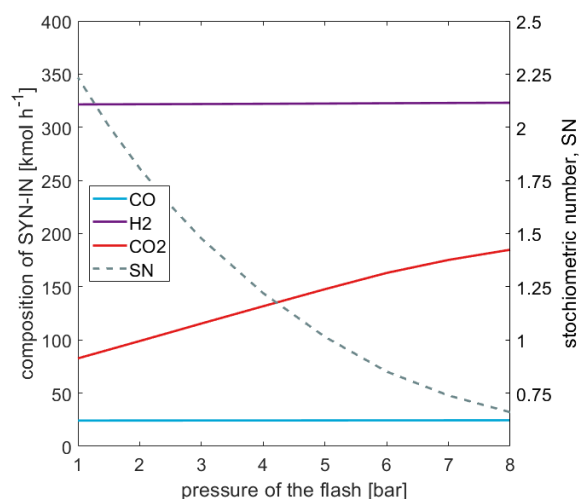


Figure 4.26: Composition of the *SYN-IN* stream after the absorber column with the resulting stoichiometric number, SN, for the operation of the flash at various pressures

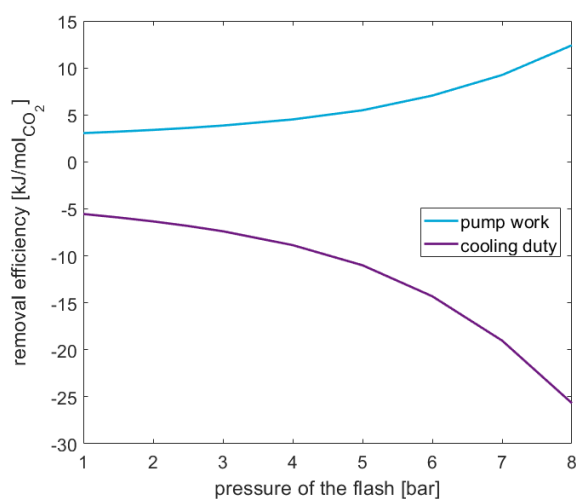


Figure 4.27: Energy requirement per removed CO₂ for the operation of the flash at various pressures

The lower power and thermal efficiencies for higher pressures in the *FLACHCCU* is due to lower regeneration. As shown in figure 4.23, the pressure has a large influence on the CO₂ content of the solvent. The more CO₂ is removed during regeneration the better the absorption within the column, as the solvent can absorb more before reaching equilibrium.

Operation of Absorber Column

The absorber column can be operated at different pressures and with different temperature feeds. Physical absorption favours low temperatures and high pressures. To achieve a higher pressure or a lower temperature within the column, additional equipment before the column is needed. Figure 4.28 and 4.29 show the behaviour of the process for different operating pressures of the column with the adjusted pump pressures. A higher pressure leads to a relatively higher absorption of CO₂ compared to the other compounds. However, it also leads to a higher total energy consumption for the process. The higher pressure of the *LEAN-IN* stream is not wasted as the following methanol production unit requires a high pressure.

Putting a compressor before the absorber column would require a cooler as well. The compression of the gas leads to an increase in temperature. This adds to the overall energy cost. Additionally, the next unit operation requires a high pressure as well as a high temperature. Therefore, this set-up needs to be examined closer for the overall optimisation. Next to the required cooler, the compressor might also exhibit problems during operation, as the gas could potentially still contain impurities that could harm the equipment. These impurities would be washed out in the column.

4.3.4. Influencing Parameters

From the sensitivity analyses the different influencing parameters are judged and identified. A very small purge and make-up stream is favoured, as it reduces the operating costs of the process. The possibility of no purge and make-up but rather an intermittent exchange of the solvent bulk could be considered.

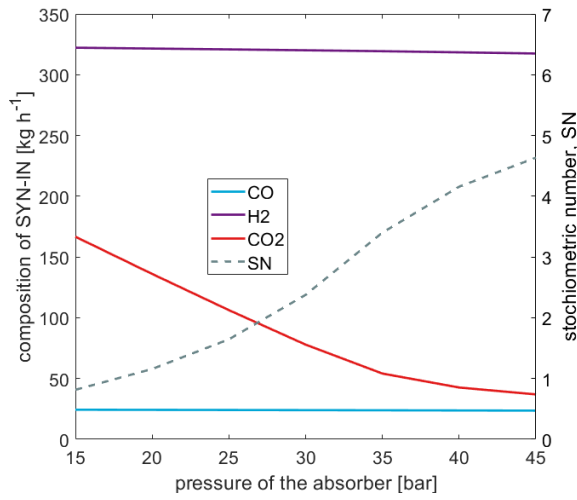


Figure 4.28: Composition of the *SYN-IN* stream after the absorber column with the resulting stoichiometric number, SN, for different operating pressures of the absorber

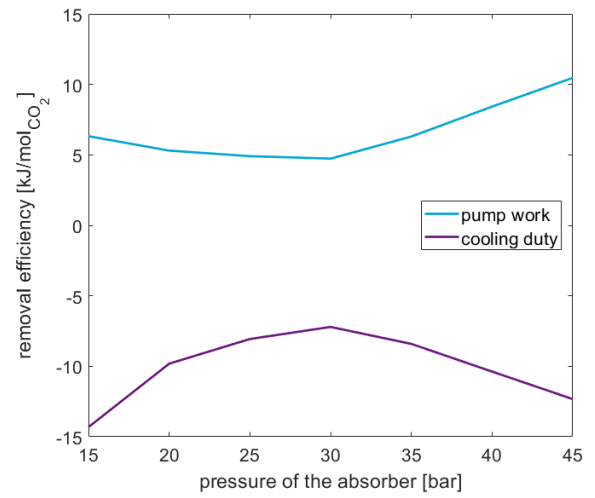


Figure 4.29: Energy requirement per removed CO₂ for different operating pressures of the absorber

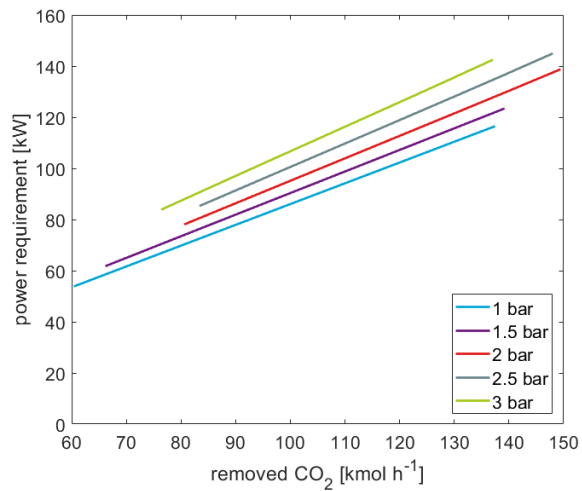


Figure 4.30: Power consumption of the CRU over the amount of removed CO₂ for various *FLACHCCU*-pressures

The pressure within the flash has a large influence on the removal efficiencies. The regeneration of the solvent increases with lower pressures. This means, that for lower pressures, less solvent is required. The energy requirement of the *PUMP* depends more on the throughput than on the pressure increase. However, lower flowrates have shown to decrease removal efficiencies. Figure 4.30 combines the influence of the flowrate as well as the pressure of the flash by comparing the amount of removed CO_2 and the required power input. It can be observed, that the influence of the regeneration pressure is higher than that of the improved removal efficiency for high flowrates.

The energy consumption of the process is lowest for an operation at 31 bar in the case of separate operation. As discussed above, integrating the CRU into the whole MSU can result in a different point of lowest energy consumption. However, the before mentioned problems with impurities within the gas can become problematic for the compressor.

4.4. Hydrogen-Recycle

A membrane was chosen to recycle the hydrogen from the *FEED-ME* stream back into the system. The need for a separation unit derives from two factors; First, the purge gas contains a lot of hydrogen. As hydrogen is the restricting quantity within this process, it is favourable to capture and recycle as much as possible. Second, the purge stream contains high quantities of inert gases for the methanol formation (CH_4 , N_2). These gases increase the volume of the methanol reactor unit but do not increase the production. This leads to the need of a separation unit to separate the hydrogen from the inert gases.

A membrane is a simple separation unit that requires little maintenance, is easy to set-up and relatively cheap. For the separation unit within this thesis a non-porous, polymer membrane was chosen as they show high selectivity for $\text{H}_2 - \text{CH}_4$ and $\text{H}_2 - \text{N}_2$ separation.

4.4.1. Modelling

To model the membrane in Aspen Plus[®], a *USER2*-Module was chosen and connected to an Excel calculation sheet. The set-up of the unit is shown in figure 4.31 where the *FEED-ME* is the stream purged from the MRU and *FEED2* is the input stream on the permeate side. The modelling is based on the assumption that the transport through the membrane is dictated by the solution-diffusion mechanism. The mechanism consists of 5 steps:

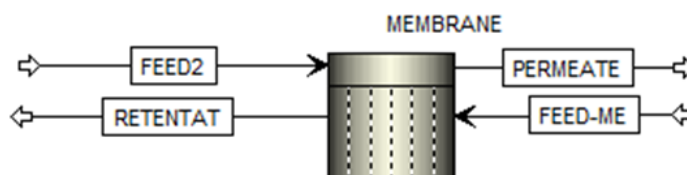


Figure 4.31: H_2 -recycle unit (HRU) with the membrane, modelled as a *USER2*-Module, and the feed and product streams

1. adsorption of the gas at the feed side of the membrane
2. solution of gas into the membrane

3. diffusion of the gas through the membrane
4. de-solution of the gas from the membrane
5. desorption of the gas from the membrane at the permeate side

The model used in this report is based on Kohl and Nielsen [62], who simplified the mechanism. They assumed that the concentration of the gas at the surface of the membrane is directly proportional to the partial pressure within the gas. This assumption is expressed through Henry's law, (see eq. 4.16). Additionally, it was assumed, that the transport through the membrane is driven by the concentration gradient within the membrane expressed through Fick's law for diffusion (see eq. 4.17).

$$c_i = k_i p_i \quad (4.16)$$

$$J_i = -D_i \frac{dc_i}{dx} \quad (4.17)$$

where c_i = local concentration of i on the membrane's surface [kmol m^{-3}]

k_i = solubility coefficient of i [$\text{kmol m}^{-3} \text{Pa}^{-1}$]

p_i = partial pressure of i in the gas [Pa]

J_i = flux of i through the membrane at steady state [$\text{kmol s}^{-1} \text{m}^{-2}$]

D_i = local diffusivity of i [$\text{m}^2 \text{s}^{-1}$]

x = distance through the membrane [m]

Combining these two equations for a parallel flow membrane Kohl and Nielsen [62] obtain equation 4.18 which gives the relation between the steady state flux expressed in the permeation rate R_i and the driving force, the partial pressures of component i on the feed and permeate side. This expression can be rewritten as eq. 4.19 for an increment of the membrane area ΔA considering ideal gas.

$$J_i = R_i (p_{i,feed} - p_{i,perm}) \quad (4.18)$$

$$M_{i,j} = R_i (y_{i,feed} \pi_{feed} - y_{i,perm} \pi_{perm}) \Delta A_j \quad (4.19)$$

where R_i = permeation rate of i [$\text{kmol m}^{-2} \text{s}^{-1} \text{Pa}^{-1}$]

y_i = mole fraction of i [-]

$M_{i,j}$ = flow rate of i through the increment j [kmol s^{-1}]

π = absolute pressure of stream [Pa]

ΔA = increment of membrane area [m^2]

The membrane used for hydrogen separation in this model is an asymmetrical polymer membrane. The active layer of the membrane is very thin and on top of a porous substrate. This means that the partial pressure of the permeate side of the active layer is effectively the partial pressure of the flow through the membrane, rather than the partial pressures of the permeate's bulk flow. With the effective mole fraction of the permeate as:

$$y_{i,j,perm} = \frac{M_{i,j}}{\sum_i M_{i,j}} \quad (4.20)$$

Equation 4.19 can be rewritten as:

$$M_{i,j} = \frac{R_i \Delta A y_{i,feed} \pi_{feed}}{1 + \frac{R_i \Delta A \pi_{perm}}{\sum_i M_{i,j}}} \quad (4.21)$$

To calculate the feed and permeate gas composition the flux has to be deducted from the feed bulk flow and added to the permeate bulk flow.

$$O_{i,j+1} = O_{i,j} + M_{i,j} \quad (4.22)$$

$$N_{i,j+1} = N_{i,j} - M_{i,j} \quad (4.23)$$

where $O_{i,j}$ = bulk flow of i in the increment j of the permeate [kmol s^{-1}]

$N_{i,j}$ = bulk flow of i in the increment j of the feed/retentate [kmol s^{-1}]

All the values within these equations are known, except for the total mass flow through the membrane for each increment. Therefore an iteration has to be performed. This iteration is started with an estimation of $M_{i,1} = M_{i,est}$ for the first increment and every following increment takes the previous flow as a first estimate.

$$M_{i,est} = R_i y_{i,feed} \frac{\pi_{feed} - \pi_{perm}}{2} \Delta A \quad (4.24)$$

Figure 4.32 shows the flows calculated within this model for one increment of membrane area.

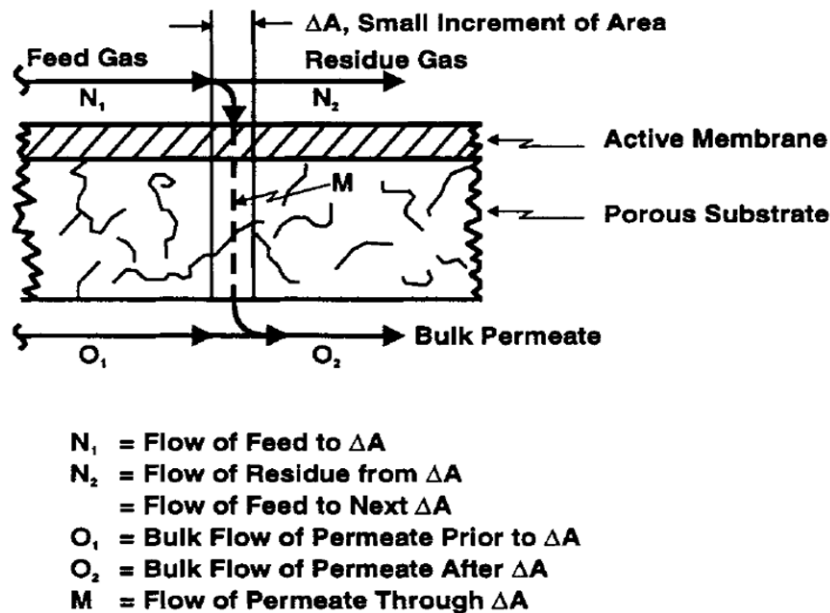


Figure 4.32: Diagram of the model by Kohl and Nielsen [62] used in this report. The flow directions of each flow are presented.

4.4.2. Sensitivity Analyses

The two main influencing parameters on the operation of the membrane, that can be modelled with the introduced mechanism, are the pressure of the feed and the size of the membrane. The pressure

Table 4.9: Permeation rates for each component [93]

Component	Permeation Rate	
	$\text{cm}^3_{\text{STP}}/(\text{cm}^2 \text{ s cmHg})$	$\text{kmol}/(\text{m}^2 \text{ s Pa})$
H ₂	5×10^{-4}	16.51×10^{-8}
CO	9×10^{-6}	0.30×10^{-8}
CO ₂	1.2×10^{-4}	3.96×10^{-8}
N ₂	6×10^{-6}	0.20×10^{-8}
CH ₄	4×10^{-6}	0.13×10^{-8}
H ₂ O	1.8×10^{-3}	59.45×10^{-8}
MeOH	assumed negligible	

increases the driving force of the permeation while the size increases the area of the flux, thus increasing the total flow through the membrane. The values used for the analysis of the membrane performance are taken from de Lathouder [10] and presented in table 4.10.

Table 4.10: Estimated feed compositions and properties from de Lathouder [10]. The composition and flowrate are used for the first optimisation of the membrane

Stream Name		FEED-ME	FEED2
Temperature	°C	50	30
Pressure	bar	85.1	32
Mole Flow	kmol hr^{-1}	232.36	109.90
Component Flow	kmol hr^{-1}		
H ₂		110.07	48.76
CO		8.05	4.94
CO ₂		31.63	40.38
N ₂		4.21	0.81
CH ₄		76.06	14.86
WATER		0.51	0.16
METHANOL		1.82	-

The influence of the size on the performance of the membrane is presented in figure 4.33. With increasing size the fraction of flow permeated from the *FEED-ME*-stream increases. The fraction of permeated H₂, CO₂, and H₂O increases quickly and then slows down for larger areas. This is due to the decrease of partial pressure of the component. For small areas, the partial pressure of hydrogen over the whole length of the membrane is very high due to the high molar stream, but with increasing size, the partial pressure decreases and thus the flux decreases. The much faster permeation of H₂, CO₂ and H₂O compared to the other components is due to their high permeation rate (table 4.9). They are between one to two magnitudes larger. Additionally, due to the simplified model, the partial pressures of each component on the permeate side have been neglected which results in a *FEED2* independent permeation stream. Through experiments it needs to be checked if this is an accurate simplification or not.

A similar effect can be observed for a fixed membrane area of 3.5 m² and changing feed pressures as displayed in figure 4.34. Lower pressures result in smaller driving forces, thus a smaller flow and smaller permeation fractions. The graph shows that the membrane is oversized for high pressures. While nearly all H₂, CO₂ and H₂O has permeated, only the other gases are increasing their permeation fraction. This effect is to be avoided as the aim of the unit is to recycle as much H₂ while rejecting N₂ and CH₄.

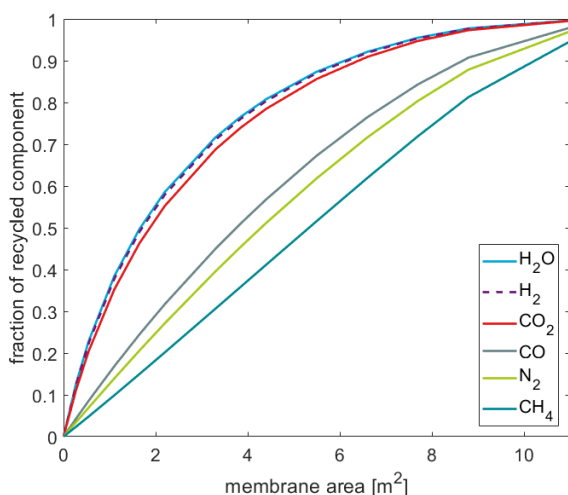


Figure 4.33: Fraction of the component flow in the *FEED-ME*-stream that permeated through the membrane over the membrane size

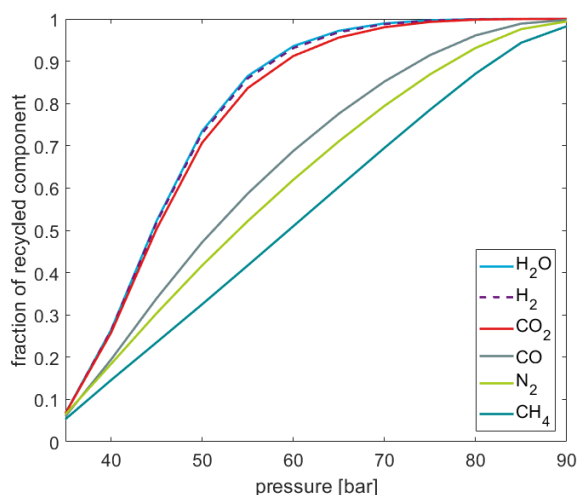


Figure 4.34: Fraction of the component flow in the *FEED-ME*-stream that permeated through the membrane over the pressure of the *FEED-ME*-stream for a membrane size of 3.5 m^2

One issue of the sizing of the membrane in the presented model is the neglect of the geometry of the membrane. The geometry of the unit influences the velocity of the flow which in turn influences the pressure drop over the membrane through the flow-regime. Assuming the same velocity, the accuracy of the model decreases, as the deviation from the actual pressure increases. Additionally, no adjustment of the permeation-rate for different temperatures has been included. The temperature of the gas has a large influence on the permeability of the membrane material. The values given in table 4.9 are for gases at 60°C . It is assumed, that they apply for the given temperature range presented here.

4.4.3. Influencing Parameters

For the following determination of the operating conditions and equipment design, the membrane will not be factored in. The cost of the unit is one of the main influences on the sizing of the membrane, it is not sensible to optimise the HRU based on energetic qualifiers. However, the estimate given by de Lathouder [10] gives a base for the possible size. This size will be used for all following analyses of the system.

4.5. Full Methanol Synthesis Unit

The complete methanol synthesis unit is realised by connecting the in- and output of the individual units as depicted in figure 4.1 (simplified) and in the flowsheet diagrams in appendix A (detailed). To find a point of operation for this unit, the process is simplified by not considering a cooling system or a heat-exchanger network. The latter is due to the framework of this thesis. The operation of the previous units and following units are not analysed which makes the creation of a heat-exchanger network impractical. Nevertheless, the cooling system can be approximated by replacing the two *FLASH*-components with heat-exchangers.

The heat-exchangers within the process are first neglected during the simulation. This includes especially the cooling of the flows within the flashes and after compression. After finding a suitable operation point, the flashes and the cooler are replaced by heat-exchangers with a cooling flow of water at 25 °C. This flow is then used to estimate the size of the required heat-exchanger equipment.

5

Evaluating the Cases

The different unit operations described in chapter 4 are put together to find the best solutions for the applications of this process. The first case looks at the process in its base setting, without any hydrogen integration from the outside. The second case operates under the condition of a constant hydrogen integration while the last case looks at a varying amount of hydrogen.

The application for the different cases is the integration of the biomass to methanol process with a renewable energy source. This energy source produces the electricity that in turn produces the hydrogen. As renewable energy sources vary in their production rates, a combined process must be able to produce methanol without additional hydrogen as well as maximum addition. The differences between the three cases are listed in table 5.1. It is assumed that the power for the hydrogen supply is produced through photovoltaic modules. As they depend on solar irradiation, there will not always be power available. The intermittent nature of photovoltaic power generation necessitates, that the process plant can operate at different hydrogen supply levels. These levels are simplified for the analysis of the system. It is assumed that the average production of hydrogen over one day can be represented through three periods (see figure 5.1).

Period 1 12 h of no additional hydrogen and the CRU runs at full capacity

Period 2 2 x 3 h of enough hydrogen to turn down the CRU-operation to its minimum capacity

Period 3 6 h of excess hydrogen, the CRU runs at minimum capacity and CO₂ is added to the process

The additional CO₂ in Period 3 comes from period 1 where CO₂ had to be removed to achieve a reasonable feed to the reactor. It is assumed that all removed CO₂ from Period 1 is inserted back into the process during Period 3.

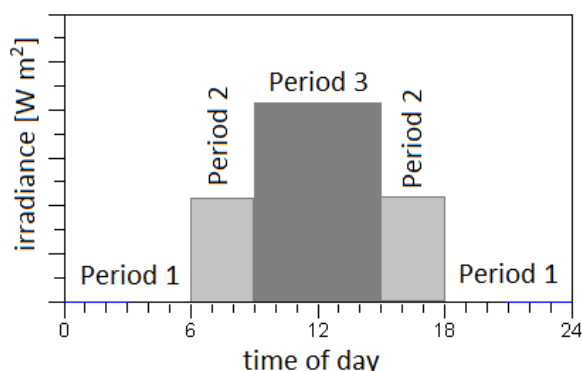


Figure 5.1: Simplified depiction of the solar irradiation during the different production periods

Table 5.1: Case overview

	Case 1	Case 2	Case 3
	Period 1	Period 2	Period 3
Length of Period	12 h	6 h	6 h
H ₂ integration	No	Yes	Yes
CO ₂ integration	No	No	Yes
CRU capacity ^a	100 %	15 % ^b	15 % ^b

^a defined by the flowrate of the solvent

^b value set through convergence limitations of Aspen Plus®

From the previous chapter the variables chosen for the optimisation of the process are:

1. Operating pressure of MRU
2. Purge fraction
3. Flowrate of Selexol® in the CRU
4. Flowrate of additional hydrogen

The size of the reactor has little influence on the process as long as the equilibrium is achieved. This means, that during the process of finding the operation conditions for each case, the reactor is oversized to not influence the results. Thus, after having decided on the operation point, the reactor is sized. For the integration of hydrogen produced by an external source, the conditions of the generation needs to be known. The chosen technology is a PEM electrolyser with an output of hydrogen at 30 bar and 25 °C and a power consumption of 64.5 kWh_{el} kg⁻¹ [94]. There are two positions for the integration of hydrogen into the process.

First, after the column before the compression to the final operating pressure of the methanol reactor unit. A potential advantage is the increased flowrate through the compressor which should increase the polytropic efficiency of the compressor [36].

Second, after the compression of the first compressor of the MRU. For this, the hydrogen has to be compressed before adding it to the process. This integration would require little change in the sizing of the first compressor, however, additional equipment for compression is required.

5.1. Case 1 - No Hydrogen Integration

The case without any hydrogen integration is the base case. The model developed in chapter 4 is calibrated to match the estimated operation condition by de Lathouder [10]. These operation conditions are listed in table 5.2. Using the same sized membrane, the operation is analysed for the above mentioned variables.

Figure 5.2 and 5.3 show the influence of the solvent flowrate and operating pressure on the mechanical ratio and thermal ratio and on the stoichiometric number. It can be observed, that the flowrate has a much smaller influence than the operating pressure. Choosing a flowrate of around 115 000 kg h⁻¹ to

Table 5.2: Operating variables for the operation similar to the first estimate by de Lathouder [10]

<i>MEMBRANE</i> Area	m ²	0.275
Output Pressure <i>COMP1</i>	bar	85.1
Output Pressure <i>COMP2</i>	bar	87.8
Pressure <i>FLASHCCU</i>	bar	1
Temperature <i>COOL-REC</i>	°C	10
Temperature <i>COOLER</i>	°C	86
Temperature <i>FLASH</i>	°C	50
Purge fraction	%	11
Temperature of <i>R-OUT1</i> at output of <i>HX1</i>	°C	230
Temperature of <i>R-IN</i> at output of <i>HX2</i>	°C	206

achieve a stoichiometric number of around 2 leads to figures 5.4 to 5.6 for effect of operating pressure and recycle ratio on the process.

While the mechanical and thermal ratio favour a low pressure, the production and flowrate of the streams become less favourable for those conditions. Figure 5.5 shows the influence of the recycle fraction and operating pressure on the production of methanol. The observations here correspond with the modelling of the single methanol reactor unit (MRU). For a higher flowrate less is produced.

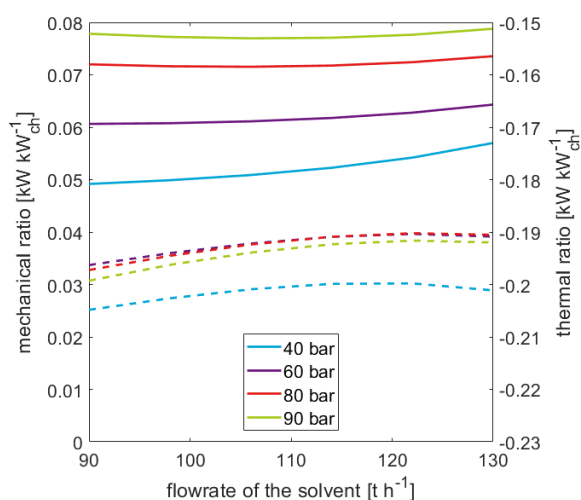


Figure 5.2: CASE1: mechanical ratio (MR) (continuous line) and thermal ratio (TR) (dashed line) over the solvent flowrate for various MRU operating pressures and a recycle fraction of 0.89

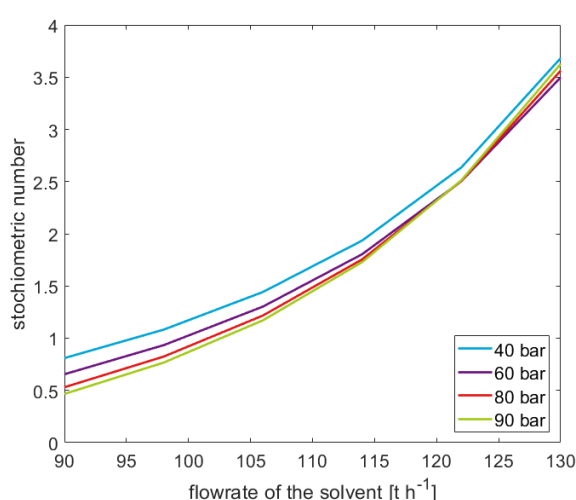


Figure 5.3: CASE1: Stoichiometric number of the reactor feed over the solvent flowrate for various MRU operating pressures and a recycle fraction of 0.89

The influence of the membrane on the process has been analysed and presented in figure 5.7 and 5.8 to determine the importance of the unit. Energetically, a smaller sized membrane is reasonable. Figure 5.8 shows that with an increased membrane area the production increases. However, the increase in required compression work outweighs the increase in production for large membranes. However, a small unit is feasible as it recycles the reaction determining hydrogen. Without a membrane, 40.5 % of the hydrogen will be lost. If no membrane is used, the input flow into the system will have less hydrogen but also less CO₂ because a side effect of the process is the permeation of CO₂. Without a membrane, a lot less CO₂ will have to be removed, which reduces the energy requirement of the process.

The purpose of the membrane was to recycle hydrogen while keeping the inert gases within the *FEED-*

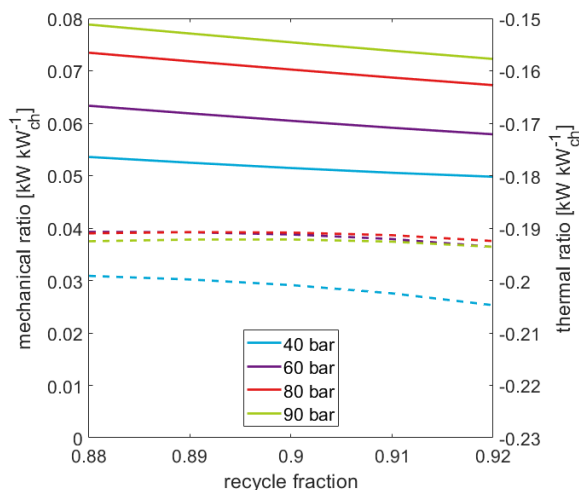


Figure 5.4: CASE1: mechanical ratio (MR) (continuous line) and thermal ratio (TR) (dashed line) over the recycle fraction for various MRU operating pressures and a solvent flowrate of $115\,000\text{ kg h}^{-1}$

ME-stream. With increasing size the amount of CO_2 permeating through the membrane increases. This influences the stoichiometric number of the gas entering the reactor. To counteract this trend a higher solvent flowrate would be required which would increase the energy requirement of the process.

5.1.1. Operating point

There is no clear best operation option for Case 1 as it is energetically most favourable to operate at low pressures with a low purge fraction and low CO_2 -removal. This results in high volumetric flowrates and a low stoichiometric number. The high volumetric flowrates result in large equipment sizes needed which generally increases CAPEX cost. The volumetric flow rate increases by 50 % for a process operated at 40 bar rather than 60 bar. The mass flowrate through the reactor does not change for different operating pressures either because at high pressures more methanol is produced and extracted from the process. Simultaneously, the higher pressure results in a much high permeation in the membrane and thus a larger *SYN-IN*-stream.

A decision based purely on the MR and TR is misleading as the energy is only one part of the production cost. This is why a minimum production mass flow of 1875 kg h^{-1} is set as a goal as well as a recycle ratio of below 5.

A production of methanol at an operating pressure above 60 bar requires more than one compressor due to the constraints of centrifugal compressors. Their pressure ratio is limited to around 2 [36]. Thus higher operating pressures, which produce higher quantities, are ignored due to their high energy ratios and the needed additional equipment. At low operating pressures, the production cannot reach the desired production volume.

Table 5.3 lists the operating conditions of the chosen process including the MR, TR and selected equipment size. The process' flows are listed in tables B.1 to B.3 in appendix B. The flowsheet depicting the process can be seen in figure A.1 in appendix A.

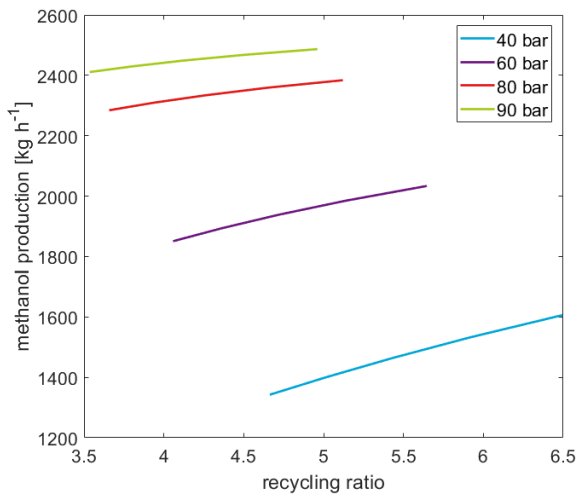


Figure 5.5: CASE1: produced methanol in the *CRUDEMEO*-stream over the recycle ratio for various MRU operating pressures and a solvent flowrate of $115\,000\text{ kg h}^{-1}$

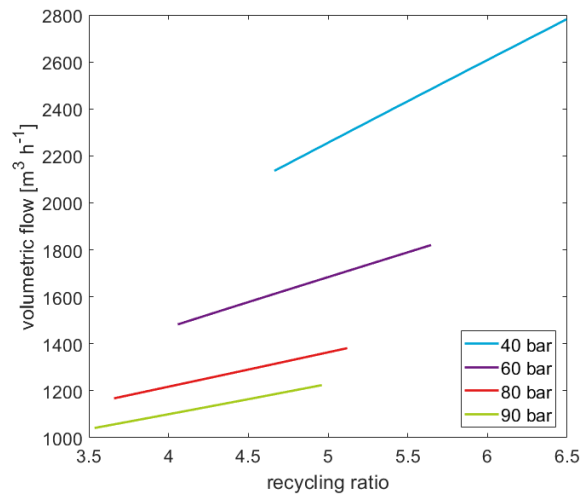


Figure 5.6: CASE1: volumetric flowrate of the reactor feed over the recycle ratio for various MRU operating pressures and a solvent flowrate of $115\,000\text{ kg h}^{-1}$

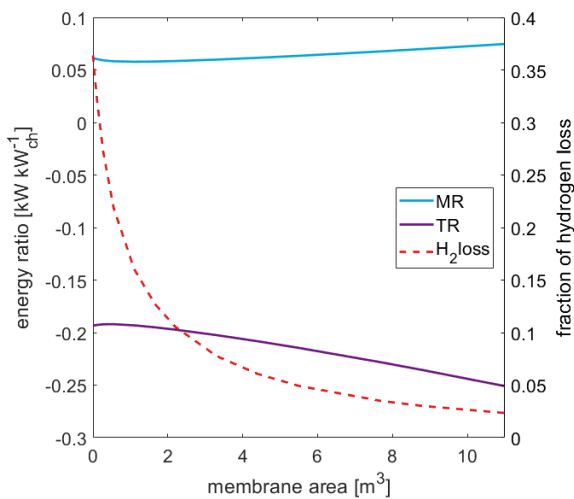


Figure 5.7: CASE1: mechanical ratio (MR), thermal ratio (TR) and the fraction of hydrogen loss over the membrane area at an operating pressure of 60 bar and a solvent flowrate of $115\,000\text{ kg h}^{-1}$

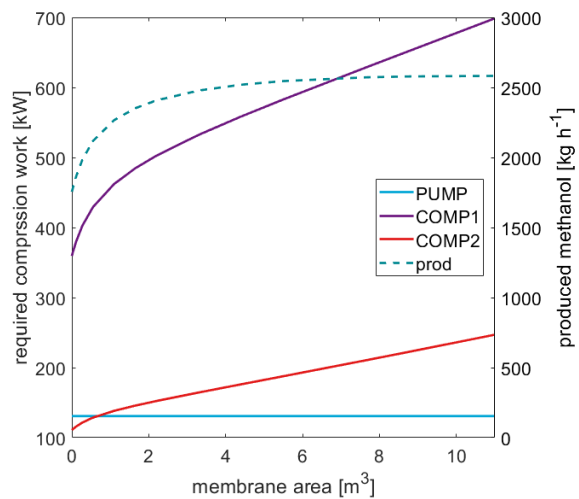


Figure 5.8: CASE1: compression work of the three pressure changers and the total flowrate of methanol in the *CRUDEMEO*-stream over the membrane at an operating pressure of 60 bar and a solvent flowrate of $115\,000\text{ kg h}^{-1}$

5.2. Case 2 - Constant Hydrogen Integration

In the case of constant hydrogen integration, the system is set up to turn down the CO_2 -removal unit to a minimum flowrate which is assumed to be 15% of Case 1. With the operating point of Case 1, an analysis of the influence of hydrogen integration into the process is conducted. The amount of hydrogen addition does not only influence the production of methanol but also the energy ratios and the loss of hydrogen through the purge stream.

While the production of methanol is not influenced by the path of integration, it increases drastically with increasing hydrogen addition. Figure 5.9 shows the 150% increase in methanol production for an supply of 350 kmol h^{-1} of hydrogen compared to no supply. The small difference between the two paths of integration results from the set up of the compressors. The set up with the integration within the MRU cools the hydrogen before entering it into the process. This results in a slightly lower mechanical

ratio as the feed for the second compressor is slightly colder. The thermal ratio is not affected as the cooling is little compared to the other cooling duties.

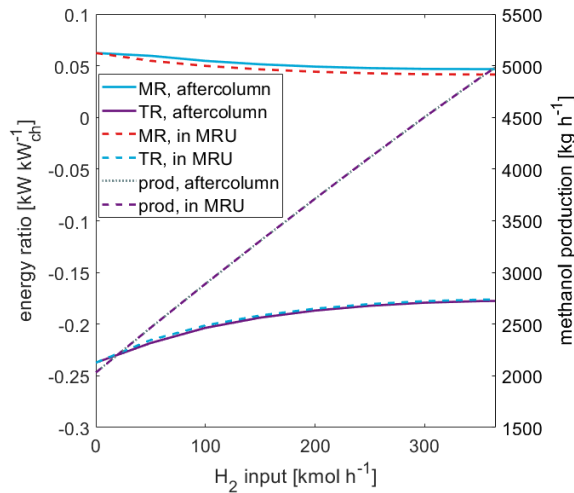


Figure 5.9: CASE2: mechanical ratio and thermal ratio as well as methanol component flow in the *CRUDEMEQ*-stream for various hydrogen inlet flows

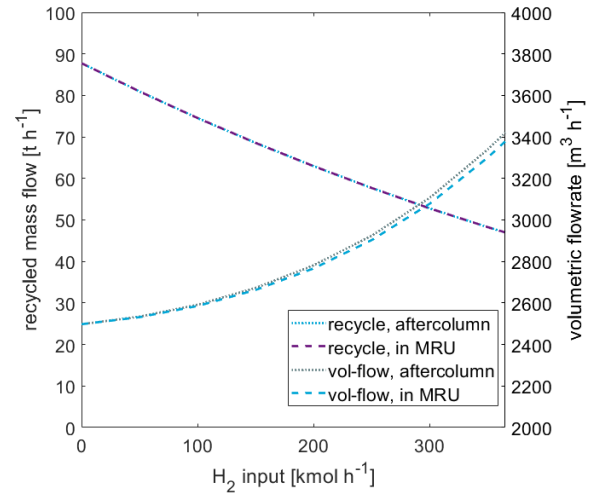


Figure 5.10: CASE2: recycled mass flow and volumetric flow entering the reactor for various hydrogen inlet flows

To find an operating point, the shared equipment between this case and the base case needs to be examined. For operational but also economical reasons, the process should not be dramatically larger than the base case. The volumetric flowrate entering the reactor was set to increase by two thirds. Case 1 has a volumetric flowrate of 1723 m³ h⁻¹, thus the volumetric flowrate of this process should be around 2870 m³ h⁻¹. This is achieved with a hydrogen input of 240 kmol h⁻¹. The characteristics of this operating point are listed in table 5.3 with the flows of the system listed in tables B.4 to B.7 in appendix B. The flowsheet picturing the process can be seen in figure A.2 in appendix A.

5.3. Case III - Varying Hydrogen Integration

During a period of over production of hydrogen, additional CO₂ can be added to the process. This addition is taken from the removed gas in the CRU in Case 1. As Period 1 is twice as long, the added CO₂ stream is equal to around twice the removed flowrate. With a flowrate of 223 kmol h⁻¹ and a CO₂ mole fraction of 0.943, the process requires higher hydrogen flowrates. The process is evaluated for a hydrogen input of up to 870 kmol h⁻¹ which equals a stream with a stoichiometric number of 3.15.

The trends of this case are similar to case 2. Figure 5.11 shows the decreasing energy ratios for higher hydrogen inflows and figure 5.12 shows the increasing volumetric flow rate while the recycled mass flow decreases. Similar to Case 2, the production increases by up to 150 % from the lowest to the highest hydrogen input.

Case 3 also has a small energetic difference between the integration in the MRU and after the column. The decision for the integration path is therefore not energetically driven but should be driven by economic and operating constraints, similar to Case 2.

Parallel to Case 1, the operating point is defined through the volumetric flowrate. The flowrate is considerably higher than the base case due to the addition of the CO₂. To find an operating point, the

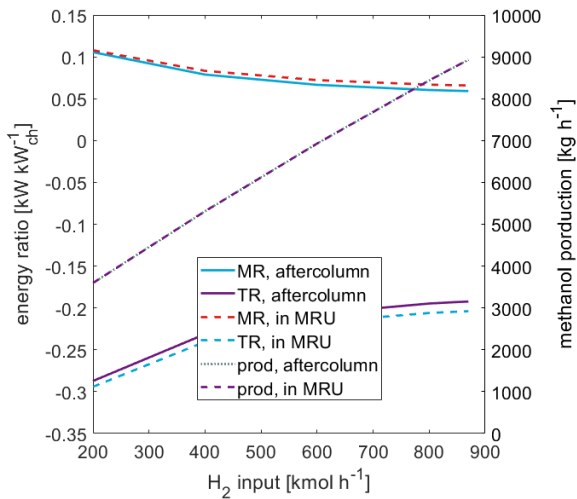


Figure 5.11: CASE3: mechanical ratio and thermal ratio as well as methanol component flow in the *CRUDEMEO*-stream for various hydrogen inlet flows

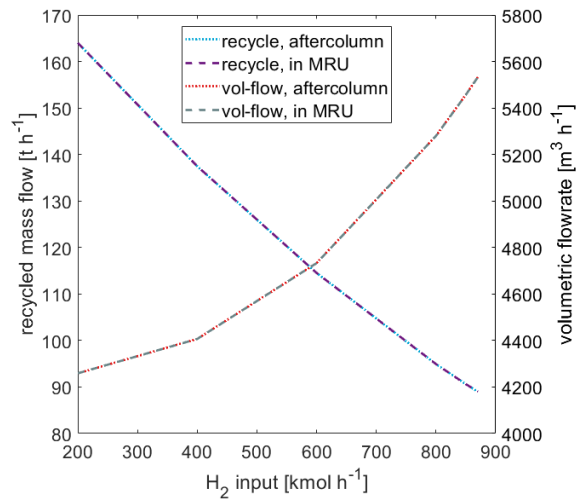


Figure 5.12: CASE3: recycled mass flow and volumetric flow entering the reactor for various hydrogen inlet flows

flowrate of case 1 is set to not be less than 35 % of the flowrate of this case. This leads to a maximum flowrate of $4923 \text{ m}^3 \text{ h}^{-1}$. To achieve the best energy ratios, a high hydrogen flowrate is desired. The operation with a hydrogen input of 680 kmol h^{-1} fulfils the requirement. The characteristics of this operating point are listed in table 5.3 with the flows of the system in tables B.8 to B.11 in appendix B. The flowsheet picturing the process can be seen in figure A.3 in appendix A.

5.4. Comparison

When comparing the characteristics of the cases in table 5.3 certain aspects stand out.

The amount of methanol produced by the different cases increases with increasing hydrogen addition. This was to be expected as more of the supplied CO_2 can be utilised for Case 2 and Case 3. Additionally, the streams increase in mass as more gas is delivered to the system. The increase in mass results in an increase of the reactor size. A larger volume is required to reach equilibrium as more catalyst surface is needed.

The stoichiometric number (SN) and the carbon ratio of CO_2 to CO become less favourable for Case 2 and Case 3. To achieve a comparable SN to Case 1, a very large amount of hydrogen would have to be added to the process which would increase the volumetric flowrate and power demand considerably. The carbon ratio of the reactor feed increases through the cases, this is a result of the constant CO content but increasing CO_2 content. This causes the low output temperatures of the reactor as the hydrogenation of CO_2 is less exothermic than of CO. In Case 1, the fraction of inert gas is much higher than for the other cases. leading to a smaller temperature rise.

Another effect of the high carbon ratio is the concentration of methanol in the *CRUDEMEO*-stream. In the flash, the condensable gases are separated from the non-condensable gases. The major components in the liquid fraction are water and methanol. A high carbon ratio increases the amount of water produced during hydrogenation. This increase in produced water is visible in the mole fractions of methanol and water within the product stream. The higher the fraction of water is, the more heat

Table 5.3: Characteristics of the processes from case 1 to 3

		CASE 1	CASE 2	CASE 3
Pressure <i>COMP1</i>	bar	60	60	60
Pressure <i>COMP2</i>	bar	62	62	62
Pressure <i>FLASH</i>	bar	60	60	60
Temperature <i>FLASH</i>	°C	50	50	50
Pressure <i>FLASHCCU</i>	bar	1	1	1
Solvent flowrate	kg h ⁻¹	115 000	17 500	17 500
Recycle Ratio		5.1	4.7	4.6
H ₂ addition	kmol h ⁻¹	-	240	680
Produced methanol	kg h ⁻¹	1981.4	4034.9	7526.2
Volumetric flowrate reactor feed	m ³ h ⁻¹	1723.3	2891.6	4944.7
Mass flowrate recycled	t h ⁻¹	30.8	58.7	106.7
Mechanical ratio (MR)	-	0.058	0.0429	0.046
Thermal ratio (TR)	-	-0.190	-0.181	-0.212
Methanol fraction in product	-	0.56	0.49	0.47
Water fraction in product	-	0.42	0.47	0.49
H ₂ loss fraction	-	0.27	0.22	0.22
stoichiometric number reactor feed	-	1.89	1.01	0.76
CO ₂ /CO ratio, reactor feed	-	3.7	5.6	6.6
T _{R-OUT}	°C	252.5	256.9	259.1
Reactor length	m	3.8	4.75	7
Reactor diameter	m	1.75	2.5	3
Reactor volume	m ³	9.1	23.3	40.5
Energy required to produce H ₂	MW _{el}	-	31.0	87.8
Energy content of the purged stream	MW _{ch}	21.00	25.22	34.58
SYSTEM EFFICIENCY				
Methanol	%	31.14	33.58	32.83
Methanol + purge gas	%	90.26	71.32	60.00

is required to separate the methanol from the *CRUDEMEO*-stream.

The hydrogen loss fraction for the cases are much lower for Case 2 and Case 3 than for the Case 1. This could be due to the amount of hydrogen present in the stream of which the purged fraction is taken. As the stoichiometric number shows, the hydrogen content is much lower for Case 2 and Case 3. With a lower hydrogen fraction in the purged gas, less hydrogen is lost after the membrane. Despite the decrease in partial pressure due to the smaller fraction, the permeation rate is still very high to ensure a good recycle of the hydrogen.

$$\eta_m = \frac{LHV_{CRUDEMEO} * \dot{m}_{CRUDEMEO}}{\sum P_i + P_{H_2prod} + LHV_{IN} * \dot{m}_{IN}} \quad (5.1)$$

$$\eta_{m+p} = \frac{LHV_{CRUDEMEO} * \dot{m}_{CRUDEMEO} + LHV_{RETENTAT} * \dot{m}_{RETENTAT}}{\sum P_i + P_{H_2prod} + LHV_{IN} * \dot{m}_{IN}} \quad (5.2)$$

where η_m = system efficiency for methanol as product
 η_{m+p} = system efficiency for methanol and purge gas as product
 LHV_i = lower heating value of stream i [MJ kg⁻¹]
 \dot{m}_i = mass flow of stream i [kg h⁻¹]

P_i = power input [kW]

P_{H_2prod} = power requirement for the production of hydrogen [kW]

The system efficiency for only methanol as a product (eq. 5.1) is within the same range for all three cases. The difference between them comes from the limitations set in the case descriptions above. A similar behaviour can be observed for the MR which is the ratio of power input to lower heating value of produced methanol as described by equation 4.1. The higher energy demand of the system for Case 1 derives from the need of the CO₂-removal unit (CRU) to run at full capacity. Case 3 requires more energy due to the compression of the CO₂, thus making Case 2 the case with the lowest MR and highest methanol-only efficiency. The trend for the thermal ratio can be explained by the same reasons.

Compared to literature, the efficiency is low as an efficiency of 55 % can be achieved for methanol synthesis from biomass [34, 95]. In Hamelinck and Faaij's [95] calculation of the efficiency, the full process including gasification, cleaning and distillation was taken into account. Additionally, the purged gas was used to produce electricity which was fed back into the system, reducing its power demand, and producing additional electricity that could be fed into the grid.

Including the purged gas as a product leads to a strong trend for the system efficiency (eq. 5.2). These values lie well above the values from literature. A proper comparison of this efficiency with the one calculated by Hamelinck and Faaij is still not viable, as the energy content of the purged stream must first be converted into electricity to their work. Also, the efficiency of the gasifier and other units are still not known for the here discussed process plant.

The trend of the efficiency for methanol and the purged gas as the product results from the energy content within the *RETENTAT*-stream. While the energy content increases from Case 1 to Case 3, the energy requirement to produce hydrogen increases much more. Hydrogen has a production efficiency of 52 % which means it requires more energy to produce the hydrogen in the purged stream than it adds to the energy content of it.

6

Conclusion

The objective of this thesis was to develop a process which converts syngas from biomass gasification into methanol. The constraints of the process were set through the application as a small-scale plant that is mobile and can be moved to the location of demand. After a comprehensive literature and technology study of the possible components for the process, a model was developed within the simulation environment of Aspen Plus[®]. The process was divided into three units, each with a different task. Where it was possible, these single units were then calibrated and compared to data from literature, before integrating them all into one process model.

The aim of this study was to use the developed model to be able to determine the operating conditions and design of the process for an operation with the integration of hydrogen supply from a renewable source. Three cases were defined depending on the availability of the hydrogen. The first case utilised the syngas fed into the system, removed a part of the CO₂ within the feed and produced methanol with no other material inputs into the system. In the second case, the feed is supplemented by hydrogen, which eliminates the need for CO₂ removal. Lastly, in the third case, there is an overproduction of hydrogen so additional CO₂ is added to the process to increase the methanol production. Being able to determine the methanol production and compositions of the product streams and predict their trends and understand the causes for them outlines the objective of this study.

The objective of this research was specified through two key question at the beginning of this thesis. Having studied the process and its influences the questions can now be answered.

What are the best reactor and separation technologies and optimal operation conditions for the production of methanol in a small-scale transportable process unit with an estimated daily production of 50 t_{MeOH} d⁻¹? For the equipment, an adiabatic reactor, separation through physical absorption with the solvent Selexol[®] and recycling of the purged gas through a membrane unit were chosen.

The reactor is a good choice as the model shows that the temperatures within the reactor never reach

critical temperatures for the catalyst. The operating pressure of the methanol reactor unit is chosen to be 60 bar. This lies outside the validated pressure range by Van den Bussche and Froment [22]. This could result in a deviation of the results, though they did determine that the kinetics were invalid outside of the validated range.

The choice of physical absorption with Selexol[®] is less obvious. It does remove the CO₂ with a very good selectivity and the removed gas has a good purity. However, it requires large mass flowrates which have a sizeable impact on the energy requirement of the process while having no or a negative effect on the production of methanol. The advantage of the correction unit comes from the reduction of the volumetric flowrates within the methanol reactor unit (MRU). The modelling of the absorption with Selexol[®] has proven to be difficult if large changes are required within the CO₂-removal unit (CRU) making the model susceptible to convergence issues.

The use of the membrane results in a lower fraction of hydrogen loss between 22 to 27 % instead of 36 %. However, there are issues with the operation of the membrane. While it recovers hydrogen from the *FEED-ME*-stream and blocks the inert gases, it also recovers CO₂. This is less good, as it leads to a higher required CO₂-removal in the CO₂-removal unit (CRU). The cause for this can lie within the membrane material chosen. However, it is more likely, that the simplified method used to describe the permeation within the membrane is too simple and ignores important factors such as the partial pressure on the side of the permeate.

The process conditions, such as operating pressure of the methanol reactor unit (MRU) and temperature of the *FLASH* within the MRU, have very little influence on the quality of the produced stream. However, the feed has a large impact as demonstrated through the comparison of the Case 1 with Case 2 and Case 3. The higher the carbon ratio is, the higher the water content of the product.

All in all, the here developed base case (Case 1) produces marginally below the desired production volume of 50 t_{MeOH} d⁻¹ as it produces 47.54 t d⁻¹. As a result, the operation has to be moved to a different operation point to produce the required amount of methanol. This operation point can differ from the original through an increase in the operating pressure of the MRU, a higher recycling ratio and/or a larger membrane.

How can integrating hydrogen improve the process yield and how does it influence the design of the process? The integration of hydrogen was studied through Case 2 and Case 3. In both cases, the desired production volume of 50 t_{MeOH} d⁻¹ was achieved. Case 2 produces 96.84 t_{MeOH} d⁻¹ while case 3 produces 180.63 t_{MeOH} d⁻¹. For both cases the production rate increases while the ratio of the energy content of the produced methanol to the required power, mechanical ratio (MR), decreases. The thermal ratio (TR) increases due to the low pressure of the CO₂ feed. However, for the MR, the power for the production of hydrogen was neglected. The system efficiency, η_{m+p} , which includes the electricity required for the hydrogen as an input as well as the energy content of the purged gas as a product, prefers no hydrogen addition. This is due to the low energy content in the purged gas compared to the high energy requirement for the production of the hydrogen. However, the factor neglected by this analysis is the much easier storage and transport technology for methanol compared to hydrogen.

An important aspect of operating the unit with varying feed flows, requires it to be flexible with its operation and reasonable for its sizing. The operation of the process such as derived in this thesis

has large issues regarding the sizing. The increased mass flowrates for each case requires larger equipment. The reactor is one example for this. The reactor for Case 3 is 4.45 times as large in volume than the base case. Considering that it is only run at full capacity for a quarter of the time, the size is probably not economically feasible. As a result, an operation of the process between the Case 1 and Case 2 could be reasonable as the increase of the reactor volume from Case 1 to Case 2 is only 2.5. Also, the CO₂ addition in Case 3 requires more equipment as it needs to compress the CO₂ which was removed in Case 1 at 1 bar to the operating pressure of the process.

6.1. Recommendations

The research conducted in this study gives a good background on the behaviour of the process, however there are still open questions.

To achieve a reasonable improved operation, a techno-economic evaluation of the process needs to be conducted. As was determined by this study, one of the largest factors determining the production of methanol from syngas is the investment and operation and maintenance cost. Without these, the process leans towards a process where the syngas is not treated and put directly into a process with a very high recycle ratio (> 9).

The model of the membrane unit interrupts the simulation due to the use of Excel. A modelling of the permeation process through an integrated program such as FORTRAN should improve the simulation. Additionally, the mechanism behind the membrane model needs to be examined to determine if the assumptions made in this study are valid. These assumptions include the simplification of the solution-diffusion mechanism as well as the independence of the permeation rate from temperature, pressure and composition of the gases.

The large energy penalty for the removal of the CO₂ inside the CRU due to the flowrate leads to the speculation that there might be a better removal technology. While researching for alternatives, special attention should be given to the energy demands.

Finally, the reactor kinetics within this study were assumed to follow Van den Bussche and Froment [22] model while ignoring limitations due to mass and heat transfer as well as the boundaries set by the validation of the kinetics. It needs to be checked through theoretical estimations if these limitations are applicable while the kinetics need to be examined if they apply outside of their boundaries, possibly through experiments. Additionally, Mignard and Pritchard's kinetics [25] should be considered if the kinetics by Van den Bussche and Froment [22] do not give accurate results.

Bibliography

- [1] UNFCCC, *Decision 1/CP.21 Adoption of the Paris Agreement*, (2015).
- [2] U.S. Energy Information Administration (EIA), *International Energy Outlook 2016 with projections to 2040*, (2016).
- [3] J. L. Sawin, K. Seyboth, and F. Sverrisson, *Ren21*, Report (Renewable Energy Policy Network for the 21st Century, 2016).
- [4] R. Perez and M. Perez, *A Fundamental Look At Supply Side Energy Reserves For The Planet*, International Energy Agency SHC programme Solar Update **62** (2015), <http://dx.doi.org/10.1016/j.enconman.2015.02.007>.
- [5] A. A. Rentizelas, A. J. Tolis, and I. P. Tatsiopoulos, *Logistics issues of biomass: The storage problem and the multi-biomass supply chain*, *Renewable and Sustainable Energy Reviews* **13**, 887 (2009).
- [6] D. Brown, A. Rowe, and P. Wild, *A techno-economic analysis of using mobile distributed pyrolysis facilities to deliver a forest residue resource*, *Bioresource Technology* **150**, 367 (2013).
- [7] Methanol Institute, *The Methanol Industry*, (2017), <http://www.methanol.org/the-methanol-industry/>.
- [8] H. Offermanns, L. Plass, and R. Heyde, *Methanol in Industrial Chemistry (General)*, in *Methanol: The Basic Chemical and Energy Feedstock of the Future*, edited by M. Bertau, H. Offermanns, L. Plass, F. Schmidt, and H.-J. Wernicke (Springer, 2014) Chap. 1.4, pp. 13–18.
- [9] J. Ott, V. Gronemann, F. Pontzen, E. Fiedler, G. Grossmann, D. B. Kersebohm, G. Weiss, and C. Witte, *Methanol*, in *Ullmann's Encyclopedia of Industrial Chemistry* (Wiley-VCH Verlag GmbH & Co. KGaA, Weinheim, Germany, 2012).
- [10] H. de Lathouder, *Personal Correspondance*, (2017).
- [11] B. Kummamuru, *WBA Global Bioenergy Statistics 2016*, Report (World Bioenergy Association, 2016).
- [12] S. Basu, A. L. Khan, A. Cano-Odena, C. Liu, and I. F. J. Vankelecom, *Membrane-based technologies for biogas separations*, *Chemical Society Reviews* **39**, 750 (2010).
- [13] A. Molino, S. Chianese, and D. Musmarra, *Biomass gasification technology: The state of the art overview*, *Journal of Energy Chemistry* **25**, 10 (2016).
- [14] L. Devi, K. J. Ptasinski, and F. J. J. G. Janssen, *A review of the primary measures for tar elimination in biomass gasification processes*, *Biomass and Bioenergy* **24**, 125 (2003).
- [15] P. J. Woolcock and R. C. Brown, *A review of cleaning technologies for biomass-derived syngas*, *Biomass and Bioenergy* **52**, 54 (2013).
- [16] P. L. Spath and D. C. Dayton, *NREL/TP-510-34929*, Report (National Renewable Energy Laboratory, Golden, CO, 2003).
- [17] J. B. Hansen and P. E. Højlund Nielsen, *Methanol Synthesis*, in *Handbook of Heterogeneous Catalysis*, edited by G. Ertl, H. Knozinger, F. Schüth, and J. Weitkamp (Wiley-VCH Verlag GmbH & Co. KGaA, Weinheim, Germany, 2008) 2nd Edition, Chap. 13.13, pp. 2920–2949.

- [18] G. H. Graaf, P. J. J. M. Sijtsema, E. J. Stamhuis, and G. E. H. Joosten, *Chemical Equilibria in Methanol Synthesis*, *Chemical Engineering Science* **41**, 2883 (1986).
- [19] G. H. Graaf, E. J. Stamhuis, and A. A. C. M. Beenackers, *Kinetics of low-pressure methanol synthesis*, *Chemical Engineering Science* **43**, 3185 (1988).
- [20] J. Skrzypek, M. Lachowska, and H. Moroz, *Kinetics of methanol synthesis over commercial Copper/ Zinc Oxide / Ammina Catalysts*, *Chemical Engineering Science* **46**, 2809 (1991).
- [21] J. Skrzypek, M. Lachowska, M. Grzesik, J. Słoczyński, and P. Nowak, *Thermodynamics and kinetics of low pressure methanol synthesis*, *The Chemical Engineering Journal and The Biochemical Engineering Journal* **58**, 101 (1995).
- [22] K. M. Van den Bussche and G. F. Froment, *A Steady-State Kinetic Model for Methanol Synthesis and the Water Gas Shift Reaction on a Commercial Cu / ZnO / Al₂O₃ Catalyst*, *Journal of Catalysis* **161**, 1 (1996).
- [23] L. Chen, Q. Jiang, Z. Song, and D. Posarac, *Optimization of Methanol Yield from a Lurgi Reactor*, *Chemical Engineering and Technology* **34**, 817 (2011).
- [24] W. L. Luyben, *Design and Control of a Methanol Reactor/Column Process*, *Industrial and Engineering Chemistry Research* **49**, 6150 (2010).
- [25] D. Mignard and C. Pritchard, *On the use of electrolytic hydrogen from variable renewable energies for the enhanced conversion of biomass to fuels*, *Chemical Engineering Research and Design* **86**, 473 (2008).
- [26] K. Klier, V. Chatikavanij, R. G. Herman, and G. W. Simmons, *Catalytic Synthesis of Methanol from CO/H₂: VI. The effects of carbon dioxide*, *Journal of catalysis* **74**, 343 (1982).
- [27] J. Holladay, J. Hu, D. King, and Y. Wang, *An overview of hydrogen production technologies*, *Catalysis Today* **139**, 244 (2009).
- [28] R. Hino, K. Haga, H. Aita, and K. Sekita, *38. R&D on hydrogen production by high-temperature electrolysis of steam*, *Nuclear Engineering and Design* **233**, 363 (2004).
- [29] B. Sørensen, *Hydrogen and Fuel Cells - Emerging Technologies and Applications*, 2nd Edition (Oxford ; Burlington, MA : Academic Press, 2012).
- [30] A. Ursua, L. M. Gandia, and P. Sanchis, *Hydrogen Production From Water Electrolysis: Current Status and Future Trends*, *Proceedings of the IEEE* **100**, 410 (2012).
- [31] R. Bhandari, C. A. Trudewind, and P. Zapp, *Life cycle assessment of hydrogen production via electrolysis - A review*, *Journal of Cleaner Production* **85**, 151 (2014).
- [32] T. Smolinka, M. Günther, and J. Garche, *NOW-Studie*, Report (Fraunhofer ISE, 2011).
- [33] V. Gronemann, L. Plass, and F. Schmidt, *Commercial Methanol Synthesis from Syngas*, in *Methanol: The Basic Chemical and Energy Feedstock of the Future*, edited by M. Bertau, H. Offermanns, L. Plass, F. Schmidt, and H.-J. Wernicke (Springer, 2014) Chap. 4.7, pp. 234–266.
- [34] G. Bozzano and F. Manenti, *Efficient methanol synthesis: Perspectives, technologies and optimization strategies*, *Progress in Energy and Combustion Science* **56**, 71 (2016).
- [35] I. Wender, *Reactions of synthesis*, *Fuel Processing Technology* **48**, 189 (1996).
- [36] R. Smith, *Chemical process design and integration* (John Wiley & Sons, Chichester, England, 2005).
- [37] F. Schmidt, N. Ringer, and L. Plass, *The Catalysis of Methanol Synthesis*, in *Methanol: The Basic Chemical and Energy Feedstock of the Future*, edited by M. Bertau, H. Offermanns, L. Plass, F. Schmidt, and H.-J. Wernicke (Springer, 2014) Chap. 4.6, pp. 218–234.
- [38] G. C. Chinchin, P. J. Denny, J. R. Jennings, K. C. Waugh, and P. Group, *Review - Synthesis of Methanol*, *Applied Catalysis* **36**, 1 (1988).

- [39] Haldor Topsøe, *Methanol*, (2017), <https://www.topsoe.com/processes/methanol>.
- [40] Toyo Engineering Corporation, *MRF-Z Methanol Reactor*, (2017), <http://www.toyo-eng.com/jp/en/products/petrochemical/methanol/>.
- [41] K. Hirotsu, H. Nakamura, and K. Shoji, *Optimum catalytic reactor design for methanol synthesis with TEC MRF-Z reactor*, *Catalysis Surveys from Japan* **2**, 99 (1998).
- [42] Linde Engineering, *Isothermal Reactor*, (2017), http://www.linde-engineering.com/en/process_plants/hydrogen_and_synthesis_gas_plants/gas_generation/isothermal_reactor/index.html.
- [43] T. Wurzel, *Lurgi MegaMethanol technology - Delivering the building blocks for the future fuel and monomer demand*, in *DGMK Conference "Synthetic Gas Chemistry"* (Dresden, Germany, 2006) pp. 9–18.
- [44] Lurgi MegaMethanol, *Brochure by engineering division of Lurgi Oel, Gas and Chemie GmbH*, (2010).
- [45] E. C. Heydorn, B. W. Diamond, and R. D. Lilly, *Commercial-scale Demonstration of the Liquid Phase Methanol (LPMEOH™) Process*, Report June 2003 (Air Products Liquid Phase Conversion Company, 2003).
- [46] B. Sea and K.-H. Lee, *Methanol synthesis from carbon dioxide and hydrogen using a ceramic membrane reactor*, *Reaction Kinetics and Catalysis Letters* **80**, 33 (2003).
- [47] F. Gallucci, L. Paturzo, and A. Basile, *An experimental study of CO₂ hydrogenation into methanol involving a zeolite membrane reactor*, *Chemical Engineering and Processing: Process Intensification* **43**, 1029 (2004).
- [48] M. V. Twigg and M. S. Spencer, *Deactivation of copper metal catalysts for methanol decomposition, methanol steam reforming and methanol synthesis*, *Topics in Catalysis* **22**, 191 (2003).
- [49] D. Y. C. Leung, G. Caramanna, and M. M. Maroto-Valer, *An overview of current status of carbon dioxide capture and storage technologies*, *Renewable and Sustainable Energy Reviews* **39**, 426 (2014).
- [50] A. B. Rao and E. S. Rubin, *A Technical, Economic, and Environmental Assessment of Amine-Based CO₂ Capture Technology for Power Plant Greenhouse Gas Control*, *Environmental Science and Technology* **36**, 4467 (2002).
- [51] T. F. Wall, *Combustion processes for carbon capture*, *Proceedings of the Combustion Institute* **31**, 31 (2007).
- [52] J. D. Figueroa, T. Fout, S. Plasynski, H. McIlvried, and R. D. Srivastava, *Advances in CO₂ capture technology-The U.S. Department of Energy's Carbon Sequestration Program*, *International Journal of Greenhouse Gas Control* **2**, 9 (2008).
- [53] K. Ramasubramanian, Y. Zhao, and W. Winston Ho, *CO₂ capture and H₂ purification: Prospects for CO₂-selective membrane processes*, *AIChE Journal* **59**, 1033 (2013).
- [54] E. Blomen, C. Hendriks, and F. Neele, *Capture technologies: Improvements and promising developments*, *Energy Procedia* **1**, 1505 (2009).
- [55] E. I. Koytsoumpa, K. Atsonios, K. D. Panopoulos, S. Karellas, E. Kakaras, and J. Karl, *Modelling and assessment of acid gas removal processes in coal-derived SNG production*, *Applied Thermal Engineering* **74**, 128 (2015).
- [56] Ekomeri, *Acid gas concentrations in natural gas*, (2015), <http://www.ekomeri.com/acid-gas-concentrations-natural-gas/>.
- [57] R. N. Tennyson and R. P. Schaaf, *Guidelines can help choose proper process for gas-treating plants*, *Oil Gas J* **75**, 78 (1977).

- [58] A. Padurean, C.-C. Cormos, and P.-S. Agachi, *Pre-combustion carbon dioxide capture by gas-liquid absorption for Integrated Gasification Combined Cycle power plants*, International Journal of Greenhouse Gas Control **7**, 1 (2012).
- [59] UOP LLC, *Presentation by UOP Selexol Technology for Acid Gas Removal*, (2009).
- [60] The Dow Chemical Company, *SELEXOL Solvents*, (2015), <http://msdssearch.dow.com/webapps/include/GetDoc.aspx?ObjectId=&filepath=productsafety/pdfs/noreg/233-00600.pdf&pdf=true&Referrer=>.
- [61] Linde Engineering, *RECTISOL® wash*, (2017), http://www.linde-engineering.com/en/process_plants/hydrogen_and_synthesis_gas_plants/gas_processing/rectisol_wash/index.html.
- [62] A. L. Kohl and R. B. Nielsen, *Gas Purification*, 5th Edition (Elsevier, Houston, Texas, 1997).
- [63] J. Xu, Z. Wang, C. Zhang, S. Zhao, Z. Qiao, P. Li, J. Wang, and S. Wang, *Parametric analysis and potential prediction of membrane processes for hydrogen production and pre-combustion CO₂ capture*, Chemical Engineering Science **135**, 202 (2015).
- [64] P. Gabrielli, M. Gazzani, and M. Mazzotti, *On the optimal design of membrane-based gas separation processes*, Journal of Membrane Science **526**, 118 (2017).
- [65] C. A. Scholes, K. H. Smith, S. E. Kentish, and G. W. Stevens, *CO₂ capture from pre-combustion processes—Strategies for membrane gas separation*, International Journal of Greenhouse Gas Control **4**, 739 (2010).
- [66] J. C. Glier and E. S. Rubin, *Assessment of solid sorbents as a competitive post-combustion CO₂ capture technology*, Energy Procedia **37**, 65 (2013).
- [67] A. H. Berger and A. S. Bhowan, *Optimizing Solid Sorbents for CO₂ Capture*, Energy Procedia **37**, 25 (2013).
- [68] A. Samanta, A. Zhao, G. K. H. Shimizu, P. Sarkar, and R. Gupta, *Post-Combustion CO₂ Capture Using Solid Sorbents : A Review*, Industrial and Engineering Chemistry Research **51**, 1438 (2012).
- [69] O. Talu, J. Li, and A. L. Myers, *Activity coefficients of adsorbed mixtures*, Adsorption **1**, 103 (1995).
- [70] M. T. Ho, G. W. Allinson, and D. E. Wiley, *Reducing the Cost of CO₂ Capture from Flue Gases Using Pressure Swing Adsorption*, Industrial and Engineering Chemistry Research **47**, 4883 (2008).
- [71] J. Zhang, P. A. Webley, and P. Xiao, *Effect of process parameters on power requirements of vacuum swing adsorption technology for CO₂ capture from flue gas*, Energy Conversion and Management **49**, 346 (2008).
- [72] A. H. Berger and A. S. Bhowan, *Comparing physisorption and chemisorption solid sorbents for use separating CO₂ from flue gas using temperature swing adsorption*, Energy Procedia **4**, 562 (2011).
- [73] S. Sjostrom and H. Krutka, *Evaluation of solid sorbents as a retrofit technology for CO₂ capture*, Fuel **89**, 1298 (2010).
- [74] S. Sjostrom, H. Krutka, T. Starns, and T. Campbell, *Pilot test results of post-combustion CO₂ capture using solid sorbents*, Energy Procedia **4**, 1584 (2011).
- [75] H. Krutka, S. Sjostrom, T. Starns, M. Dillon, and R. Silverman, *Post-combustion CO₂ capture using solid sorbents: 1 MW e pilot evaluation*, Energy Procedia **37**, 73 (2013).
- [76] J. R. Rumble, ed., *CRC Handbook of Chemistry and Physics (Internet Version 2018)*, 98th Edition (CRC Press/Taylor & Francis, Boca Raton, FL, 2017).

- [77] A. Hinchliffe and K. Porter, *A Comparison of Membrane Separation and Distillation*, Chemical Engineering Research and Design **78**, 255 (2000).
- [78] D. Berstad, R. Anantharaman, and P. Neksa, *Low-temperature CO₂ capture technologies – Applications and potential*, International Journal of Refrigeration **36**, 1403 (2013).
- [79] D. Berstad, R. Anantharaman, and P. Neksa, *Low-temperature CCS from an IGCC Power Plant and Comparison with Physical Solvents*, Energy Procedia **37**, 2204 (2013).
- [80] D. Jansen, M. Gazzani, G. Manzolini, E. V. Dijk, and M. Carbo, *Pre-combustion CO₂ capture*, International Journal of Greenhouse Gas Control **40**, 167 (2015).
- [81] N. A. Al-Mufachi, N. V. Rees, and R. Steinberger-Wilkens, *Hydrogen selective membranes: A review of palladium-based dense metal membranes*, Renewable and Sustainable Energy Reviews **47**, 540 (2015).
- [82] L. Shao, B. T. Low, T.-S. Chung, and A. R. Greenberg, *Polymeric membranes for the hydrogen economy: Contemporary approaches and prospects for the future*, Journal of Membrane Science **327**, 18 (2009).
- [83] S. Adhikari and S. Fernando, *Hydrogen Membrane Separation Techniques*, Industrial and Engineering Chemistry Research **45**, 875 (2006).
- [84] L. M. Robeson, *The upper bound revisited*, Journal of Membrane Science **320**, 390 (2008).
- [85] B. D. Freeman, *Basis of Permeability/Selectivity Tradeoff Relations in Polymeric Gas Separation Membranes*, Macromolecules **32**, 375 (1999).
- [86] S. Iyer, T. Renganathan, S. Pushpavanam, M. Vasudeva Kumar, and N. Kaisare, *Generalized thermodynamic analysis of methanol synthesis: Effect of feed composition*, Journal of CO₂ Utilization **10**, 95 (2015).
- [87] S. Lee, *Methanol synthesis technology* (CRC Press, 1990).
- [88] H. Bakhtiary-Davijany, F. Dadgar, F. Hayer, X. K. Phan, R. Myrstad, H. J. Venvik, P. Pfeifer, and A. Holmen, *Analysis of External and Internal Mass Transfer at Low Reynolds Numbers in a Multiple-Slit Packed Bed Microstructured Reactor for Synthesis of Methanol from Syngas*, Industrial & Engineering Chemistry Research **51**, 13574 (2012).
- [89] G. Towler and R. Sinnott, *Chemical Engineering Design - Principles, Practice and Economics of Plant and Process Design*, 2nd Edition (Elsevier Ltd., 2013).
- [90] Z. Tan, *Air Pollution and Greenhouse Gases*, Green Energy and Technology (Springer Singapore, Singapore, 2014).
- [91] Aspen Technology, *Physical Property Methods*, Aspen Physical Property System (2009).
- [92] Aspen Technology, *Aspen Plus Model of the CO₂ Capture Process by DEPG*, Report (Aspen Technology, 2014).
- [93] Undisclosed Company, *Gas Separation System by Membrane*, Product Brochure (1993).
- [94] Proton On Site, *Hydrogen Generation Systems*, (2017), <http://www.protononsite.com/products-proton-site/c10-c20-c30>.
- [95] C. N. Hamelinck and A. P. C. Faaij, *Future prospects for production of methanol and hydrogen from biomass*, Journal of Power Sources **111**, 1 (2002).

A

Flowsheets

The figures A.1 to A.3 show the flowsheets for the operation of the three discussed cases. The figures include the power and heat requirements of the equipment as well as the pressure and temperature of the flows.

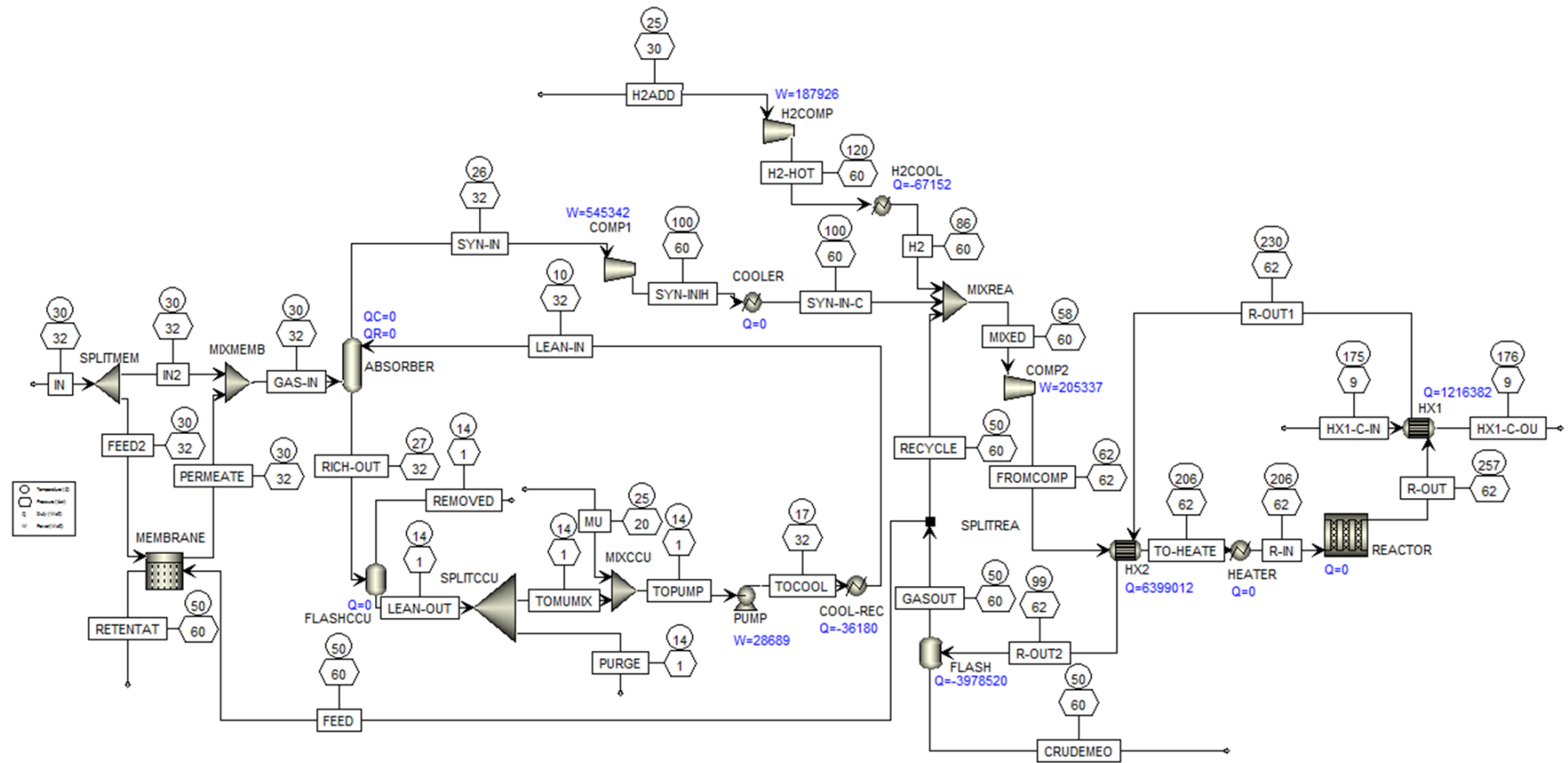


Figure A.2: Aspen Plus® Model flow-sheet for case 2: Methanol synthesis with hydrogen integration

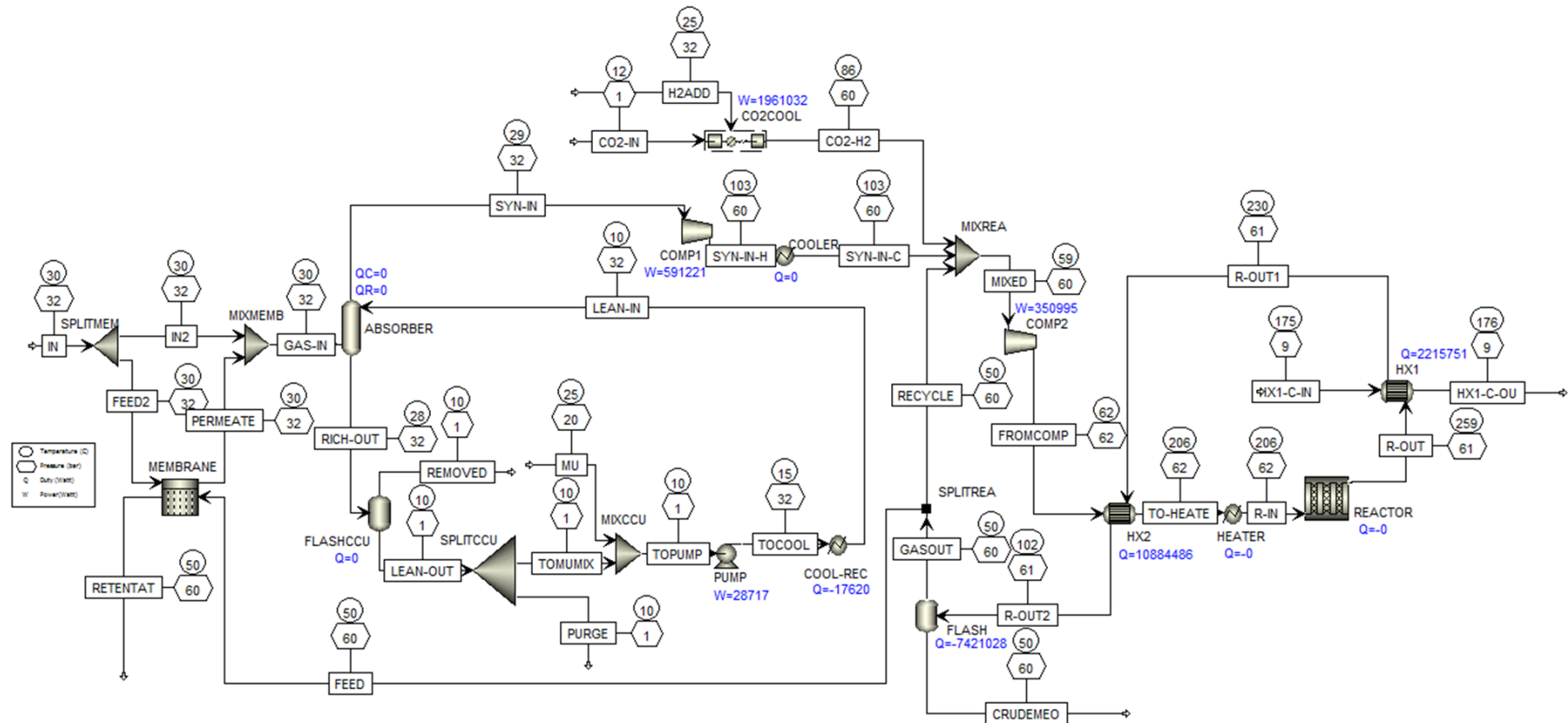


Figure A.3: Aspen Plus® Model flow-sheet for case 3: Methanol synthesis with hydrogen and CO₂ integration

B

Flows of the cases

In the following pages, the flows of each case as defined in chapter 5 are listed alphabetically. The placement of the streams within the processes can be seen in figures A.1 to A.3 respectively

Table B.1: Stream summary for case 1: Methanol synthesis without hydrogen integration (part1)

	Units	CRUDEMEO	FEED-ME	FEED2	FROMCOMP	GAS-IN	GASOUT	HX1-C-IN	HX1-C-OU	IN	IN2
From		FLASH	SPLITREA	SPLITMEM	COMP2	MIXMEMB	FLASH		HX1		SPLITMEM
To			MEMBRANE	MEMBRANE	HX2	ABSORBER	SPLITREA	HX1		SPLITMEM	MIXMEMB
Phase:		Liquid	Vapor	Vapor	Vapor	Mixed	Vapor	Liquid	Mixed	Vapor	Vapor
Component Mass Flow											
H2	KG/HR	0,1	197,0	98,3	2540,3	554,3	2188,8	0,0	0,0	491,4	393,2
CO	KG/HR	0,2	208,2	138,4	2796,4	707,0	2313,0	0,0	0,0	691,8	553,5
CO2	KG/HR	110,8	1276,4	1777,0	16344,2	9225,0	14182,3	0,0	0,0	8885,0	7108,0
N2	KG/HR	0,1	118,4	22,8	1315,8	120,4	1315,6	0,0	0,0	113,9	91,1
CH4	KG/HR	6,7	1167,7	238,3	12981,4	1234,4	12974,7	0,0	0,0	1191,4	953,1
WATER	KG/HR	832,1	9,4	3,0	97,3	18,0	104,7	5000,0	5000,0	14,8	11,9
MEOH	KG/HR	1981,4	64,6	0,0	653,3	0,0	718,0	0,0	0,0	0,0	0,0
SELEXOL	KG/HR	0,0	0,0	0,0	0,0	0,0	0,0	0,0	0,0	0,0	0,0
Mole Flow	KMOL/HR	111,0	213,7	109,9	2613,3	592,1	2374,5	277,5	277,5	549,5	439,6
Mass Flow	KG/HR	2931,5	3041,7	2277,7	36728,7	11859,2	33797,0	5000,0	5000,0	11388,4	9110,7
Volume Flow	CUM/HR	4,7	95,3	84,7	1172,2	458,2	1059,2	7,7	233,3	423,4	338,7
Temperature	C	50,0	50,0	30,0	60,4	30,1	50,0	175,0	175,5	30,0	30,0
Pressure	BAR	60,0	60,0	32,0	62,0	31,9	60,0	9,0	9,0	32,0	32,0
Vapor Fraction		0,0	1,0	1,0	1,0	1,0	1,0	0,0	0,2	1,0	1,0
LHV	MJ/KG	13,6	28,1	11,0	27,1	11,4	28,1	0,0	0,0	11,0	11,0
Molar Enthalpy	MJ/KMOL	-260,0	-84,7	-160,1	-84,4	-154,3	-84,7	-275,6	-267,6	-160,1	-160,1
Mass Enthalpy	MJ/KG	-9,8	-5,9	-7,7	-6,0	-7,7	-5,9	-15,3	-14,9	-7,7	-7,7
Enthalpy Flow	MW	-8,0	-5,0	-4,9	-61,3	-25,4	-55,8	-21,2	-20,6	-24,4	-19,6
Mass Entropy	J/KG-K	-7478,9	-3320,5	-1210,4	-3089,5	-1249,2	-3320,5	-7493,3	-6504,8	-1210,4	-1210,4
Mass Density	KG/CUM	629,6	31,9	26,9	31,3	25,9	31,9	650,3	21,4	26,9	26,9

Table B.2: Stream summary for case 1: Methanol synthesis without hydrogen integration (part2)

	Units	LEAN-IN	LEAN-OUT	MIXED	PERMEATE	PURGE	MU	RECYCLE	REMOVED	RETENTAT	RICH-OUT
From		COOL-REC	FLASHCCU	MIXREA	MEMBRANE	SPLITCCU		SPLITREA	FLASHCCU	MEMBRANE	ABSORBER
To		ABSORBER	SPLITCCU	COMP2	MIXMEMB		MIXCCU	MIXREA			FLASHCCU
Phase:		Liquid	Liquid	Vapor	Liquid	Mixed	Liquid	Vapor	Vapor	Mixed	Liquid
Component Mass Flow											
H2	KG/HR	0,0	0,0	2540,3	161,2	0,0	0,0	1991,8	5,8	134,1	5,8
CO	KG/HR	0,1	0,1	2796,4	153,5	0,0	0,0	2104,8	15,4	193,0	15,4
CO2	KG/HR	655,6	655,6	16344,2	2116,9	0,0	0,0	12905,9	5786,7	936,5	6442,3
N2	KG/HR	0,0	0,0	1315,8	29,3	0,0	0,0	1197,2	1,9	111,9	1,9
CH4	KG/HR	0,5	0,5	12981,4	281,3	0,0	0,0	11807,0	60,0	1124,7	60,5
WATER	KG/HR	1347,2	1347,2	97,3	6,1	0,0	0,1	95,3	16,0	6,3	1363,2
MEOH	KG/HR	0,0	0,0	653,3	0,0	0,0	0,0	653,3	0,0	64,6	0,0
SELEXOL	KG/HR	112999,0	112999,0	0,0	0,0	1,9	1,9	0,0	0,0	0,0	112999,0
Mole Flow	KMOL/HR	493,3	493,3	2613,3	152,5	0,0	0,0	2160,8	139,6	171,1	632,9
Mass Flow	KG/HR	115002,0	115002,0	36728,7	2748,4	2,0	2,0	30755,3	5885,8	2571,0	120888,0
Volume Flow	CUM/HR	107,4	108,0	1195,7	118,7	0,0	0,0	963,9	3289,8	75,8	115,0
Temperature	C	10,0	11,8	56,6	30,0	11,8	25,0	50,0	11,8	50,0	21,1
Pressure	BAR	31,9	1,0	60,0	31,9	1,0	20,0	60,0	1,0	59,9	31,9
Vapor Fraction		0,0	0,0	1,0	1,0	0,0	0,0	1,0	1,0	1,0	0,0
LHV	MJ/KG	0,0	0,0	27,1	12,7	0,0	0,0	28,1	0,7	29,4	0,0
Molar Enthalpy	MJ/KMOL	-137,6	-137,3	-84,6	-137,4	-137,3	-165,9	-84,7	-375,1	-86,4	-189,8
Mass Enthalpy	MJ/KG	-0,6	-0,6	-6,0	-7,6	-0,6	-1,0	-5,9	-8,9	-5,8	-1,0
Enthalpy Flow	MW	-18,9	-18,8	-61,4	-5,8	0,0	0,0	-50,8	-14,5	-4,1	-33,4
Mass Entropy	J/KG-K	-882,7	-867,7	-3097,1	-1384,0	-867,7	-886,8	-3320,5	33,5	-3504,7	-850,5
Mass Density	KG/CUM	1070,7	1065,0	30,7	23,1	1065,0	1057,0	31,9	1,8	33,9	1050,9

Table B.3: Stream summary for case 1: Methanol synthesis without hydrogen integration (part3)

	Units	R-IN	R-OUT	R-OUT1	R-OUT2	SYN-IN	SYN-IN-H	TOCOOL	TO-HEATE	TOMUMIX	TOPUMP
From		HEATER	REACTOR	HX1	HX2	ABSORBER	COMP1	PUMP	HX2	SPLITCCU	MIXCCU
To		REACTOR	HX1	HX2	FLASH	COMP1	MIXREA	COOL-REC	HEATER	MIXCCU	PUMP
Phase:		Vapor	Vapor	Vapor	Mixed	Vapor	Vapor	Liquid	Vapor	Liquid	Liquid
Component Mass Flow											
H2	KG/HR	2540,3	2188,9	2188,9	2188,9	548,5	548,5	0,0	2540,3	0,0	0,0
CO	KG/HR	2796,4	2313,2	2313,2	2313,2	691,6	691,6	0,1	2796,4	0,1	0,1
CO2	KG/HR	16344,1	14293,1	14293,1	14293,1	3438,3	3438,3	655,6	16344,2	655,6	655,6
N2	KG/HR	1315,8	1315,8	1315,8	1315,8	118,5	118,5	0,0	1315,8	0,0	0,0
CH4	KG/HR	12981,4	12981,4	12981,4	12981,4	1174,5	1174,5	0,5	12981,4	0,5	0,5
WATER	KG/HR	97,3	936,8	936,8	936,8	2,0	2,0	1347,2	97,3	1347,1	1347,2
MEOH	KG/HR	653,3	2699,3	2699,3	2699,3	0,0	0,0	0,0	653,3	0,0	0,0
SELEXOL	KG/HR	0,0	0,0	0,0	0,0	0,0	0,0	112999,0	0,0	112997,0	112999,0
Mole Flow	KMOL/HR	2613,3	2485,6	2485,6	2485,6	452,5	452,5	493,3	2613,3	493,3	493,3
Mass Flow	KG/HR	36728,6	36728,6	36728,6	36728,6	5973,4	5973,4	115002,0	36728,7	115000,0	115002,0
Volume Flow	CUM/HR	1717,8	1797,8	1719,0	1212,5	342,0	231,9	107,7	1717,8	108,0	108,0
Temperature	C	206,3	252,5	230,0	91,4	15,9	90,3	12,9	206,3	11,8	11,8
Pressure	BAR	62,0	61,6	61,6	61,6	31,9	60,0	31,9	62,0	1,0	1,0
Vapor Fraction		1,0	1,0	1,0	1,0	1,0	1,0	0,0	1,0	0,0	0,0
LHV	MJ/KG	27,1	26,9	26,9	26,9	22,0	22,0	0,0	27,1	0,0	0,0
Molar Enthalpy	MJ/KMOL	-79,1	-83,2	-84,1	-89,7	-86,5	-84,2	-136,4	-79,1	-137,3	-137,3
Mass Enthalpy	MJ/KG	-5,6	-5,6	-5,7	-6,1	-6,6	-6,4	-0,6	-5,6	-0,6	-0,6
Enthalpy Flow	MW	-57,4	-57,4	-58,1	-61,9	-10,9	-10,6	-18,7	-57,4	-18,8	-18,8
Mass Entropy	J/KG-K	-2150,2	-2110,0	-2227,4	-3113,5	-2157,9	-2015,7	-863,5	-2150,2	-867,7	-867,7
Mass Density	KG/CUM	21,4	20,4	21,4	30,3	17,5	25,8	1067,6	21,4	1065,0	1065,0

Table B.4: Stream summary for case 2: Methanol synthesis with hydrogen integration (part1)

	Units	CRUDEMEO	FEED-ME	FEED2	FROMCOMP	GAS-IN	GASOUT	H2	H2ADD	H2-HOT
From		FLASH	SPLITREA	SPLTMEM	COMP2	MIXMEMB	FLASH	H2COOL		H2COMP
To			MEMBRANE	MEMBRANE	HX2	ABSORBER	SPLITREA	MIXREA	H2COMP	H2COOL
Phase:		Liquid	Vapor	Vapor	Vapor	Mixed	Vapor	Vapor	Vapor	Vapor
Component Mass Flow										
H2	KG/HR	0,3	342,1	98,3	4562,7	620,2	3801,2	483,8	483,8	483,8
CO	KG/HR	0,5	440,3	138,4	5165,5	714,6	4892,4	0,0	0,0	0,0
CO2	KG/HR	377,4	3579,3	1777,0	45401,6	9872,7	39770,3	0,0	0,0	0,0
N2	KG/HR	0,1	118,6	22,8	1317,4	118,8	1317,3	0,0	0,0	0,0
CH4	KG/HR	7,9	1208,3	238,3	13433,7	1221,2	13425,7	0,0	0,0	0,0
WATER	KG/HR	2148,9	16,2	3,0	178,1	21,5	179,9	0,0	0,0	0,0
MEOH	KG/HR	4035,1	102,0	0,0	1031,1	0,0	1133,1	0,0	0,0	0,0
SELEXOL	KG/HR	0,0	0,0	0,0	0,0	0,0	0,0	0,0	0,0	0,0
Mole Flow	KMOL/HR	254,4	350,4	109,9	4405,9	639,1	3893,2	240,0	240,0	240,0
Mass Flow	KG/HR	6570,2	5806,8	2277,7	71090,1	12569,1	64519,9	483,8	483,8	483,8
Volume Flow	CUM/HR	10,2	155,5	84,7	1979,6	495,2	1727,7	123,4	202,0	134,9
Temperature	C	50,0	50,0	30,0	62,2	30,1	50,0	86,0	25,0	120,3
Pressure	BAR	60,0	60,0	32,0	62,0	31,9	60,0	60,0	30,0	60,0
Vapor Fraction		0,0	1,0	1,0	1,0	1,0	1,0	1,0	1,0	1,0
LHV	MJ/KG	12,3	18,6	11,0	18,2	11,4	18,6	120,0	120,0	120,0
Molar Enthalpy	MJ/KMOL	-264,5	-114,3	-160,1	-112,1	-152,0	-114,3	1,8	0,0	2,8
Mass Enthalpy	MJ/KG	-10,2	-6,9	-7,7	-6,9	-7,7	-6,9	0,9	0,0	1,4
Enthalpy Flow	MW	-18,7	-11,1	-4,9	-137,2	-27,0	-123,7	0,1	0,0	0,2
Mass Entropy	J/KG-K	-7401,9	-2160,7	-1210,4	-2051,5	-1251,1	-2160,7	-14198,0	-14007,4	-12869,3
Mass Density	KG/CUM	643,0	37,3	26,9	35,9	25,4	37,3	3,9	2,4	3,6

Table B.5: Stream summary for case 2: Methanol synthesis with hydrogen integration (part2)

	Units	HX1-C-IN	HX1-C-OU	IN	IN2	LEAN-IN	LEAN-OUT	MIXED	MU	PERMEATE
From			HX1		SPLITMEM	COOL-REC	FLASHCCU	MIXREA		MEMBRANE
To		HX1		SPLITMEM	MIXMEMB	ABSORBER	SPLITCCU	COMP2	MIXCCU	MIXMEMB
Phase:		Liquid	Mixed	Vapor	Vapor	Liquid	Liquid	Vapor	Liquid	Mixed
Component Mass Flow										
H2	KG/HR	0,0	0,0	491,4	393,2	0,0	0,0	4562,6	0,0	227,1
CO	KG/HR	0,0	0,0	691,8	553,5	0,0	0,0	5165,5	0,0	161,1
CO2	KG/HR	0,0	0,0	8885,0	7108,0	96,6	96,6	45402,1	0,0	2764,7
N2	KG/HR	0,0	0,0	113,9	91,1	0,0	0,0	1317,4	0,0	27,7
CH4	KG/HR	0,0	0,0	1191,4	953,1	0,0	0,0	13433,7	0,0	268,1
WATER	KG/HR	5000,0	5000,0	14,8	11,9	1778,1	1778,1	178,1	0,0	9,6
MEOH	KG/HR	0,0	0,0	0,0	0,0	0,0	0,0	1031,1	0,0	0,0
SELEXOL	KG/HR	0,0	0,0	0,0	0,0	15625,4	15625,4	0,0	0,2	0,0
Mole Flow	KMOL/HR	277,5	277,5	549,5	439,6	156,7	156,7	4405,9	0,0	199,5
Mass Flow	KG/HR	5000,0	5000,0	11388,4	9110,7	17500,2	17500,2	71090,5	0,2	3458,3
Volume Flow	CUM/HR	7,7	454,6	423,4	338,7	16,4	16,5	2019,2	0,0	155,7
Temperature	C	175,0	175,5	30,0	30,0	10,0	13,7	58,3	25,0	30,0
Pressure	BAR	9,0	9,0	32,0	32,0	31,9	1,0	60,0	20,0	31,9
Vapor Fraction		0,0	0,4	1,0	1,0	0,0	0,0	1,0	0,0	1,0
LHV	MJ/KG	0,0	0,0	11,0	11,0	0,0	0,0	18,2	0,0	12,2
Molar Enthalpy	MJ/KMOL	-275,6	-259,8	-160,1	-160,1	-206,8	-206,7	-112,2	-165,9	-134,1
Mass Enthalpy	MJ/KG	-15,3	-14,4	-7,7	-7,7	-1,9	-1,9	-7,0	-1,0	-7,7
Enthalpy Flow	MW	-21,2	-20,0	-24,4	-19,6	-9,0	-9,0	-137,3	0,0	-7,4
Mass Entropy	J/KG-K	-7493,3	-5541,3	-1210,4	-1210,4	-1176,1	-1160,6	-2058,0	-886,8	-1370,7
Mass Density	KG/CUM	650,3	11,0	26,9	26,9	1068,3	1063,2	35,2	1057,0	22,2

Table B.6: Stream summary for case 2: Methanol synthesis with hydrogen integration (part3)

	Units	PURGE	RECYCLE	REMOVED	RETENTAT	RICH-OUT	R-IN	R-OUT	R-OUT1	R-OUT2
From		SPLITCCU	SPLITREA	FLASHCCU	MEMBRANE	ABSORBER	HEATER	REACTOR	HX1	HX2
To			MIXREA			FLASHCCU	REACTOR	HX1	HX2	FLASH
Phase:		Liquid	Vapor	Vapor	Mixed	Liquid	Vapor	Vapor	Vapor	Mixed
Component Mass Flow										
H2	KG/HR	0,0	3459,1	0,5	213,3	0,5	4562,7	3801,5	3801,5	3801,5
CO	KG/HR	0,0	4452,1	1,2	417,5	1,2	5165,5	4892,9	4892,9	4892,9
CO2	KG/HR	0,0	36190,9	661,6	2591,6	758,2	45401,6	40147,6	40147,6	40147,6
N2	KG/HR	0,0	1198,7	0,2	113,6	0,2	1317,4	1317,4	1317,4	1317,4
CH4	KG/HR	0,0	12217,4	4,9	1178,5	5,0	13433,7	13433,7	13433,7	13433,7
WATER	KG/HR	0,0	163,7	7,0	9,5	1785,2	178,1	2328,8	2328,8	2328,8
MEOH	KG/HR	0,0	1031,1	0,0	102,0	0,0	1031,1	5168,2	5168,2	5168,2
SELEXOL	KG/HR	0,2	0,0	0,0	0,0	15625,4	0,0	0,0	0,0	0,0
Mole Flow	KMOL/HR	0,0	3542,8	16,0	260,8	172,7	4405,9	4147,6	4147,6	4147,6
Mass Flow	KG/HR	0,2	58713,1	675,5	4626,1	18175,7	71090,1	71090,1	71090,1	71090,1
Volume Flow	CUM/HR	0,0	1572,2	380,3	114,7	17,2	2891,6	3017,2	2859,0	2042,7
Temperature	C	13,7	50,0	13,7	50,0	27,2	206,3	256,9	230,0	98,7
Pressure	BAR	1,0	60,0	1,0	59,9	31,9	62,0	61,6	61,6	61,6
Vapor Fraction		0,0	1,0	1,0	1,0	0,0	1,0	1,0	1,0	1,0
LHV	MJ/KG	0,0	18,6	0,5	19,6	0,0	18,2	18,0	18,0	18,0
Molar Enthalpy	MJ/KMOL	-206,7	-114,3	-377,0	-118,8	-222,5	-106,8	-113,5	-114,5	-120,1
Mass Enthalpy	MJ/KG	-1,9	-6,9	-8,9	-6,7	-2,1	-6,6	-6,6	-6,7	-7,0
Enthalpy Flow	MW	0,0	-112,5	-1,7	-8,6	-10,7	-130,8	-130,8	-132,0	-138,4
Mass Entropy	J/KG-K	-1160,6	-2160,7	35,8	-2260,2	-1137,9	-1248,7	-1203,5	-1322,8	-2078,8
Mass Density	KG/CUM	1063,2	37,3	1,8	40,3	1054,5	24,6	23,6	24,9	34,8

Table B.7: Stream summary for case 2: Methanol synthesis with hydrogen integration (part4)

	Units	SYN-IN	SYN-IN-C	SYN-INIH	TOCOOL	TO-HEATE	TOMUMIX	TOPUMP
From		ABSORBER	COOLER	COMP1	PUMP	HX2	SPLITCCU	MIXCCU
To		COMP1	MIXREA	COOLER	COOL-REC	HEATER	MIXCCU	PUMP
Phase:		Vapor	Vapor	Vapor	Liquid	Vapor	Liquid	Liquid
Component Mass Flow								
H2	KG/HR	619,7	619,7	619,7	0,0	4562,7	0,0	0,0
CO	KG/HR	713,4	713,4	713,4	0,0	5165,5	0,0	0,0
CO2	KG/HR	9211,1	9211,1	9211,1	96,6	45401,6	96,6	96,6
N2	KG/HR	118,7	118,7	118,7	0,0	1317,4	0,0	0,0
CH4	KG/HR	1216,2	1216,2	1216,2	0,0	13433,7	0,0	0,0
WATER	KG/HR	14,4	14,4	14,4	1778,1	178,1	1778,1	1778,1
MEOH	KG/HR	0,0	0,0	0,0	0,0	1031,1	0,0	0,0
SELEXOL	KG/HR	0,0	0,0	0,0	15625,4	0,0	15625,2	15625,4
Mole Flow	KMOL/HR	623,0	623,0	623,0	156,7	4405,9	156,7	156,7
Mass Flow	KG/HR	11893,6	11893,6	11893,6	17500,2	71090,1	17500,0	17500,2
Volume Flow	CUM/HR	479,4	322,8	322,8	16,4	2891,6	16,5	16,5
Temperature	C	25,9	99,6	99,6	16,8	206,3	13,7	13,7
Pressure	BAR	31,9	60,0	60,0	31,9	62,0	1,0	1,0
Vapor Fraction		1,0	1,0	1,0	0,0	1,0	0,0	0,0
LHV	MJ/KG	12,0	12,0	12,0	0,0	18,2	0,0	0,0
Molar Enthalpy	MJ/KMOL	-146,3	-143,9	-143,9	-206,0	-106,8	-206,7	-206,7
Mass Enthalpy	MJ/KG	-7,7	-7,5	-7,5	-1,8	-6,6	-1,9	-1,9
Enthalpy Flow	MW	-25,3	-24,9	-24,9	-9,0	-130,8	-9,0	-9,0
Mass Entropy	J/KG-K	-1305,4	-1208,2	-1208,2	-1150,2	-1248,7	-1160,6	-1160,6
Mass Density	KG/CUM	24,8	36,8	36,8	1064,3	24,6	1063,2	1063,2

Table B.8: Stream summary for case 3: Methanol synthesis with hydrogen and CO₂ integration (part1)

	Units	CO2-H2	CO2-IN	CRUDEMEO	FEED-ME	FEED2	FROMCOMP	GAS-IN	GASOUT	H2ADD
From		CO2COOL		FLASH	SPLITREA	SPLITMEM	COMP2	MIXMEMB	FLASH	
To		MIXREA	CO2COOL		MEMBRANE	MEMBRANE	HX2	ABSORBER	SPLITREA	CO2COOL
Phase:		Vapor	Mixed	Liquid	Vapor	Vapor	Vapor	Mixed	Vapor	Vapor
Component Mass Flow										
H2	KG/HR	1379,5	8,7	0,5	601,5	98,3	8142,4	682,0	6682,9	1370,8
CO	KG/HR	24,5	24,5	1,0	833,1	138,4	9165,1	717,9	9256,9	0,0
CO2	KG/HR	9253,7	9253,7	872,8	7512,0	1777,0	95053,3	10442,3	83466,0	0,0
N2	KG/HR	3,0	3,0	0,1	120,1	22,8	1334,7	117,4	1334,6	0,0
CH4	KG/HR	94,4	94,4	9,1	1291,6	238,3	14360,5	1210,2	14351,4	0,0
WATER	KG/HR	28,4	28,4	4405,3	27,7	3,0	327,3	24,8	307,9	0,0
MEOH	KG/HR	0,0	0,0	7525,8	168,8	0,0	1707,3	0,0	1876,1	0,0
SELEXOL	KG/HR	0,0	0,0	0,0	0,0	0,0	0,0	0,0	0,0	0,0
Mole Flow	KMOL/HR	903,0	223,0	500,1	590,4	109,9	7540,4	682,2	6560,0	680,0
Mass Flow	KG/HR	10783,4	9412,6	12814,7	10554,9	2277,7	130090,0	13194,4	117276,0	1370,8
Volume Flow	CUM/HR	458,5	5257,2	19,7	261,3	84,7	3383,7	529,2	2903,6	537,4
Temperature	C	86,0	11,9	50,0	50,0	30,0	62,4	30,0	50,0	25,0
Pressure	BAR	60,0	1,0	60,0	60,0	32,0	62,0	31,9	60,0	32,0
Vapor Fraction		1,0	1,0	0,0	1,0	1,0	1,0	1,0	1,0	1,0
LHV	MJ/KG	15,8	0,6	11,7	14,1	11,0	14,0	11,3	14,1	120,0
Molar Enthalpy	MJ/KMOL	-90,8	-375,7	-266,5	-131,5	-160,1	-127,5	-149,9	-131,5	0,0
Mass Enthalpy	MJ/KG	-7,6	-8,9	-10,4	-7,4	-7,7	-7,4	-7,8	-7,4	0,0
Enthalpy Flow	MW	-22,8	-23,3	-37,0	-21,6	-4,9	-267,1	-28,4	-239,7	0,0
Mass Entropy	J/KG-K	-1958,5	32,9	-7354,3	-1637,2	-1210,4	-1599,1	-1257,4	-1637,2	-14275,8
Mass Density	KG/CUM	23,5	1,8	649,3	40,4	26,9	38,4	24,9	40,4	2,6

Table B.9: Stream summary for case 3: Methanol synthesis with hydrogen and CO₂ integration (part2)

	Units	HX1-C-IN	HX1-C-OU	IN	IN2	LEAN-IN	LEAN-OUT	MIXED	MU	PERMEATE
From			HX1		SPLITMEM	COOL-REC	FLASHCCU	MIXREA		MEMBRANE
To		HX1		SPLITMEM	MIXMEMB	ABSORBER	SPLITCCU	COMP2	MIXCCU	MIXMEMB
Phase:		Liquid	Mixed	Vapor	Vapor	Liquid	Liquid	Vapor	Liquid	Mixed
Component Mass Flow										
H2	KG/HR	0,0	0,0	491,4	393,2	0,0	0,0	8142,4	0,0	288,8
CO	KG/HR	0,0	0,0	691,8	553,5	0,0	0,0	9165,1	0,0	164,4
CO2	KG/HR	0,0	0,0	8885,0	7108,0	110,3	110,3	95052,5	0,0	3334,2
N2	KG/HR	0,0	0,0	113,9	91,1	0,0	0,0	1334,7	0,0	26,2
CH4	KG/HR	0,0	0,0	1191,4	953,1	0,0	0,0	14360,5	0,0	257,1
WATER	KG/HR	5000,0	5000,0	14,8	11,9	2580,0	2580,1	327,3	0,0	12,9
MEOH	KG/HR	0,0	0,0	0,0	0,0	0,0	0,0	1707,3	0,0	0,0
SELEXOL	KG/HR	0,0	0,0	0,0	0,0	14809,8	14809,8	0,0	0,2	0,0
Mole Flow	KMOL/HR	277,5	277,5	549,5	439,6	198,6	198,6	7540,4	0,0	242,6
Mass Flow	KG/HR	5000,0	5000,0	11388,4	9110,7	17500,2	17500,2	130090,0	0,2	4083,7
Volume Flow	CUM/HR	7,7	822,9	423,4	338,7	16,4	16,5	3451,4	0,0	189,7
Temperature	C	175,0	175,5	30,0	30,0	10,0	10,4	58,6	25,0	30,0
Pressure	BAR	9,0	9,0	32,0	32,0	31,9	1,0	60,0	20,0	31,9
Vapor Fraction		0,0	0,7	1,0	1,0	0,0	0,0	1,0	0,0	1,0
LHV	MJ/KG	0,0	0,0	11,0	11,0	0,0	0,0	14,0	0,0	12,0
Molar Enthalpy	MJ/KMOL	-275,6	-246,8	-160,1	-160,1	-221,5	-221,7	-127,6	-165,9	-131,3
Mass Enthalpy	MJ/KG	-15,3	-13,7	-7,7	-7,7	-2,5	-2,5	-7,4	-1,0	-7,8
Enthalpy Flow	MW	-21,2	-19,0	-24,4	-19,6	-12,2	-12,2	-267,3	0,0	-8,8
Mass Entropy	J/KG-K	-7493,3	-3938,1	-1210,4	-1210,4	-1373,8	-1371,5	-1605,2	-886,8	-1381,0
Mass Density	KG/CUM	650,3	6,1	26,9	26,9	1064,6	1061,8	37,7	1057,0	21,5

Table B.10: Stream summary for case 3: Methanol synthesis with hydrogen and CO₂ integration (part3)

	Units	PURGE	RECYCLE	REMOVED	RETENTAT	RICH-OUT	R-IN	R-OUT	R-OUT1	R-OUT2
From		SPLITCCU	SPLITREA	FLASHCCU	MEMBRANE	ABSORBER	HEATER	REACTOR	HX1	HX2
To			MIXREA			FLASHCCU	REACTOR	HX1	HX2	FLASH
Phase:		Liquid	Vapor	Vapor	Mixed	Liquid	Vapor	Vapor	Vapor	Mixed
Component Mass Flow										
H2	KG/HR	0,0	6081,4	0,5	410,9	0,5	8142,4	6683,4	6683,4	6683,4
CO	KG/HR	0,0	8423,7	1,0	807,1	1,0	9165,1	9257,9	9257,9	9257,9
CO2	KG/HR	0,0	75954,1	597,5	5954,8	707,8	95053,2	84338,8	84338,8	84338,8
N2	KG/HR	0,0	1214,5	0,1	116,7	0,1	1334,7	1334,7	1334,7	1334,7
CH4	KG/HR	0,0	13059,8	3,9	1272,8	4,0	14360,5	14360,5	14360,5	14360,5
WATER	KG/HR	0,0	280,2	6,0	17,7	2586,1	327,3	4713,2	4713,2	4713,2
MEOH	KG/HR	0,0	1707,3	0,0	168,8	0,0	1707,3	9401,9	9401,9	9401,9
SELEXOL	KG/HR	0,2	0,0	0,0	0,0	14809,8	0,0	0,0	0,0	0,0
Mole Flow	KMOL/HR	0,0	5969,6	14,4	457,7	213,0	7540,4	7060,1	7060,1	7060,1
Mass Flow	KG/HR	0,2	106721,0	609,0	8748,8	18109,2	130090,0	130090,0	130090,0	130090,0
Volume Flow	CUM/HR	0,0	2642,3	338,0	201,0	17,2	4944,7	5185,6	4892,0	3513,6
Temperature	C	10,4	50,0	10,4	50,0	27,9	206,3	259,1	230,0	102,2
Pressure	BAR	1,0	60,0	1,0	59,9	31,9	62,0	61,2	61,2	61,2
Vapor Fraction		0,0	1,0	1,0	1,0	0,0	1,0	1,0	1,0	1,0
LHV	MJ/KG	0,0	14,1	0,4	14,2	0,0	14,0	13,8	13,8	13,8
Molar Enthalpy	MJ/KMOL	-221,7	-131,5	-378,3	-138,7	-232,3	-122,3	-130,6	-131,8	-137,3
Mass Enthalpy	MJ/KG	-2,5	-7,4	-9,0	-7,3	-2,7	-7,1	-7,1	-7,2	-7,5
Enthalpy Flow	MW	0,0	-218,1	-1,5	-17,6	-13,7	-256,2	-256,2	-258,4	-269,3
Mass Entropy	J/KG-K	-1371,5	-1637,2	27,4	-1618,8	-1344,8	-852,9	-801,8	-920,2	-1622,0
Mass Density	KG/CUM	1061,8	40,4	1,8	43,5	1054,3	26,3	25,1	26,6	37,0

Table B.11: Stream summary for case 3: Methanol synthesis with hydrogen and CO₂ integration (part4)

	Units	SYN-IN	SYN-IN-C	SYN-IN-H	TOCOOL	TO-HEATE	TOMUMIX	TOPUMP
From		ABSORBER	COOLER	COMP1	PUMP	HX2	SPLITCCU	MIXCCU
To		COMP1	MIXREA	COOLER	COOL-REC	HEATER	MIXCCU	PUMP
Phase:		Vapor	Vapor	Vapor	Liquid	Vapor	Liquid	Liquid
Component Mass Flow								
H2	KG/HR	681,5	681,5	681,5	0,0	8142,4	0,0	0,0
CO	KG/HR	716,9	716,9	716,9	0,0	9165,1	0,0	0,0
CO2	KG/HR	9844,8	9844,8	9844,8	110,3	95053,3	110,3	110,3
N2	KG/HR	117,2	117,2	117,2	0,0	1334,7	0,0	0,0
CH4	KG/HR	1206,3	1206,3	1206,3	0,0	14360,5	0,0	0,0
WATER	KG/HR	18,7	18,7	18,7	2580,0	327,3	2580,0	2580,0
MEOH	KG/HR	0,0	0,0	0,0	0,0	1707,3	0,0	0,0
SELEXOL	KG/HR	0,0	0,0	0,0	14809,8	0,0	14809,6	14809,8
Mole Flow	KMOL/HR	667,8	667,8	667,8	198,6	7540,4	198,6	198,6
Mass Flow	KG/HR	12585,4	12585,4	12585,4	17500,2	130090,0	17500,0	17500,2
Volume Flow	CUM/HR	519,7	349,8	349,8	16,5	4944,7	16,5	16,5
Temperature	C	28,8	103,1	103,1	14,8	206,3	10,4	10,4
Pressure	BAR	31,9	60,0	60,0	31,9	62,0	1,0	1,0
Vapor Fraction		1,0	1,0	1,0	0,0	1,0	0,0	0,0
LHV	MJ/KG	11,9	11,9	11,9	0,0	14,0	0,0	0,0
Molar Enthalpy	MJ/KMOL	-144,9	-142,5	-142,5	-221,2	-122,3	-221,7	-221,7
Mass Enthalpy	MJ/KG	-7,7	-7,6	-7,6	-2,5	-7,1	-2,5	-2,5
Enthalpy Flow	MW	-26,9	-26,4	-26,4	-12,2	-256,2	-12,2	-12,2
Mass Entropy	J/KG-K	-1287,3	-1188,7	-1188,6	-1361,0	-852,9	-1371,5	-1371,5
Mass Density	KG/CUM	24,2	36,0	36,0	1062,5	26,3	1061,8	1061,8